

POLITECNICO DI MILANO

Dipartimento di Meccanica

TECHNISCHE UNIVERSITÄT MÜNCHEN

Fachgebiet für Risikoanalyse und Zuverlässigkeit

Reliability of structural components under variable  
amplitude high cycle fatigue

Doctoral Dissertation of:

Alessandra Altamura

Supervisors:

Prof. Stefano Beretta

Prof. Daniel Straub

The Chair of the Doctoral Program:

Prof. Bianca Maria Colosimo

Doctoral Program in Engineering of Mechanical Systems

Year 2013 - Cycle XXIII

To Giulia and Andrea

## Acknowledgements

In 2008 I started to pursue my doctoral degree in the frame of my activity as research and development engineer at Tenaris, a leading supplier of tubes. The challenge to combine an advanced technical study program with applied activities in the company was great and I decided it was worth a try. The first part of the work was carried out between Politecnico di Milano and Tenaris Research & Development centre, the second part was developed at the Engineering Risk Analysis group at the Technische Universität München.

This thesis is the outcome of the interaction with many people.

Mario Rossi, director of Tenaris Research & Development centre in Italy, and Tenaris University are kindly acknowledged for their support and for the permission to publish the experimental data contained in this work.

I thank Prof. Stefano Beretta, my supervisor at Politecnico di Milano, for his will to start my doctoral research and his ability to link the academic world and the industrial demands.

A special thank goes to Mauro Madia, researcher at Politecnico di Milano, for his illuminating explanations on fracture mechanics, for his kindness and friendship.

The experimental activities have been supported by Luca Signorelli at Politecnico di Milano and by Enrico Palermo, at the Tenaris Research and Development centre laboratory.

I am grateful to Gabriel Solari for the support during the software implementation and for the time spent discussing statistical issues, to Ettore Anelli and Emanuele Paravicini for their precious advices on metallurgical issues.

A key contribution to this work has been given by my supervisor at the Technische Universität München, Prof. Daniel Straub, who welcomed me in his research group and accompanied me in the discovery of the logic and the rationale of the scientific approach. I am also very grateful to Iason Papaioannou, researcher in the Engineering Risk Analysis group, for his clear explanations of random processes and the support during the implementation of the Subset simulation algorithm.



# Contents

<b>List of Figures</b>	<b>ix</b>
<b>List of Tables</b>	<b>xv</b>
<b>1 Introduction</b>	<b>1</b>
1.1 This work: motivation and innovative features . . . . .	4
<b>2 Background</b>	<b>9</b>
2.1 Introduction . . . . .	9
2.2 Fatigue: crack initiation and growth . . . . .	10
2.2.1 Pre-existing surface flaws and probability of detection . . . . .	11
2.2.2 Parameters influencing the fatigue threshold . . . . .	12
2.3 Variable amplitude loading . . . . .	15
2.3.1 Historical background . . . . .	15
2.3.2 Load as a random process . . . . .	17
2.4 Fatigue crack growth evaluation under constant and variable loading . .	18
2.4.1 Models of fatigue crack growth . . . . .	18
2.4.2 Evaluation of fatigue crack growth . . . . .	20
2.4.2.1 One-dimensional crack growth with constant amplitude loading . . . . .	20
2.4.2.2 Two-dimensional crack growth with constant amplitude loading . . . . .	21
2.4.2.3 One-dimensional crack growth with variable loading . .	22
2.4.2.4 Two-dimensional crack growth with variable amplitude loading . . . . .	25
2.5 Probabilistic fatigue crack growth . . . . .	26

## CONTENTS

---

2.5.1	Random process approach . . . . .	27
2.5.2	Random variable approach . . . . .	28
2.6	Failure evaluation . . . . .	29
2.6.1	Limit state function . . . . .	29
2.6.2	Failure criteria . . . . .	29
2.6.3	Numerical evaluation of the limit state function for variable amplitude loading . . . . .	31
2.7	Reliability evaluation methods . . . . .	32
2.7.1	Monte Carlo Simulation Method . . . . .	32
2.7.2	First Order Reliability Method . . . . .	33
2.7.3	Subset simulation . . . . .	34
<b>3</b>	<b>Experimental investigation on crack growth and threshold for structural steels</b> . . . . .	<b>35</b>
3.1	Introduction . . . . .	35
3.2	Materials . . . . .	36
3.2.1	Microstructural characterization . . . . .	36
3.2.2	Mechanical characterization . . . . .	37
3.2.2.1	Monotonic tensile properties . . . . .	37
3.2.2.2	Cyclic behaviour . . . . .	37
3.2.2.3	Fracture toughness . . . . .	38
3.3	Fatigue crack growth tests . . . . .	38
3.3.1	Design of experiments . . . . .	40
3.3.2	Test method . . . . .	41
3.3.3	Data analysis method . . . . .	46
3.3.4	Test results . . . . .	46
3.4	Fatigue threshold statistical analysis . . . . .	51
3.4.1	Equality of the variance . . . . .	53
3.4.2	Equality of the mean . . . . .	53
3.4.3	Pooled data analysis . . . . .	55
3.5	Crack paths, crack closure and microstructure in the threshold region . . . . .	55
3.6	Discussion . . . . .	58
3.7	Concluding remarks . . . . .	59

<b>4 Case study: description of the adopted models</b>	<b>61</b>
4.1 Introduction . . . . .	61
4.2 Case study . . . . .	62
4.3 Model for the pre-existing flaws distribution and POD model . . . . .	62
4.4 Structural integrity model . . . . .	63
4.4.1 Semi-elliptical surface cracks in flat plates . . . . .	63
4.4.2 Semi-elliptical external surface cracks in thick tubes . . . . .	64
4.5 Fatigue crack growth algorithm and Nasgro equation . . . . .	65
4.6 Failure evaluation . . . . .	66
4.6.1 Failure criteria . . . . .	66
4.6.2 Proposed algorithm for the evaluation of the limit state function	68
4.7 Verification . . . . .	69
4.8 Probabilistic model . . . . .	72
4.9 Validity and limits of the models . . . . .	73
4.10 Concluding remarks . . . . .	73
<b>5 Fracture mechanics based fatigue reliability under variable amplitude loading: random variable approach</b>	<b>75</b>
5.1 Introduction . . . . .	75
5.2 Experimental assessment of the distribution of initial surface flaws depth	76
5.2.1 Methodology . . . . .	76
5.2.2 Experimental results . . . . .	77
5.3 Reliability assessment method . . . . .	81
5.4 Case Study . . . . .	82
5.4.1 Service stress measurements . . . . .	82
5.4.2 Approaches for the evaluation of the probability of failure . . . . .	83
5.4.3 Results and discussion . . . . .	84
5.5 Concluding remarks . . . . .	86
<b>6 Fracture mechanics based fatigue reliability under variable amplitude loading: random process model</b>	<b>89</b>
6.1 Introduction . . . . .	89
6.2 Markov process model of the load . . . . .	90
6.2.1 Discretization of the fatigue load process into blocks . . . . .	91



## CONTENTS

---

6.2.2	Generation of a Markov process load sequence for reliability analysis	92
6.2.3	Variable amplitude stress for numerical investigation . . . . .	94
6.3	Innovative solutions for the reliability evaluation . . . . .	95
6.4	Results - critical crack size failure criterion . . . . .	96
6.4.0.1	FORM sensitivity analysis . . . . .	100
6.5	Results - Critical crack size failure and crack driving force failure criteria	102
6.6	Discussion . . . . .	104
6.7	Concluding remarks . . . . .	106
<b>7</b>	<b>Conclusions</b>	<b>107</b>
7.1	Validity and limits of the results . . . . .	109
7.2	Future work . . . . .	110
<b>A</b>	<b>Influence of mechanical properties and microstructural features on the fatigue threshold of steels</b>	<b>111</b>
A.1	Introduction . . . . .	111
A.2	Closure mechanisms and their influence on the fatigue threshold . . . . .	112
A.2.1	Plasticity induced closure . . . . .	112
A.2.2	Oxide induced closure . . . . .	113
A.2.3	Roughness induced closure . . . . .	113
A.2.4	Measurement of closure . . . . .	113
A.3	Parameters influencing the threshold . . . . .	114
A.3.1	Influence of stress ratio . . . . .	114
A.3.2	Influence of microstructural domain size and yield strength . . . . .	115
A.3.3	Influence of microstructural inhomogeneities and second phases . . . . .	116
A.4	Intrinsic and extrinsic threshold concept . . . . .	117
A.5	Two parameters threshold representation . . . . .	117
A.6	Factors affecting the fatigue threshold . . . . .	117
<b>B</b>	<b>Fatigue crack growth model: Nasgro equation</b>	<b>119</b>
<b>C</b>	<b>Verification of the subset simulation algorithm</b>	<b>123</b>
	<b>References</b>	<b>125</b>

# List of Figures

2.4	Crack with a near semi-elliptical shape and various cracks advance directions, where $O$ is the origin. . . . .	18
2.5	Scheme of an elliptical crack with semi-axes $a$ and $c$ , corresponding to the main growth directions. . . . .	19
2.6	Scheme of a one-dimensional crack with crack depth $a$ . . . . .	20
3.1	Ramberg-Osgood interpolation of the experimental data: stress $\sigma$ versus strain $\epsilon$ . . . . .	39
3.2	Specimen mounted on a resonant test machine during pre-cracking . . .	41
3.3	Inner surface of a tested specimen where precrack is marked with heat tinting. The precrack is larger at the sample boundary where plain stress conditions act. . . . .	42
3.4	<i>CPCA</i> experimental procedure: the test is carried out at constant amplitude loading, increasing at each step the applied stress intensity factor untill the crack starts growing. . . . .	43
3.5	<i>CPLR</i> experimental procedure: in the first part a constant amplitude load is applied, then a $\Delta K$ decreasing procedure. . . . .	43
3.6	Three Paris curves obtained applying the same test procedures by the three laboratories: <i>TenarisDalmine Research and Development laboratory (TD)</i> , <i>Centro Sviluppo Materiali (CSM)</i> and <i>Politecnico di Milano (PM)</i> . The data are superimposed. . . . .	44
3.7	Specimen mounted on a servo-hydraulic test machine during the tests at TenarisDalmine laboratory. . . . .	44
3.8	Specimen mounted on a servo-hydraulic test machine during the tests at Politecnico di Milano. . . . .	45

## LIST OF FIGURES

---

3.9	Fatigue crack growth experimental data for material 355L and the corresponding fitted Nasgro equation: fatigue crack growth rate $\frac{da}{dN}$ versus the stress intensification factor range $\Delta K$ . . . . .	47
3.10	Fatigue crack growth experimental data for material 355H and the corresponding fitted Nasgro equation: fatigue crack growth rate $\frac{da}{dN}$ versus the stress intensification factor range $\Delta K$ . . . . .	48
3.11	Fatigue crack growth experimental data for material 410L and the corresponding fitted Nasgro equation: fatigue crack growth rate $\frac{da}{dN}$ versus the stress intensification factor range $\Delta K$ . . . . .	49
3.12	Fatigue crack growth experimental data for material E410H and the corresponding fitted Nasgro equation: fatigue crack growth rate $\frac{da}{dN}$ versus the stress intensification factor range $\Delta K$ . . . . .	50
3.13	Normalized fatigue threshold experimental data for material 355L and the corresponding fitted Nasgro equation with its 95% confidence interval.	51
3.14	Normalized fatigue threshold experimental data for material 355H and the corresponding fitted Nasgro equation with its 95% confidence interval.	52
3.15	Normalized fatigue threshold experimental data for material 410L and the corresponding fitted Nasgro equation with its 95% confidence interval.	52
3.16	Normalized fatigue threshold experimental data for material 410H and the corresponding fitted Nasgro equation with its 95% confidence interval.	53
3.17	Multiple comparison procedure: the normalized mean values of the threshold and its 95% confidence interval for each load ratio for the four investigated materials. . . . .	54
3.18	Crack path observed with the optical microscopy: deviations and branching (material 355L). . . . .	56
3.19	Crack path observed with the optical microscopy: deviations are evident (material 410L) . . . . .	57
3.20	Crack path observed with the optical microscopy arresting at a pearlite island (material 355H). . . . .	57
3.21	Crack path observed with the optical microscopy: no influence of the microstructure (material 410H). . . . .	58

**LIST OF FIGURES**

---

4.1	Transversal and longitudinal sections of the tube subjected to internal pressure, $P$ . On the external surface an initial flaw characterized by the depth $a$ and the semi-length $c$ is present. The geometry of the tube is defined by the outer diameter, $OD$ , the wall thickness, $WT$ , and the inner diameter, $ID$ . . . . .	62
4.2	Scheme of the model of a semi-elliptical surface crack in a flat plate: membrane stress $\sigma_m$ and bi-dimensional fatigue crack growth. . . . .	64
4.6	Full scale test data (32) (cylinders with 0.3 mm EDM notches ) with their maximum likelihood interpolation and its 90% scatter band compared with the present crack growth model prediction and AFGROW evaluation (13). For confidentiality reasons no quantitative data concerning the number of cycles to failure can be disclosed. . . . .	72
5.1	SEM image of the longitudinal section of micro-defects (13). . . . .	77
5.2	Surface flaws of the same order of magnitude as the NDT threshold (13). . . . .	77
5.3	Lognormal, Weibull and LEVD probability papers of the crack depth, $a$ , expressed as percentage of tube wall thickness (for confidentiality reasons no absolute values can be disclosed) (13). . . . .	79
5.4	Simultaneous confidence interval tests: $\frac{\lambda}{\lambda}$ , $\frac{\delta}{\delta}$ and $\frac{\lambda}{\delta}$ versus outer diameter and wall thickness (13). . . . .	80
5.6	Stress spectra measured on earth moving machines extrapolated to 360 working hours (13). . . . .	83
5.7	Approaches adopted to evaluate the probability of failure (13). . . . .	84
5.8	Probability of failure for the various approaches. The probability of failure is normalized with respect to the highest value. . . . .	85
6.1	Randomly generated sequences of the stress range $\Delta\sigma$ , with identical marginal distribution and varying correlation length $z$ . . . . .	91
6.2	Approximated load sequences built as blocks of length $b = 20$ cycles, superimposed on the load sequences shown in figure 6.1. The value of $\Delta\sigma$ at each block is equal to the mid-point value of the original random process at each block. . . . .	92

## LIST OF FIGURES

---

6.4	Probability of failure $p_F$ versus correlation length of the stress range process $z$ corresponding to the three models: $C1$ , $C2$ , $CW$ . Results for $z = 1, 10^3, 10^5, 10^7, 10^9$ are obtained describing the load as Markov random process and applying a subset simulation algorithm (SuS RP). Results for $z = \infty$ refer to the case of the load described as a random variable and solved with Monte Carlo simulation or with first order reliability method (MCS RV and FORM RV). Results for $z = 0$ are obtained applying the mean approximation with respect to the stress process and solving with FORM (FORM MA). . . . .	97
6.5	Mean approximation for cases $C1$ and $CW$ : (a) expected value of the fatigue crack growth rate $E[\frac{da}{dn}] = h'_a(a, \frac{a}{c}, \delta, \gamma)$ as a function of the crack length $a$ ; (b) crack depth $a$ versus the number of fatigue cycles $n$ calculated with the mean approximation at the design point $u^*$ of the FORM solution for case $C1$ . . . . .	99
6.6	Crack depth $a$ versus number of fatigue cycles $n$ with initial crack depth $a_0 = 0.0003$ m or $a_0 = 0.00056$ m and fixed fatigue threshold. . . . .	100
6.7	Crack depth (black) and stress range (gray) versus number of cycles with initial crack depth $a_0 = 0.56$ mm and fixed fatigue threshold. The crack growth is evaluated for realizations of the stress range modeled as a random process with a correlation $z = 10^7$ based on the empirical $C1$ . Three randomly generated load histories are exemplarily shown. . . . .	101
6.8	CDF of the maximum stress range in a block of $b = 10^4$ number of cycles for the random variable model of the stress range and for the random process model with correlation length ( $z = 1$ ). . . . .	102
6.9	Probability of failure versus correlation length $z$ when applying either the critical crack size failure criterion alone or in combination with the crack driving force failure criteria. For $z = 1$ , results are computed with SuS; for $z = \infty$ , the MCS is applied. . . . .	103

C.1 Probability of failure versus correlation length of the stress random process, having cumulative distribution function  $CDF1$ , obtained applying subset simulation method ( $SuS RP$ ) and Monte Carlo simulation method ( $MCS RP$ ). The results are obtained considering the critical crack size failure condition and evaluating the fatigue crack growth using  $b = 10^4$  cycles for each block. . . . . 124

## **LIST OF FIGURES**

---

# List of Tables

3.1	Chemical composition of the steels investigated in this work. Chemical components are expressed in terms of percentage by mass. $C_{eq} = C + \frac{Mn}{6} + \frac{Cr+Mo+V}{5} + \frac{Ni+Cu}{15}$ . . . . .	36
3.2	Steel grade according to EN 10305-1 (9) and tubes' dimension ( $OD$ is the outer diameter and $WT$ is the wall thickness). . . . .	36
3.3	Average size $D$ of the characteristic microstructural domain. . . . .	37
3.4	Monotonic tensile properties. . . . .	37
3.5	Monotonic tensile properties . . . . .	38
3.6	Number of replicates for experimental conditions . . . . .	40
3.7	ANOVA: probability that the samples at $R=0.1$ , $R=0.3$ and $R=0.7$ have the same mean . . . . .	54
5.1	Geometry of the inspected tubes. . . . .	78
5.2	Case studies of service stress measurements . . . . .	83
6.1	Properties of the three applied load models: maximum stress range $\Delta\sigma_{max}$ , number of fatigue cycles during the service life $N$ , mean of the stress range $\mu_{\Delta\sigma}$ , and standard deviation $\sigma_{\Delta\sigma}$ . . . . .	95
6.2	FORM sensitivity analysis for the random variable approach . . . . .	101
6.3	FORM sensitivity analysis for the mean approximation approach . . . . .	101
B.1	Forman-Mettu equation parameters . . . . .	120
B.2	Mechanical properties . . . . .	121



## **LIST OF TABLES**

---

# 1

## Introduction

Fatigue of materials is a phenomenon which implies a structural damage due to cyclic loading and it is one of the most studied subjects in the field of structural and mechanical engineering.

High cycle fatigue refers to the application of more than  $10^3$  loading cycles to the structure or to the component. Since its discovery in the 19<sup>th</sup> century by Wöhler, fatigue of metals has been constantly studied in the field of engineering, unfortunately being the driver often constituted by the many accidents caused by this phenomenon. More than 15.000 papers have been written on this topic in the last 20 years. Nevertheless fatigue failures still occur, causing not only costs but also disasters, such as the Aloha Airlines Flight 243 accident in 1988, or the Comet 1 accident in 1954, just to cite two of the most known accidents, for which fatigue has been officially recognized to be the cause of failure.

The service loading conditions, which in the case of fatigue are given by cyclic loading, may cause the nucleation and growth of cracks from the free surface or from pre-existing imperfections. Cracks often grow from the free surface, because stresses usually reach their highest value on the surface and because small imperfections due to the surface roughness facilitate the crack nucleation. Cracks can also easily grow from pre-existing imperfections, such as for example welding defects or surface flaws deriving from the manufacturing process or resulting from the deterioration during the service. The nucleation phase of the cracks is usually longer in comparison to the growth phase, therefore the presence of preexisting imperfections must be taken into account when

## 1. INTRODUCTION

---

analyzing the behavior of a structures subjected to fatigue. Once nucleated, cracks may grow in the structure without causing macroscopic or visible damage from the beginning. However unexpected failure occurs, when critical conditions of crack size and applied stress are reached.

Fatigue crack growth is possible only when the fatigue threshold or the fatigue limit are exceeded. The fatigue threshold is a characteristic property of the material and it is expressed in terms of a stress intensity factor (SIF). The SIF accounts for the geometry of the structure, the crack's shape and dimension, the applied nominal stress. When the applied SIF exceeds the fatigue threshold ( $SIF \geq SIF_{th}$ ) the crack grows, when the applied SIF is lower than the fatigue threshold ( $SIF \leq SIF_{th}$ ) the crack does not grow, even though cyclic stresses are applied. Generally, the fatigue crack growth depends on the combination of crack's dimension and applied stress and it is also influenced by the geometry of the structure and by the cracks' shape.

Due to the presence of the fatigue threshold, a cyclic loading acting on a structure does not imply the generation of fatigue damage. In this respect two design approaches can be distinguished: i) safe-life and ii) damage tolerant.

The safe-life design approach avoids crack nucleation and crack growth in the structures, maintaining the SIF below the fatigue threshold and assuming the structure will have an infinite service life. In case pre-existing cracks are present in the structure, an hypothesis on their maximum or expected size must be formulated in order to avoid the exceedance of the fatigue threshold. This approach is simple to apply and often conservative; its drawback is the over-dimensioning of the components.

The damage tolerant design approach allows the nucleation and growth of cracks, i.e. this approach permits the application of a SIF higher than the threshold. However it ensures that the damage does not cause failure. In some cases non destructive inspections are carried out during the structure's life to detect the presence of cracks. This is for example the case of aeronautical components or expensive components of power generation plants. In other cases only initial non destructive tests are planned, and no intermediate inspections is foreseen. This approach requires the definition of a finite service life.

---

The loading to which a structure is subjected might be constant or variable.

In the simplest case, a structure is subjected to a constant amplitude stress with constant stress ratio, as depicted in figure 1.1. In this case the stress condition is described by the stress range  $\Delta\sigma = \sigma_{max} - \sigma_{min}$  and by the stress ratio,  $R = \frac{\sigma_{min}}{\sigma_{max}}$ , or by the stress amplitude  $\sigma_a = \frac{\Delta\sigma}{2}$ .

Usually structures are subjected to variable amplitude loads, which imply a variable stress amplitude and a variable stress ratio during the fatigue life (see figure 1.2).

A constant stress sequence of the type shown in figure 1.1 can be very easily described, while a variable amplitude stress sequence is not always predictable, it is not easy to simulate for experimental testing and it is difficult to obtain analytically for numerical evaluations.

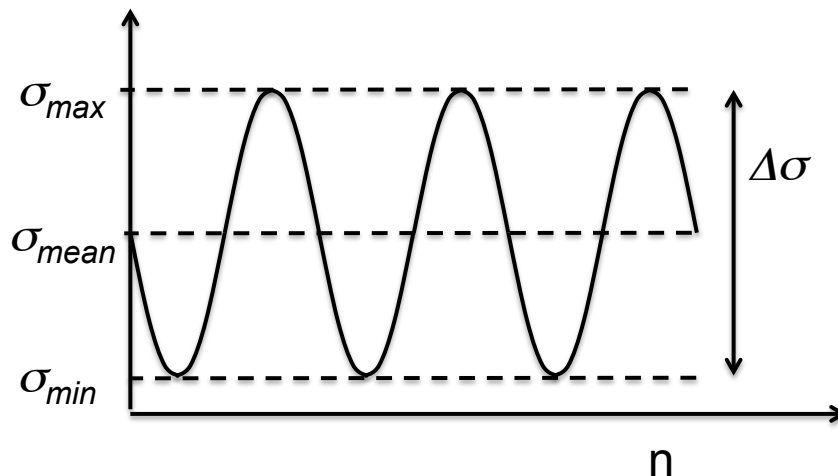


**Figure 1.1:** Scheme of a constant amplitude stress versus the number of fatigue cycles  $n$ .

The stress to which structural components is subjected depends on the specific application and on the particular service conditions. For example the stress sequence experienced by a structural component of an airplane is very demanding during landing and take off, while it is lighter during the cruise. This implies that airplanes traveling a long way experience less severe loading than those landing and taking off more often. The stress sequences experienced by off shore structures depend by the water current of the particular area where they are installed. The mechanical components of a car, such as axles and suspensions, are subjected to very different types of loading when the

## 1. INTRODUCTION

---

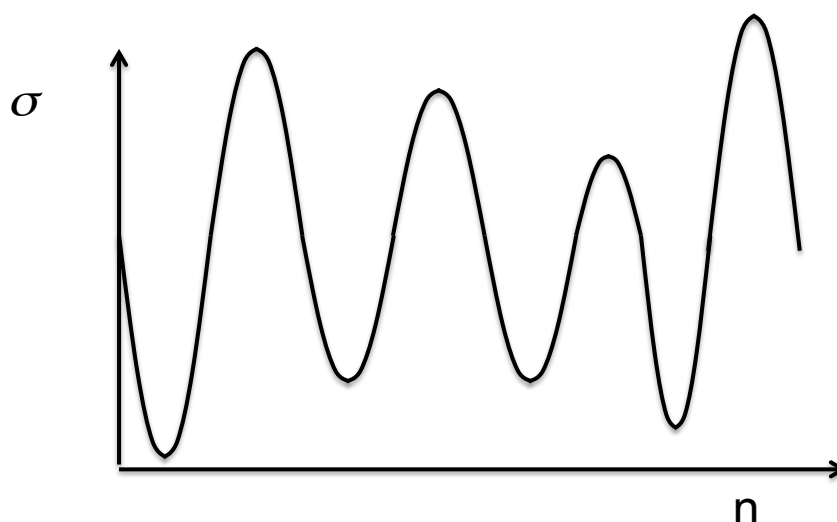


**Figure 1.2:** Scheme of a variable stress versus the number of fatigue cycles  $n$ .

car is traveling on a highway or when it is traveling off-road. On average, the type of stress to which a car is subjected depends on the quality of the road network on which the car is traveling, and can vary for different countries or regions. Steel bridges are also subjected to variable stresses and the estimation of their fatigue damage as well as of the possibility to extend their life are relevant topics in the civil engineering field.

### 1.1 This work: motivation and innovative features

The first studies on the influence of variable amplitude loading on fatigue date back to the 1930s when, in the aeronautical field, engineers aimed at optimizing the performance of the components and reducing their weight. Many improvements have been done in the high cycle fatigue design with variable loading, but many aspects of this topic are still open for investigation.

To achieve an optimized design not only the sequence of variable stress has to be described, but also the uncertainty in the other input variables has to be taken into account. For example the presence of initial flaws and their size are uncertain, as well as the mechanical and the fatigue properties of the material, which are often given as minimum guaranteed values and vary depending on the manufacturing process or even on the production batch. Sometimes, also the residual stresses, due for example to the

## 1.1 This work: motivation and innovative features

---

manufacturing or welding process, play an important role in the fatigue phenomenon. Besides, fatigue presents considerable scatter even under controlled experimental conditions and its intrinsic stochastic nature has also to be considered.

For this reason, an exhaustive fatigue design must be based on a statistically based reliability evaluation, accounting for all the uncertainties affecting the case study and properly describing the applied stress sequence.

The current standard fatigue reliability evaluation procedures, such as (6), do not treat the fatigue life assessment with a probabilistic approach and do not consider variable amplitude fatigue stress sequences and the stochastic fatigue crack growth (21). Therefore there is a gap between the fatigue reliability evaluation available standard procedures, the state of the art methods for fatigue crack growth and reliability evaluation, the actual in-service conditions of the structures subjected to high cycle fatigue. The present work aims at covering this gap, proposing a comprehensive reliability evaluation method for structures subjected to high cycle variable amplitude fatigue. In particular this work is characterized by the following novelties :

- Initial flaws are described with a probabilistic approach based on experimental data.
- An original model of the load is presented, which permits representing different types of service histories (section 6.2).
- A comprehensive fatigue crack growth and fatigue threshold model based on experimental data is proposed and validated. The model accounts for the stochasticity of the crack growth phenomenon and for plasticity induced closure (chapter 3 and section 3.6). The model is more accurate than the usually applied models, but simpler from a statistical point of view.
- A new bi-dimensional fatigue crack growth and failure evaluation algorithm is implemented based on the integration of the Forman-Mettu model (or Nasgro equation) and a block approximation of the stress sequence (sections 2.4.2.4, 4.5, 4.6, 6.2.1).
- Original and very efficient probabilistic reliability evaluation schemes are proposed, implemented, and verified on a case study. They are based on state of

## 1. INTRODUCTION

---

the art fracture mechanics concepts, most recent fatigue crack growth and failure assessment methods, advanced statistical approaches (sections 4.8, 5.3, 6.3).

In the following the key steps for fatigue reliability evaluation are identified and the way they are tackled and developed in this work is summarized.

First of all hypothesis on the presence of preexisting flaws, which may behave like cracks or from which cracks may grow, must be formulated. Manufacturing and welding processes, as well as non destructive tests have to be considered when defining the probability of the existence of flaws and their dimensions and shape. Usually in the literature the maximum size of the flaws, corresponding to the non-destructive tests threshold, or an equivalent flaw size, is adopted (82). In this work a probabilistic model for the preexisting surface flaws is developed (section 4.3) based on experimental data. The presence of preexisting flaws and the distribution of their depth is experimentally analyzed, as reported in the first part of chapter 5.2.

A further key factor for the fatigue reliability analysis is the description of the stress sequence. In many studies concerning fatigue reliability, the stress is assumed constant or deterministic block sequences are adopted (56, 167). These sequences are however often not representative of the real service load to which the structure is subjected. In this work in-service stress measurements, presented in section 5.4.1 are used to produce two types of stress sequences. For the analysis presented in chapter 5 completely randomized stress sequences are generated from the empirical cumulative distribution function of the measured stress amplitude. For the analysis presented in chapter 6, the concept of Markov random processes is applied (see sections 2.3 and 6.2). An innovative method to generate random stress sequences and simulate different service conditions is proposed and implemented. The method permits to obtain different stress sequences varying only one parameters, that is the correlation length of the sequence.

Once the model for the stresses is defined, it is necessary to evaluate the fatigue life and the failure mode. This task can be accomplished either with a cumulative damage approach (81) or with a fatigue crack growth approach. In this work a fatigue crack growth evaluation approach is adopted, because it is more suitable to variable stress cases. An overview on fatigue crack growth is offered to the reader in sections 2.2 and 2.4. Section 2.5 addresses the topic of probabilistic fatigue crack growth, which is related to the intrinsic stochastic nature of the fatigue phenomenon. The evaluation of

## 1.1 This work: motivation and innovative features

---

crack growth implies not only a fatigue crack growth algorithm, but also a structural integrity model and failure evaluation criteria. In this thesis a new comprehensive fatigue crack growth model and an original algorithm for the fatigue crack growth evaluation and failure are presented (chapter 3 and sections 4.5, 4.4, 2.6 and 4.6). Chapter 3 describes the large experimental activity aimed at investigating the influence of material properties on the fatigue threshold and to propose a suitable description of the fatigue crack growth stochasticity. The stochasticity of the fatigue crack growth is expressed with one random variable (the fatigue threshold), while usually two or more random variables are used: the models developed up to now are more complicated and the fatigue life prediction is less accurate (17). The threshold variation with the stress ratio and the related crack closure are expressed using cyclic yield strength and the applied stress intensity factor, while usually the yield stress related to the maximum applied stress is considered, which does not permit to take into account the specimen geometry (88). The fatigue crack growth and failure algorithm herein presented have unique features, which are not present in any commercial software. It permits to take into account any kind of randomly generated stress sequence and uses a comprehensive and validate fatigue crack growth model as well as a state of the art failure evaluation approach. The main lack of fatigue crack growth algorithm proposed in the literature is the application of simple and unrealistic fatigue crack growth model which do not describe precisely the fatigue threshold region, which is actually the most influent one when treating high cycle fatigue (127). The algorithm herein proposed can describe very accurately the experimental data and indeed it is computationally efficient.

Finally, a proper reliability evaluation method has to be chosen, based on the number of random variables and on the expected probability of failure. An overview of the state of the art reliability evaluation methods is given in 2.7. In this work efficient reliability evaluation schemes are proposed and are used to investigate the influence of the stress sequence and of the failure criteria on the reliability (section 6.3). For the first time a fatigue reliability evaluation is approached applying a time discretization of the Markov stress process with subset simulation method. This scheme joins the subset simulation method, a random process model of the load and the state of the art Forman-Mettu model applied to a bi-dimensional fatigue crack growth scheme. This represents an extremely innovative efficient method in the field of high cycle fatigue. Additionally, also a mean approximation of the stress process is applied and solved



## 1. INTRODUCTION

---

with the first order reliability method (FORM): this is a new solution of the fatigue life evaluation problem and represents an extremely efficient method to solve the fatigue life evaluation problem. It is also proven that this approximated method gives good predictions in the case of uncorrelated stress sequences. Finally the numerical example demonstrates that a random variable approach can be used with FORM to obtain correct reliability predictions in the case of high correlated sequences.

## 2

# Background

## 2.1 Introduction

The reliability of components subjected to high cycle fatigue can be evaluated using two approaches. One is based on S-N curves and damage accumulation rules. The other one is based on fatigue crack growth evaluation.

Damage accumulation approaches are aimed at predicting fatigue life under variable amplitude loading taking into account the number of fatigue cycles applied at various stress levels and evaluating the damage level with a simple linear rule, as in the classical formulation of the Palmgren-Miners rule (93, 111) or with more complex non-linear rules (115, 160). A review of cumulative fatigue damage theories can be found in (44). This approach is used basically because experimental data in terms of S-N curves are easy to obtain, even though experiments are costly. However the S-N approach does not provide any information regarding the crack depth during the fatigue crack growth and the failure mode. An additional limitation is that this approach is based on experimental data and no extrapolation to conditions different from the experimental ones is possible. For example in (24), a stochastic crack growth model for variable loading is developed and compared with the results obtained using the Miner's rule, demonstrating that the S-N diagram does not predict the influence of load order on the fatigue crack growth.

Approaches based on fatigue crack growth evaluation are applied in this work, because they have the following advantages:

- the crack depth as a function of the number of cycles can be calculated;

## 2. BACKGROUND

---

- the sequence of applied stress cycles can be taken into account;
- the stochasticity of any input parameter, such as the initial crack depth, the material properties, the parameters describing the fatigue crack growth curve, can be accounted for and the distribution of crack depths as a function of the number of cycles can be determined;
- experimental data collected in different conditions can be extrapolated and used.

This section offers to the reader an overview and an historical background on fatigue, crack growth, variable amplitude loading and reliability evaluation. These concepts and knowledge are the basis on which the reliability evaluation models presented in the further sections are developed.

### 2.2 Fatigue: crack initiation and growth

The phenomena of fatigue can be divided into four phases: crack initiation, small-crack growth, long-crack growth and failure.

*Crack initiation* When no pre-existing imperfections are present, cracks initiate on the surface by the mechanism of persistent slip bands, which are the embryonic fatigue cracks (144). Alternatively, cracks may nucleate from pre-existing imperfections, such as micro voids or inclusions, or defects which act as stress intensifiers. The number of cycles for initiation is highest when cracks nucleate from a defect-free surface and it is smallest when pre-existing imperfections or notches lead to crack initiation.

*Small-crack growth* Depending on their size, cracks can be divided into two groups: small and long cracks, which exhibit a very different fatigue crack growth behavior. According to standard ASTM E647 (7) "a crack is defined as being small when all physical dimensions (in particular, both length and depth of a surface crack) are small in comparison to a relevant microstructural scale, continuum mechanics scale, or physical size scale". Small cracks can grow at faster growth rate than long cracks and can also grow below the so called "long crack threshold" (92, 116, 129, 145). Among the different approaches to identify the small cracks regime, it is worth mentioning the one proposed by Kitagawa and Takahashi (67), which shows that the threshold for the crack growth varies with the crack size, depending on the fatigue limit of a plain specimen and on the fatigue threshold for long cracks. The model identifies a characteristic dimension,

called El Haddad's parameter (38), which is the boundary between the small crack region and the long crack region. Murakami contributed to a further development of this model by proposing the square root of the crack area as characteristic dimension (100).

*Long-crack growth* The growth of long cracks can be fully described with linear elastic fracture mechanics models, while the same does not hold for small cracks. Cracks nucleating from a defect-free surface go through the small crack phase until they reach the long crack dimension. Cracks generated from pre-existing imperfections can behave right from the start as long cracks, depending on the initial dimension of the imperfection.

*Failure* Failure occurs when a critical condition is reached, given by the combination of crack size and stress. failure can occur according to different failure modes.

### 2.2.1 Pre-existing surface flaws and probability of detection

The present work is concerned with the reliability of structural components containing initial surface flaws. In particular, the work is focused on tubes having some surface imperfections deriving from the manufacturing process and constituting pre-existing cracks. The crack initiation phase and the small-crack growth phase are absent in this particular case. The surface imperfections are usually monitored after the production, in order to assure that their size is limited and below a given value, called non-destructive test threshold. To this aim, non-destructive tests (NDT) are carried out, mainly using ultrasonic or eddy current methods. The inspection performance of the NDT equipment is influenced by many variables, such as the flaw size, its orientation, the environmental conditions as well as by the signal noise (142). Therefore a curve indicating the probability of detection (POD) as a function of the defect size can be drawn, as depicted in figure 2.1.

In this work the depth of the characteristic flaw or crack size is called  $a_0$ . The probability density function of the crack depth after the manufacturing process before the NDT tests is the prior probability density function  $f'(a_0)$ . The probability density function of the crack depth after the NDT tests is the posterior probability density function  $f''(a_0)$  and can be evaluated considering the probability of detection  $POD(a_0)$  and applying the Bayes' rule (122). The posterior probability density function  $f''(a_0)$

## 2. BACKGROUND

---

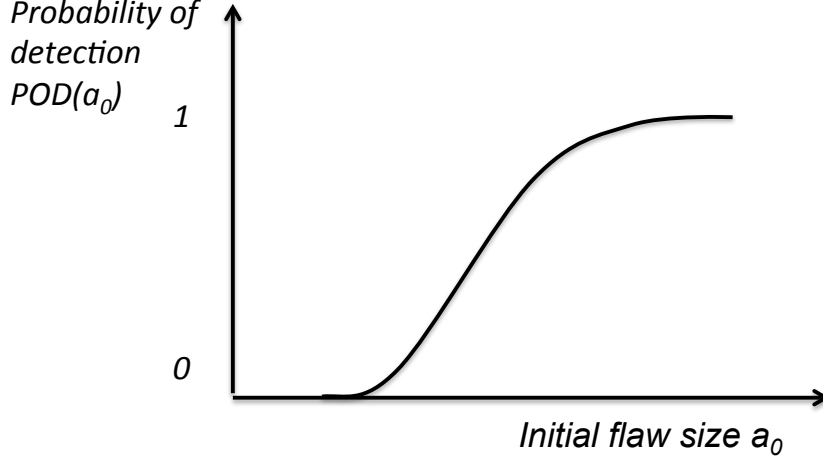


**Figure 2.1:** Curve of the probability of detection,  $POD$ , versus the flaw size: there is a transition region where the probability of detection increases from 0 to 1 with the flaw size.

is the probability density function of the cracks given the event of no detection  $ND$  and can be expressed as:

$$f''(a_0) = f(a_0|ND) = \frac{f'(a_0)[1 - POD(a_0)]}{\int_0^{\infty} f'(a_0)[1 - POD(a_0)]da_0} \quad (2.1)$$

### 2.2.2 Parameters influencing the fatigue threshold

The third phase identified above is the long-crack growth. The long-crack growth is driven by the applied stress intensity factor range ( $\Delta K$ ), a parameter which accounts for the geometry of the structure, the crack's shape and dimension, the applied nominal stress range. A threshold in terms of stress intensity factor range  $\Delta K_{th}$  exists for long cracks fatigue growth, defining the applied  $\Delta K$  value above which cracks grow and below which no fatigue crack growth is possible. The long crack growth fatigue behavior is usually expressed in terms of fatigue crack growth rate  $\frac{da}{dn}$  versus  $\Delta K$ . During the long crack growth three domains can be identified: the near-threshold region, the straight-line region, also called Paris region, because it is described by the Paris law, the unstable growth and failure region. These three domains are illustrated in figure 2.2.

When treating the reliability of components subjected to high cycle fatigue, the fatigue threshold is a parameter of paramount interest, being the boundary between

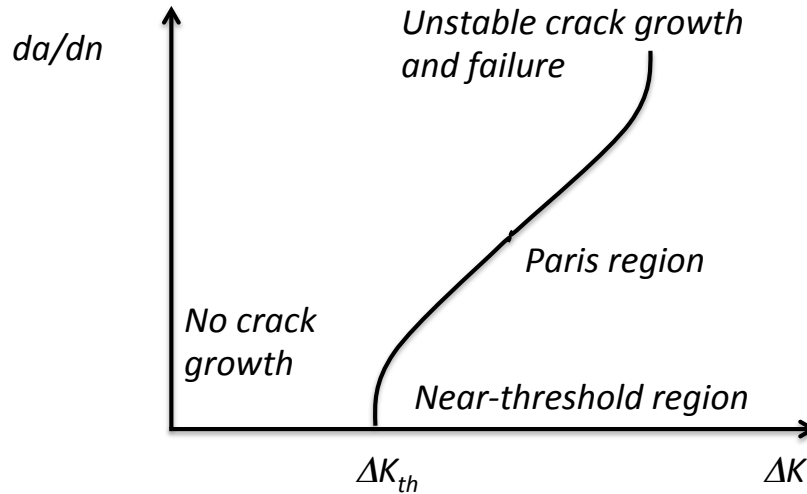


**Figure 2.2:** The three crack growth curve's domains: the near-threshold region, the straight-line region, also called Paris region, because it is described by the Paris law, the unstable growth and failure region.

crack propagation and non-propagation. In other words it represents the boundary between a safe-life and a damage tolerant design. The fatigue threshold is defined as the value of stress intensity factor under which no propagation occurs. For practical purposes, in the standard ASTM E647 (7) the fatigue threshold of long cracks is defined as the stress intensity factor causing a propagation rate of  $10^{-7}$  mm/cycle.

Many experimental observations reported in the literature show that the near threshold region is affected by load ratio, microstructural features and mechanical properties, while the Paris region is not influenced by these parameters (79, 126, 148). The reason for this behavior is that the crack tip opening displacement and the crack tip plastic zone size in the near threshold region are of the same order of magnitude of the microstructural features, while in the Paris region they are much larger than the characteristic microstructural dimension. In other words, in the near threshold region, the stress field at the crack tip is directly influenced by the microstructural features that surround the tip, while in the Paris region the average material properties contribute to the crack growth.

To understand why the above mentioned parameters influence the threshold zone, crack closure has to be considered. When a crack grows due to cyclic loading, theoretically one expects that the crack surfaces open during the positive part of the stress

## 2. BACKGROUND

---

cycle, i.e. when the stress is increasing from zero to a positive value. When the stress decreases the surfaces are expected to close and adhere completely when the applied stress is zero. The mechanism of closure causes the crack to open at an applied stress level  $\sigma_{open}$  higher than the minimum applied stress  $\sigma_{min}$  even if this is equal or higher than zero. Therefore the effective stress intensity factor applied to the crack is reduced: the effective stress range is  $\Delta\sigma_{eff} = \sigma_{max} - \sigma_{open}$  and the corresponding effective stress intensity factor range is  $\Delta K_{eff} = K_{max} - K_{open}$ . A higher level of closure increases  $K_{open}$  and decreases  $\Delta K_{eff}$ , as schematically depicted in figure A.1. Thus, in presence of closure, the measured fatigue threshold is higher than that measured in absence of closure, due to the lower  $\Delta K_{eff}$  actually acting on the crack. The amount of closure is related to the stress ratio  $R = \frac{\sigma_{min}}{\sigma_{max}}$ , to the yield stress of the material and to the microstructural features.

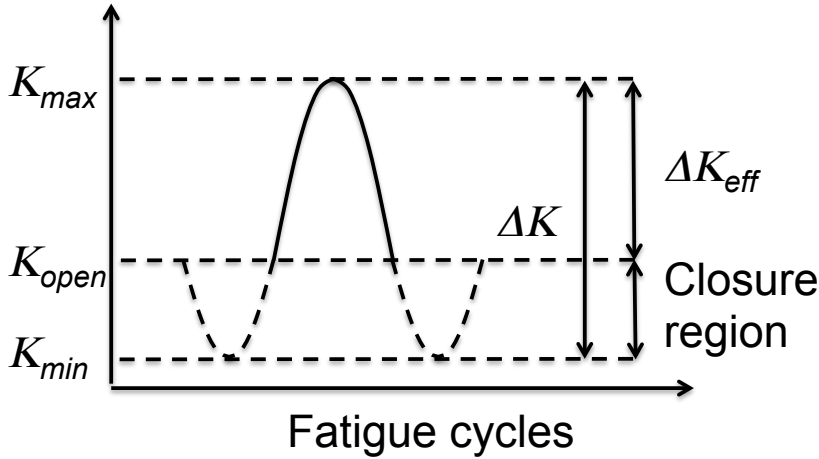


**Figure 2.3:** Crack closure: the applied stress is  $\Delta K = K_{max} - K_{min}$ , but the effective stress is  $\Delta K_{eff} = K_{max} - K_{open}$ . The crack tip opens at  $K_{open}$

The threshold value in absence of closure is often called intrinsic component of the threshold of the material. The intrinsic component, according to most of the models, is described through considerations based on the energy necessary for dislocation movement to permit the crack advance. The threshold increment due to closure is called extrinsic component of the threshold and can be observed at low values of  $R$ . The extrinsic component is also affected by microstructural morphology (39, 68, 125, 126, 148, 168) and by the monotonic or cyclic yield strength, which determines the extension of the

plastic zone size at the crack tip (29). Closure can be induced by plasticity, roughness and oxide (148). The plasticity induced closure was the first one to be observed by Elber (40, 41), later other mechanisms were discovered.

It is observed in most of the materials that the threshold value decreases as the stress ratio  $R$  increases, since at low stress ratio  $K_{open} > K_{min}$ . The yield stress influences the threshold mostly through the plasticity induced closure, which increases as the yield strength decreases, because the size of the plastic zone size at the crack tip is larger for lower yield strength's materials. Therefore it is generally expected that a lower yield strength leads to higher threshold values. Finally, the microstructure exerts an influence on threshold through the roughness-induced closure, caused by crack deflections in correspondence to microstructural inhomogeneities and grain boundaries. It has to be underlined that all the above mentioned mechanisms interact simultaneously and a model able to predict the closure level for various types of materials is not available. The influence of material properties and closure on the fatigue threshold are explained in more detail in appendix A.

## 2.3 Variable amplitude loading

Most structural components are subjected to variable amplitude loading, also called spectrum loading (10), during their service life. Early on, scientists realized the need for describing and properly modeling the load sequences to which components are subjected during their service life. Most of the structures and the mechanical components are actually subjected to variable stress during their service life and predictions using data related to constant stress experiments require a model for the variable stress sequence.

### 2.3.1 Historical background

In the 1930s, engineers working in aeronautics realized that in-service stress cycles have variable amplitude. Measurements of service loads were carried out and first load spectra were published by Kaul (65). In 1939, Gassner introduced the first variable amplitude load sequence (49) for testing aeronautical structures. Laboratory experiments require simple load sequences, which however should be representative of the real service conditions. The Eight-Block-Program Test proposed by Gassner is a sequence of loading blocks, now known as Gassner sequence. Within each block, stress cycles are



## 2. BACKGROUND

---

identical; between blocks, the stress amplitude changes while the mean value remains the same. The lengths of the blocks are defined such that stress amplitudes follow the lognormal distribution. The Gassner sequence consists of eight varying blocks, whose sequence is fixed and predetermined. After eight blocks, the sequence is repeated (140). This procedure is the core of the *operational fatigue strength* approach to the design of components under variable amplitude loading (50, 136). With the availability of hydraulic testing machines, more realistic load sequences could be applied for testing. Such load sequences can be derived from experimental measurements. For example, the SAE Fatigue and Evaluation Committee selected test load sequences from existing strain measurements (43, 151). Exhaustive information on fatigue testing under variable amplitude loading can be found in (141), while a review of the standard load sequences used for fatigue testing and on the generation of testing load histories from experimental measurements can be found in (56).

For the first time Lardner (71, 72, 73) and Rau (124) proposed to model variable amplitude loading by random processes. In (71, 72) an approach for the reliability evaluation under random loading is described using the crack propagation law proposed by (55). Rau (124) describes the fatigue crack growth as a random process, since it is the consequence of the application of loads, which are viewed as a random process. In his work, the hypothesis that the propagation of the fatigue crack is independent of the order of application of the stresses is formulated. This assumption holds when the load is a stationary and ergodic random process and when a high number of cycles is applied, so that variations due to the order of application of the stresses average out.

At the beginning of the 1970s, Schijve investigated the influence of the load sequence on fatigue life (133). In his study, the effect of the load sequence on crack propagation is investigated by performing experiments applying random loading sequence with short and long blocks of cycles. It was observed that the random load sequences could lead to fatigue lives that differ from those evaluated using laboratory tests with simplified load sequences, demonstrating the importance of appropriately representing the randomness of fatigue loads. According to (133), the predicted life does not depend so much on the sequence, provided that it is random in some way or programmed with a short period, which confirms the findings by (124). Simplified loading sequences consisting of repeated large blocks may lead to non conservative fatigue life predictions due to

sequence effects. Following these studies, the need to account for the stochasticity of fatigue crack growth under variable loading was recognized.

### 2.3.2 Load as a random process

When describing load sequences from experimental load measurements, procedures for identifying load cycles from the stress time history are necessary (84). Standardized procedures reported in (10) are: level-crossing counting, peak counting, simple-range counting and rainflow counting. These methods result in a sequence of stress cycles that are characterized by their stress ranges,  $\Delta\sigma$ , and stress ratios  $R$ , or alternatively by their minimum and maximum stresses  $\sigma_{min}$  and  $\sigma_{max}$ . Consequently, the load sequence can be statistically described by the random processes  $\{\Delta\sigma(n)\}, \{R(n)\}$ , i.e. for every stress cycle  $n$  there is a random variable pair  $\{\Delta\sigma(n)\}$  and  $\{R(n)\}$ . Values of  $\{\Delta\sigma(n)\}$  and  $\{R(n)\}$  at different cycles are generally correlated.

In this work the discussion is limited to stationary load processes, since the assumption of stationarity is sufficient for most relevant applications, and for ease of notation the processes are denoted by  $\{\Delta\sigma\}$  and  $\{R\}$ .

Under the assumption of a Gaussian copula model, a stationary random process is fully characterized by its marginal distribution and its autocovariance function (83). These can both be determined from observed load sequences. Alternatives are presented by Markov chain models as presented e.g. in (86, 112, 130), which require the definition of the stress cumulative distribution function and autocovariance function. In general, Markov process models, due to their flexibility, can represent the real dependence among stress cycles more accurately. For example, switching Markov models (112) can well represent different modes of operations of mechanical systems and structures, and representation of non-stationary processes is facilitated by Markov chains (86). However, given the uncertainties associated with determining in-service stresses in real structures, the Gaussian copula model is sufficiently accurate for many engineering applications. It is pointed out that the marginal distribution of the stress ranges,  $\Delta\sigma$ , and stress ratio,  $R$ , is not affected by these modeling assumptions.

## 2. BACKGROUND

---

### 2.4 Fatigue crack growth evaluation under constant and variable loading

#### 2.4.1 Models of fatigue crack growth

Starting from an initial flaw or notch, cracks will form and grow under cyclic loading. Cracks that grow in two directions usually exhibit a near elliptical or semi-elliptical shape (105). Thereby, the crack front advances in all directions, with coordinates  $x_i, x_j, x_k$ , as depicted in figure 2.4:

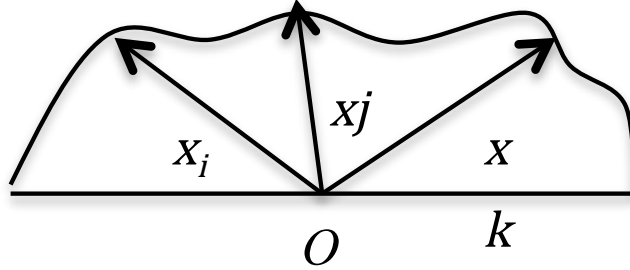


**Figure 2.4: Crack with a near semi-elliptical shape and various cracks advance directions, where  $O$  is the origin.**

Crack growth in any direction  $x_i$  is described by a differential equation expressing the crack growth rate,  $\frac{dx_i}{dn}$ , as a function of the stress intensity factor range along the crack front in the  $x_i$  direction,  $\Delta K_{x_i}$ :

$$\frac{dx_i}{dn} = h_{x_i}(\Delta K_{x_i}, R, \delta) \quad (2.2)$$

where  $R$  is the stress ratio and  $\delta$  is a set of parameters related to the material properties. For the case of the Paris law we have  $\frac{dx_i}{dn} = C \cdot \Delta K_{x_i}^m$  with parameters  $\delta = [C, m]$ . Alternative models for  $h_{x_i}$  include different modifications of the Paris law, e.g. the bilinear crack growth model adopted in (5, 127) or the Forman-Mettu model, which is detailed in appendix B and which is used in the numerical investigations presented later.

The evaluation of fatigue crack growth requires knowledge of the stress intensity factor along the entire crack front. A large body of research has focused on deriving analytical or numerical expressions for  $\Delta K_{x_1}$ , including (45, 99, 105, 146, 161). For

## 2.4 Fatigue crack growth evaluation under constant and variable loading

certain geometries, exact or approximated analytical solutions are available, in other cases FEM analysis is necessary, e.g. (25, 51, 98, 135). If the geometry of the crack is approximated by a perfect semi-elliptical or elliptical shape, then it is fully described by the semi-lengths of the two axes, called  $a$  and  $c$ , which correspond to the two main growth directions (105), as shown in figure 2.5. In the following, this approximation will be used.

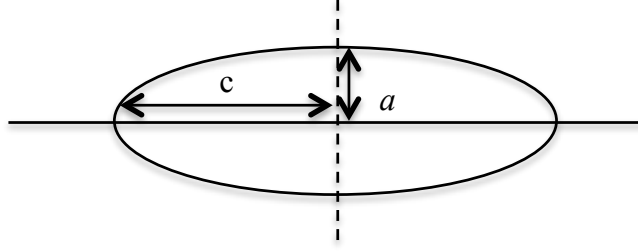


**Figure 2.5: Scheme of an elliptical crack with semi-axes  $a$  and  $c$ , corresponding to the main growth directions.**

The stress intensity factor ranges in the two directions  $a$  or  $c$ , denoted by  $\Delta K_a$  and  $\Delta K_c$ , are a function of the geometry of the component, the crack dimensions  $a$  and  $c$ , and the applied stress range. It is distinguished between the membrane stress range,  $\Delta\sigma_m$ , and the bending stress range,  $\Delta\sigma_b$ , which varies along the section. In absence of residual stresses, both components can be directly evaluated from a total stress range  $\Delta\sigma = \Delta\sigma_m + \max(\Delta\sigma_b)$  (165). For ease of presentation, only  $\Delta\sigma$  is considered. Therefore, the stress intensity factor range can be written in terms of  $\Delta K_a = \Delta K_a(a, c, \Delta\sigma, \gamma)$  and  $\Delta K_c = \Delta K_c(a, c, \Delta\sigma, \gamma)$  and equation 2.2 can be rewritten as follows:

$$\frac{da}{dn} = h_a(\Delta K_a(a, c, \Delta\sigma, \gamma), R, \delta) \quad (2.3)$$

$$\frac{dc}{dn} = h_c(\Delta K_c(a, c, \Delta\sigma, \gamma), R, \delta) \quad (2.4)$$

where:

- $\frac{da}{dn}$  and  $\frac{dc}{dn}$  are the crack growth rates in directions  $a$  and  $c$ ;
- $h_a$  and  $h_c$  are the functions describing the crack growth rate;

## 2. BACKGROUND

---

- $R$  is the stress ratio;
- $\delta$  is a set of parameters describing material properties;
- $\gamma$  is a set of parameters describing the geometry of the component containing the crack.

If crack closure and load interaction effects are taken into account, a corresponding model has to be included in the fatigue crack growth rate equations. Different models for crack closure are available to describe the delaying effects of high loads, such as the Wheeler model (157), the Wilenbourg model (158), the more realistic Newman model based on a strip yield type plastic zone (104), the partial crack closure model valid in the near-threshold region (37, 114).

### 2.4.2 Evaluation of fatigue crack growth

In the following, the evaluation of one- and two-dimensional crack growth under constant and variable amplitude loading is presented. The parameters  $R$ ,  $\delta$  and  $\gamma$  are assumed constant. Generally they may be modeled as deterministic or random variables.

#### 2.4.2.1 One-dimensional crack growth with constant amplitude loading

For one-dimensional crack growth, the crack is fully characterized by its depth  $a$ , as shown in figure 2.6. Crack growth is thus fully described by equation 2.3 where  $c$  disappears.

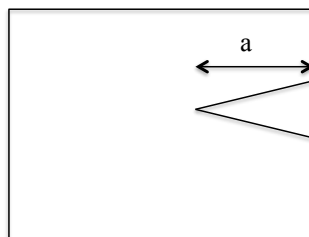


Figure 2.6: Scheme of a one-dimensional crack with crack depth  $a$ .

With constant amplitude  $\Delta\sigma$ , the crack growth can be evaluated from the boundary condition on the initial value of crack depth  $a_0$ . By reformulating equation 2.3 and integrating on both sides, one obtains:

## 2.4 Fatigue crack growth evaluation under constant and variable loading

$$n = \int_0^n dn = \int_0^n \frac{da}{h_a(\Delta K_a(a, \Delta\sigma, \gamma), R, \delta)} \quad (2.5)$$

where  $n$  is the number of stress cycles to reach the crack depth  $a$ .

Equation 2.5 can be solved numerically. For special cases, analytical solutions exist (e.g. for the simple Paris law (84)). If the interest is in finding the crack depth  $a$  as a function of the number of stress cycles  $n$ , a root finding algorithm can be employed; this algorithm requires evaluating the integral in equation 2.5 for different values of  $a$ .

### 2.4.2.2 Two-dimensional crack growth with constant amplitude loading

In case of two-dimensional crack growth, the crack is described by its depth  $a$  and its width  $c$ . Crack growth is described by two coupled differential equations given in equations 2.3 and 2.4. An approximate solution of these coupled differential equations is obtained through a step-wise solution. Let  $b$  denote the number of cycles in each step. In the  $i^{th}$  step, the crack advances from  $a_i, c_i$  to  $a_{i+1}, c_{i+1}$ . If the ratio of crack depth to width is fixed in each step to  $(\frac{a}{c})_i$ , then the stress intensity factors can be rewritten as  $\Delta K_a = \Delta K_a(a, (\frac{a}{c})_i, \Delta\sigma, \gamma)$  and  $\Delta K_c = \Delta K_c(c, (\frac{a}{c})_i, \Delta\sigma, \gamma)$ . The two differential equations can be integrated separately, as shown in equations 2.6 and 2.7.

$$\Delta n_a = \int_{n_i}^{n_{i+1}=n_i+\Delta n_a} dn = \int_{a_i}^{a_{i+1}} \frac{da}{h_a(\Delta K_a(a, (\frac{a}{c})_i, \Delta\sigma, \gamma), R, \delta)} \quad (2.6)$$

$$\Delta n_c = \int_{n_i}^{n_{i+1}=n_i+\Delta n_c} dn = \int_{c_i}^{c_{i+1}} \frac{dc}{h_c(\Delta K_c(c, (\frac{a}{c})_i, \Delta\sigma, \gamma), R, \delta)} \quad (2.7)$$

In equations 2.6 and 2.7, the integrals are evaluated for fixed values of  $a_{i+1}$  and  $c_{i+1}$ . In order to find the crack dimensions after  $b$  cycles, an iterative procedure is required. A root-finding algorithm is employed to find values of  $a_{i+1}$  and  $c_{i+1}$  which assure that  $\Delta n_a = \Delta n_c = b$ . The above is an approximation due to the assumption of a constant ratio  $(\frac{a}{c})_i$ . An exact solution could only be obtained by cycle-by-cycle evaluation of the increment of  $a$  and  $c$ , which corresponds to setting  $b = 1$  in equations 2.6 and 2.7, with associated large computational efforts. The error of the approximation increases with increasing  $b$ . The two-dimensional problem could be simplified and reduced to a one-dimensional problem if  $(\frac{a}{c})$  were assumed constant throughout the entire process or if a parametric relation between  $a$  and  $c$  were defined as  $c = c(a)$ , see e.g. (142).

## 2. BACKGROUND

---

### 2.4.2.3 One-dimensional crack growth with variable loading

With random variable amplitude fatigue loading, the stress range  $\Delta\sigma$  and the stress ratio  $R$  are a function of  $n$ . Therefore, equation 2.3 is rewritten to:

$$\frac{da}{dn} = h_a(\Delta K_a(a, \Delta\sigma(n), \gamma), R(n), \delta) \quad (2.8)$$

In the following, the evaluation of crack growth described through equation 2.8 for a deterministic realization of the random stress process  $\{\Delta\sigma\}, \{R\}$  is presented. Thereafter, the solution for a random stress process  $\{\Delta\sigma\}, \{R\}$  through a mean approximation is described.

**Solutions for deterministic realizations of a random stress process** For a given realization of the stress process,  $\{(\tilde{\Delta}\sigma(1), \tilde{R}(1)); \dots; (\tilde{\Delta}\sigma(l), \tilde{R}(l)); \dots; (\tilde{\Delta}\sigma(N), \tilde{R}(N))\}$ , an exact solution can be obtained through performing a cycle-by-cycle calculation. The crack increment during the  $l^{th}$  cycle is simply:

$$da(l) = h_a(\Delta K_a(a, \tilde{\Delta}\sigma(l), \gamma), \tilde{R}(l), \delta) \quad (2.9)$$

and the crack depth  $a(l+1)$  is;

$$a(l+1) = a(l) + da(l) \quad (2.10)$$

Unfortunately, the cycle-by-cycle calculation is not computationally feasible for high-cycle fatigue. This holds in particular when the randomness of the stress process must be taken into account. An approximate solution can be obtained by representing the load sequence with blocks of  $b$  cycles with constant stress amplitude and constant stress ratio, as presented in section 6.2.1 and 6.2.2. The crack growth during the  $i^{th}$  block  $\Delta a_i$  is now obtained from the solution for constant amplitude loading given in section 2.4.2.1, i.e.  $\Delta a_i$  is found from the following condition:

$$b = \int_{a_i}^{a_{i+1}=a_i+\Delta a_i} \frac{da}{h_a(\Delta K_a(a, \tilde{\Delta}\sigma_i, \gamma), \tilde{R}_i, \delta)} \quad (2.11)$$

$\tilde{\Delta}\sigma_i$  and  $\tilde{R}_i$  are the values of the stress process realization at the midpoint of the  $i^{th}$  block. Equation 2.11 can be used whenever the load is given as a deterministic sequence of stress ranges and stress ratio values, as for example in (13, 49, 78, 94, 109).

## 2.4 Fatigue crack growth evaluation under constant and variable loading

If the stress process is random, equation 2.11 can be used to evaluate the crack growth for realizations of the stress process in a simulation approach, as presented later in this work.

**Solutions for a mean approximation of a random stress process** Crack growth is a cumulative process, in which the contributions of the individual stress cycles are added up. This motivates a piecewise approximation of the random crack growth process by the mean crack growth. This approach has been followed by a number of authors, e.g. (85, 127). The crack growth rate,  $\frac{da}{dn}$ , expressed in equation 2.8, is approximated by its expected value with respect to  $\{\Delta\sigma\}$  and  $\{R\}$ :

$$\frac{da}{dn} \approx E_{\{\Delta\sigma\},\{R\}}[h_a(\Delta K_a(a, \Delta\sigma(n), \gamma), R(n), \delta)] \quad (2.12)$$

$$\frac{da}{dn} \approx \int_{-\infty}^{\infty} \int_0^{\infty} h_a(\Delta K_a(a, \Delta\sigma, \gamma), R, \delta) \cdot f_{\Delta\sigma,R}(\Delta\sigma, R) d\Delta\sigma dR \quad (2.13)$$

Where  $f_{\Delta\sigma,R}$  is the joint cumulative distribution function of  $\Delta\sigma(n)$  and  $R(n)$  and  $n$  can be dropped if the process is stationary.

The expected value of the fatigue crack growth rate,  $E_{\{\Delta\sigma\},\{R\}}[h_a(\Delta K_a(a, \Delta\sigma(n), \gamma), R(n), \delta)]$ , does not depend on  $n$  if the process is stationary. Therefore, for given distribution of  $\Delta\sigma(n)$  and  $R(n)$ , the crack growth becomes a function of  $a$ ,  $\delta$  and  $\gamma$  only:

$$\frac{da}{dn} \approx E_{\{\Delta\sigma\},\{R\}}[h_a(\Delta K_a(a, \Delta\sigma(n), \gamma), R(n), \delta)] = h'_a(a, \delta, \gamma) \quad (2.14)$$

The validity of the mean approximation is based on the following conditions for the stress process:

- strong stationarity: the probability distribution of the stress process does not depend on  $n$ ;
- ergodicity, i.e. the statistics of the entire process can be deduced from a single realization of the process;
- sufficiently mixing, i.e. the total number of cycles considered,  $N$ , is much larger than the correlation length of the process.



## 2. BACKGROUND

---

The requirement of a sufficiently mixing stress process will be further substantiated in the numerical investigations presented later in section 6. With the mean approximation, crack growth can be evaluated through the direct integration of equation 2.5, where  $h_a$  is replaced by  $h'_a$ .

To illustrate the mean approximation, let us consider the original Paris law, where  $R(n)$  is disregarded and where the material parameters are  $\gamma = [C, m]$ :

$$\frac{da}{dn} = C \cdot \Delta K^m = C \cdot (Y(a) \cdot \Delta\sigma(n) \cdot \sqrt{\pi a})^m \quad (2.15)$$

Separating the variables and integrating on both sides:

$$\int_{a_0}^a (Y(a) \cdot \sqrt{\pi a})^{-m} da = C \cdot \int_0^N (\Delta\sigma(n))^m dn \quad (2.16)$$

Under the condition that  $\{\Delta\sigma(n)\}$  is stationary, ergodic, sufficiently mixing and that  $N$  is large, the integral over  $n$  on the right hand side of equation 2.16 is approximated by an integral over  $\Delta\sigma(n)$ :

$$\int_0^N (\Delta\sigma(n))^m dn \approx N \cdot \int_0^\infty f_{\Delta\sigma}(\Delta\sigma) \cdot \Delta\sigma^m d\Delta\sigma = N \cdot E_{\{\Delta\sigma\}}[\Delta\sigma^m] \quad (2.17)$$

Note that the approximation is correct in the limit as  $N \rightarrow \infty$ . Inserting this approximation into equation 2.16 leads to:

$$\int_{a_0}^a (Y(a) \cdot \sqrt{\pi a})^{-m} \cdot da \approx C \cdot N \cdot E_{\{\Delta\sigma\}}[\Delta\sigma^m] \quad (2.18)$$

Solving for  $N$  gives:

$$N = \int_{a_0}^a \frac{da}{C \cdot (Y(a) \cdot \sqrt{\pi a})^m \cdot E_{\{\Delta\sigma\}}[\Delta\sigma^m]} \quad (2.19)$$

This is equal to the solution of equation 2.5, where  $h_a$  is replaced by the mean approximation of the crack growth in equation 2.15:

$$h_a = E_{\{\Delta\sigma\}}[C \cdot (Y(a) \cdot \Delta\sigma(n) \cdot \sqrt{\pi a})^m] = C \cdot (Y(a) \sqrt{\pi a})^m \cdot E_{\{\Delta\sigma\}}[\Delta\sigma^m] \quad (2.20)$$

The quantity  $\{E_{\{\Delta\sigma\}}[\Delta\sigma^m]\}^{\frac{1}{m}}$  can be viewed as an equivalent stress range (61, 159).

## 2.4 Fatigue crack growth evaluation under constant and variable loading

As shown above, the mean approximation is asymptotically correct as  $N \rightarrow \infty$  for the case of the Paris law. This is due to the fact that Paris law allows to separate the variables  $a$  and  $\Delta\sigma$  and, therefore, the integration can be performed as in equation 2.16. For the general case of a crack growth law  $h_a(\Delta K_a(a, \Delta\sigma(n), \gamma), R(n), \delta)$ , this separation is not possible. However, for common crack growth laws, the mean approximation is still reasonably close under the stated conditions. This is also demonstrated by the numerical investigations presented later.

### 2.4.2.4 Two-dimensional crack growth with variable amplitude loading

With random variable amplitude fatigue loading, equations 2.3 and 2.4, are rewritten to:

$$\frac{da}{dn} = h_a(\Delta K_a(a, \frac{a}{c}, \Delta\sigma(n), \gamma), R(n), \delta) \quad (2.21)$$

$$\frac{dc}{dn} = h_c(\Delta K_c(a, \frac{a}{c}, \Delta\sigma(n), \gamma), R(n), \delta) \quad (2.22)$$

When the load history is given as a realization of a random process, an exact solution can be obtained performing a cycle-by-cycle crack growth evaluation, as reported in equations 2.9 and 2.10 for the one-dimensional case. However, this is not practically feasible for most applications. Alternatively, an approximated crack growth evaluation is possible by representing the load sequence with blocks of  $b$  cycles with constant stress amplitude and constant stress ratio, in analogy to the solution in equation 2.11 for the one-dimensional case:

$$b = \int_{a_1}^{a_{i+1}=a_i+\Delta a_i} \frac{da}{h_a(\Delta K_a(a, (\frac{a}{c})_i, \tilde{\Delta}\sigma_i, \gamma), \tilde{R}, \delta)} \quad (2.23)$$

$$b = \int_{c_1}^{c_{i+1}=c_i+\Delta c_i} \frac{dc}{h_c(\Delta K_c(c, (\frac{a}{c})_i, \tilde{\Delta}\sigma_i, \gamma), \tilde{R}, \delta)} \quad (2.24)$$

Equations 2.23 and 2.24 must be solved iteratively for  $\Delta a_i$  and  $\Delta c_i$ , respectively, using a root finding algorithm as described earlier. The approach of equations 2.23 and 2.24 is implemented in commercial software such as NASGRO (47) and AFGROW (12). In analogy to the one-dimensional crack growth model, a mean approximation can be used to compute the crack growth under a random process fatigue load. The

## 2. BACKGROUND

---

fatigue crack growth rate in both directions  $a$  and  $c$  are approximated by their expected value with respect to the loading process.

$$\frac{da}{dn} \approx E_{\{\Delta\sigma\},\{R\}}[h_a(\Delta K_a(a, \frac{a}{c}, \Delta\sigma(n), \gamma), R(n), \delta)] = h'_a(a, \frac{a}{c}, \delta, \gamma) \quad (2.25)$$

$$\frac{dc}{dn} \approx E_{\{\Delta\sigma\},\{R\}}[h_c(\Delta K_c(c, \frac{a}{c}, \Delta\sigma(n), \gamma), R(n), \delta)] = h'_c(c, \frac{a}{c}, \delta, \gamma) \quad (2.26)$$

Using the mean approximation, the crack growth evaluation is reduced to the problem described in section 2.4.2.2, where  $h_a$  and  $h_c$  are replaced by  $h'_a$  and  $h'_c$ , respectively. The resulting coupled differential equations cannot be solved in one integration step but must be computed for blocks of cycles following equations 2.6 and 2.7.

### 2.5 Probabilistic fatigue crack growth

So far, the random nature of fatigue loads is considered, which are ideally modeled as random processes. However, fatigue crack growth involves additional intrinsically random factors and the model parameters are subject to uncertainty. When evaluating the reliability under fatigue crack growth, these random factors and uncertainties must be addressed.

The scatter in fatigue data was discussed as early as 1927 (97), but it was only after the large replicate experiments at constant amplitude loading performed by Virkler (155) that the intrinsic stochasticity of fatigue crack growth was investigated in more details. This intrinsic stochasticity of fatigue crack growth is due to variability of material properties and material inhomogeneities. As can be observed from the data obtained by Virkler, shown in figure 2.7, two random effects can be distinguished (110): (a) each curve has an irregular shape (high frequency stochasticity); (b) the mean crack growth curve of each experiment is different (low frequency stochasticity).

High frequency stochasticity (a) can be modeled with a random process approach, such as the one proposed by Yang and Manning (164). Low frequency stochasticity (b) can be modeled with a random variable approach, i.e. by randomizing the coefficients of the fatigue crack growth law (17, 42, 76, 110, 153). In addition to the inherent stochasticity, which can be observed in experiments, the evaluation of fatigue crack

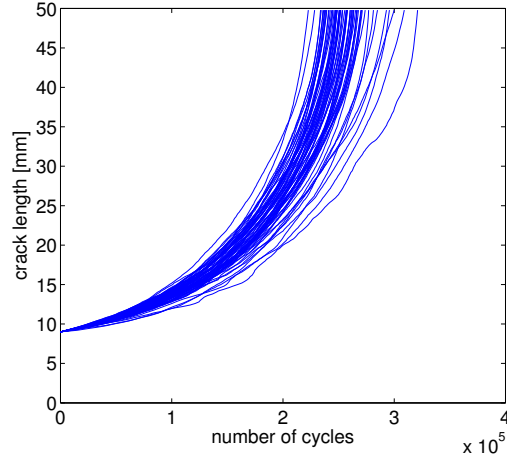


**Figure 2.7:** Virkler’s experiments (155): the 68 curves of crack length versus number of cycles.

growth under service conditions is subject to variability of the loading, as has been addressed earlier, and model uncertainties. The latter can also be addressed by a random variable approach (84).

### 2.5.1 Random process approach

Approaches based on random processes have been developed in the 1980s to describe the intrinsic stochasticity of the crack growth observed during large replicate tests with constant amplitude loading, such as those shown in figure 2.7. The aim is to describe the stochasticity of fatigue crack growth under constant or variable loading due to the heterogeneous material structure. The random process model adopted by many authors, e.g. (30, 31, 63, 64, 74, 110, 150, 162, 164), is:

$$\frac{dx_i}{dn} = X(n) \cdot h_{x_i}(x_i, \Delta\sigma, R, \delta, \gamma) \quad (2.27)$$

where  $X(n)$  is a random process and  $x_i$  is either crack depth,  $a$ , or half-width  $c$ . Most authors do not provide a physical interpretation of  $X(n)$ , but its correlation length can be fitted to experimental data (119). The resulting crack size has the smallest statistical dispersion if  $X(n)$  is uncorrelated as in (31), and the highest statistical dispersion if  $X(n)$  is fully correlated.

## 2. BACKGROUND

---

The main limitation of this approach is the lack of physical meaning of the random process  $\{X(n)\}$ .

### 2.5.2 Random variable approach

The parameters of the fatigue crack growth models can be represented as random variables (139) (163). The assumption is that these parameters are random or uncertain but do not vary during the crack growth process. They can represent specimen-to-specimen variability, randomness in the initial condition as well as model uncertainties.

Proper attention has to be paid to the modeling of the correlation among the random variables (17). As an example, the parameters  $C$  and  $m$  of Paris law are highly correlated, and the same holds for most empirically determined material parameters. To obtain the distribution of the crack size one has to solve functions of random variables. For special, simplified cases, analytical solutions are available. In the general case, numerical solutions are required, such as Monte Carlo simulation. For computing the reliability under fatigue crack growth, structural reliability methods are available, which are discussed in section 2.7.

A realistic description of the fatigue crack growth requires a combination of the random variable approach with the random process model. To reproduce the randomness of the crack growth curves shown in figure 2.7, random processes are necessary to represent the variability within each curve and random variables are required to reproduce the observed specimen-to-specimen variability. In principle, the random process model can include the latter as well, by using correlation functions that do approach a non-zero, positive value for values of  $n \rightarrow \infty$ . However, such correlation functions cannot be modeled by markovian processes and a combined modeling approach is thus preferable.

A number of authors have combined the random variable model with the random process model e.g. (36) (110) (138). To evaluate the combined model, the statistics of the fatigue crack growth process for given values of the random variables are computed. These conditional statistics must then be integrated over the outcome space of the random variables, using the total probability theorem. Methods for the computation of the reliability for the combined model are presented in paragraph 2.7 of this section.

## 2.6 Failure evaluation

When fatigue crack growth evaluation is carried out for reliability assessment, failure criteria have to be defined. In the context of reliability analysis, these criteria are expressed by limit state functions.

### 2.6.1 Limit state function

Let  $X$  denote the set of random variables of the model. By definition, a failure event is defined through a limit state function  $g(X)$  in such a way that failure occurs when  $g(X) \leq 0$ . The probability of failure is thus evaluated as  $p_F = Pr\{g(X) \leq 0\}$ . In the case of fatigue crack growth,  $X$  includes the initial crack dimensions  $a_0$  and  $c_0$ , the material properties and fatigue crack growth parameters  $\delta$ , the set of the geometric parameters  $\gamma$  and the applied stress amplitude and stress ratio  $\{\Delta\sigma\}, \{R\}$ . Furthermore, to make explicit the dependence of the limit state function on the total number of fatigue stress cycles  $N$ , the limit state function is written as  $g(X, N) = g(a_0, c_0, \{\Delta\sigma\}, \{R\}, \delta, \gamma, N)$ .

In structural reliability, it is convenient to define a failure domain  $\Omega_F$  in the outcome space of the random variables as:

$$\Omega_F(N) = \{g(X, N) \leq 0\} \quad (2.28)$$

The probability of failure can then be expressed as a multidimensional integral of the joint PDF of  $X$  over the failure domain (35, 91, 121):

$$p_F(N) = Pr\{g(X, N) \leq 0\} = \int_{\Omega_F(N)} f_X(x) dx \quad (2.29)$$

where  $dx = dx_1, dx_2, \dots, dx_n$ . In general, the solution is an n-dimensional integral cannot be obtained analytically. Structural reliability methods have been especially developed to solve integrals of this form. These methods are explained in section 2.7.

### 2.6.2 Failure criteria

In case of a fatigue crack growth evaluation based on a fracture mechanics approach, the failure criteria can be of two types:

- failure occurs when a critical crack size, typically the wall thickness, is reached;

## 2. BACKGROUND

---

- failure occurs by plastic collapse failure or unstable crack growth.

The expression of the first criterion (critical crack size failure, *CCSF*) is straightforward, as failure occurs when  $a(N) \geq a_{cr}$ , where  $a_{cr}$  is the critical crack depth. The corresponding limit state function for this failure criterion can be written as:

$$g_1(X, N) = a_{cr} - a(X, N) \quad (2.30)$$

where  $a(X, N)$  is the crack depth as evaluated following section 2.4.

As far as the second criterion is concerned, in this work the critical crack driving force failure (*CDF*) condition is adopted from (165).

The *CDF* involves a limit value for the ligament yielding factor,  $L_{r,max}$ , and a limit value for the applied J-integral,  $J_{applied}$ . Failure occurs when either one of those is exceeded during any stress cycle  $n$ , i.e. when  $J_{applied} \geq J_{mat}$  or when  $L_r \geq L_{r,max}$ . These two failure modes thus lead to the following two limit state functions:

$$\begin{cases} g_2(X, n) = L_{r,max} - L_r(X, n) \\ g_3(X, n) = J_{mat} - J_{applied}(X, n) \end{cases} \quad (2.31)$$

With random variable amplitude loading, both  $J_{applied}(X, n)$  and  $L_r(X, n)$  become random processes. To assess the *CDF* failure condition therefore implies the solution of a first passage problem (84). An exact solution is obtained by evaluating the limit state functions at every cycle.

The failure occurs if any of the limit state functions becomes negative. Therefore, combining all failure conditions into a single limit state function gives:

$$g(X, N) = \min[g_1(X, N), \min_{|n=1:N} g_2(X, n), \min_{|n=1:N} g_3(X, n)] \quad (2.32)$$

Alternatively, the limit state function can be expressed in terms of the number of cycles to failure  $N_{fail}$ , which can be evaluated with a crack growth algorithm considering the three failure modes defined above. The numbers of cycles to failure for each failure mode are  $N_{fail,1}$ ,  $N_{fail,2}$  and  $N_{fail,3}$  and are defined as

$$\begin{aligned} N_{fail,1}(X) &= \min\{n\} \\ \text{s.t. } a_{cr} &\leq a(X, n) \end{aligned} \quad (2.33)$$

$$\begin{aligned} N_{fail,2}(X) &= \min\{n\} \\ \text{s.t. } J_{mat} &\leq J_{applied}(X, n) \end{aligned} \quad (2.34)$$

$$\begin{aligned} N_{fail,3}(X) &= \min\{n\} \\ s.t. \ L_{r,max} &\leq L_r(X, n) \end{aligned} \quad (2.35)$$

The actual number of cycles to failure  $N_{fail}$  is the minimum of the three. The corresponding limit state function becomes:

$$g(X, N) = \min[N_{fail,1}(X), N_{fail,2}(X), N_{fail,3}(X)] - N \quad (2.36)$$

The limit state functions 2.32 and 2.36 are equivalent. However, equation 2.36 has the advantage that the three failure criteria are all expressed in the same unit, the number of cycles. This is beneficial for most structural reliability methods, as it ensures that the limit state function is not ill-conditioned.

### 2.6.3 Numerical evaluation of the limit state function for variable amplitude loading

Under variable amplitude loading, an exact solution requires an evaluation of the failure criteria 2 and 3 at each stress cycle (we are dealing with a first passage problem). For most practical problems, an approximate solution is required. In the following, we consider an approximated crack growth evaluation that is based on the block approximation introduced in section 2.4.2.4. In the block approximation to the fatigue crack growth the stress range  $\Delta\sigma$  and the load ratio  $R$  in each block are fixed. However, for assessing the failure criteria 2 and 3 (equation 2.31), it is the maximum stress  $\sigma_{max}$  in each block that is of relevance. Therefore, the block approximation proceeds by assessing the failure criteria in each block where the applied ligament yielding factor  $L_r$  and the applied J-integral are computed with  $\sigma_{max}$ . In each block  $i$ ,  $\sigma_{max,i}$  is a random variable, which is dependent on the fixed value  $\Delta\sigma_i$  and  $R_i$ . Unfortunately, an analytical solution for this distribution is not available in the general case. For the special case of no correlation among stress cycles, one can neglect the dependence of the maximum  $\sigma_{max}$  on the midpoint value of the stress range  $\Delta\sigma$ ; the cumulative distribution function of the maximum stress is obtained as:

$$F_{\sigma_{max,i}}(\sigma) = [F_{\sigma}(\sigma)]^b \quad (2.37)$$

If the stress cycles are correlated, i.e. when the correlation length  $z$  increases, the distribution of the maximum stress  $\sigma_{max,i}$  conditional on the fixed value  $\sigma_i$  (which is a



## 2. BACKGROUND

---

function of  $\Delta\sigma_i$  and  $R_i$ ) can be evaluated numerically. However, this is a cumbersome procedure. In many instances, the CDF criteria are not leading to significantly different results than the critical crack depth criterion. Therefore, a practical solution is to assess the relevance of the CDF criteria under the assumption of no correlation and under the assumption of constant amplitude loading (full correlation). If the influence of the CDF criteria under these two limiting cases is found to be small, this indicates that these criteria can be neglected for practical purposes. Otherwise, the evaluation of  $F_{\sigma_{max,i}}$  conditional on  $\sigma_i$  is required. Further discussion is written later in chapter 6.

### 2.7 Reliability evaluation methods

This section presents three methods to evaluate the reliability. The Monte Carlo simulation method is the most common one and most straightforward and is applied in section 5. The first order reliability method (FORM) offers the advantage of reducing the computational time, but it is applicable only to small dimensional problems, i.e. when a reduced number of random variables are considered. The subset simulation method is suitable to evaluate small probability of failure with a reasonable number of simulations without restrictions on the number of random variables. FORM and subset simulation method are applied in the analysis presented in chapter 6.

#### 2.7.1 Monte Carlo Simulation Method

The Monte Carlo Simulation (MCS) method (123) is generally used for solving multi-dimensional integrals or integrals for which no analytical solution is available.

When solving Eq. (44), MCS consists in generating  $n_s$  samples,  $u_i, i = 1, \dots, n_s$ , of  $U$ , and evaluating the limit state function  $G(U_i)$  for each sample. The number  $n_F$  of samples for which  $G(U_i) \leq 0$  is evaluated, and an estimate of the probability of failure is computed as:

$$p_F = \frac{n_F}{n_s} \quad (2.38)$$

The MCS method is straightforward to apply, but often requires a significant computational effort, especially when the probability of failure is low. This is due to the fact that the MCS estimate has a coefficient of variation of approximately  $\frac{1}{\sqrt{n_s p_F}} = \frac{1}{\sqrt{n_F}}$ .

As an example, in order to estimate a probability of failure of  $10^{-4}$  with a c.o.v. of 20%, a total of  $2.5 \cdot 10^5$  samples are required.

The latin hypercube is a sampling method which ensures that all the portions of the distributions of the input random variables are represented and permits more precise estimations in respect to the standard random sampling method (90).

### 2.7.2 First Order Reliability Method

The First Order Reliability Method (FORM)(54, 121) is an efficient alternative to the MCS method for reliability problems with a limited number of random variables. It utilizes a linear approximation to the limit state function in the space of standard normal random variables  $U$ . The limit state function is linearized at the so-called design point,  $u^* = [u_1^*; u_2^*; \dots; u_n^*]$ , which is point in the failure domain with the highest probability. Sometimes,  $u^*$  is referred to as the most likely failure point, and is obtained by solving the following constrained optimization problem (120):

$$\begin{aligned} u^* &= \min |u| \\ \text{s.t. } G(u) &\leq 0 \end{aligned} \quad (2.39)$$

where  $|u|$  is the Euclidian norm of  $u$ . The limit state function is linearized at  $u^*$ :

$$G'(u) = G(u^*) + \frac{\partial G(u)}{\partial u_1} \Big|_{u=u^*} \cdot (u_1 - u_1^*) + \dots + \frac{\partial G(u)}{\partial u_n} \Big|_{u=u^*} \cdot (u_n - u_n^*) \quad (2.40)$$

The probability of failure associated with this linearized limit state function is the FORM approximation, and it is defined entirely by  $|u^*|$ , as:

$$p_F = Pr\{G'(U) \leq 0\} = \Phi_U(-|u^*|) \quad (2.41)$$

$\Phi_U$  is the standard normal CDF. The FORM reliability index is defined as  $\beta_{FORM} = |u^*|$ .

FORM facilitates a sensitivity analysis of the random variables  $U$  or  $X$ . Sensitivity factors  $\alpha_i$  are obtained as the normalized gradient vector at the design point:

$$\alpha_i = \frac{u_i^*}{|u_i^*|} \quad (2.42)$$

## 2. BACKGROUND

---

The sensitivity factors  $\alpha_i$  take values between -1 and 1. The larger their absolute value, the higher the influence on the reliability. Positive values of  $\alpha_i$  indicate that an increase in  $u_i$  or  $x_i$  leads to an increase of the probability of failure, while negative values of  $\alpha_i$  are related to a decrease of the probability of failure for an increasing  $u_i$  or  $x_i$ .

FORM is computationally efficient in low dimensions, but can become cumbersome and inefficient with increasing number of random variables, due to the optimization problem in equation 2.39. For this reason, FORM is not practical when modeling the fatigue load as a random process, which involves a large number of random variables. It is however applicable in combination with the mean approximation approach.

### 2.7.3 Subset simulation

The subset simulation method (19) is a technique based on the Monte Carlo method, which can be used to efficiently evaluate small probabilities of failure in problems involving a large number of random variables is involved. In subset simulation, intermediate failure events  $E_i = \{G(U) \leq o_i\}$ ,  $i = 1, \dots, B$ , are defined. By requiring  $o_1 \geq o_2 \geq \dots \geq o_B = 0$ , it holds  $E_1 \supset E_2 \supset \dots \supset E_B = \Omega_F$ , i.e.  $E_i$  is a subset of  $E_{i-1}$ , which in turn is a subset of  $E_{i-2}$  and so on. The probability of failure can be expressed as:

$$P_F = Pr\left(\bigcap_{i=1}^B E_i\right) = Pr(E_B|E_{B-1}) \cdot Pr\left(\bigcap_{i=1}^{B-1} E_i\right) = Pr(E_1) \prod_{i=2}^B Pr(E_i|E_{i-1}) \quad (2.43)$$

where  $P(E_i|E_{i-1})$  is the conditional probability of  $E_i$  given  $E_{i-1}$ . The samples required to estimate the conditional probabilities  $Pr(E_i|E_{i-1})$  are obtained by means of a Markov Chain Monte Carlo (MCMC) sampling approach using the modified Metropolis-Hastings (M-H) algorithm from (19). This algorithm allows to generate samples from the conditional distribution of  $U$  given  $E_{i-1}$ ,  $F(U|E_{i-1})$ . The conditional probability  $Pr(E_i|E_{i-1})$  is then evaluated from these samples using a Monte Carlo approach. The constants  $o_i$  are selected so that the probabilities  $Pr(E_i|E_{i-1})$  are large, typically around 0.1. Therefore, the number of samples required for computing each conditional probability is relatively small, typically around 500. Furthermore, the required number of samples increases only linearly with a decrease in the order of magnitude of the probability of failure.

# 3

## Experimental investigation on crack growth and threshold for structural steels

### 3.1 Introduction

When investigating high cycle fatigue behavior of components carrying some initial surface flaws, the fatigue threshold is a key input for the fatigue crack growth evaluation, since it defines the minimum stress intensity factor required for crack growth.

Since the fatigue crack growth rate is proportional to the crack length, most of the crack life is spent in the near threshold region and only a small portion is spent in the Paris region. Additionally, it is well known that the fatigue threshold is a stochastic parameter and the fatigue crack growth behavior is a stochastic phenomenon (17) (23). Therefore, a correct fatigue crack growth evaluation requires an accurate model for the transition from the threshold zone to the Paris region and a proper description of the stochasticity of crack growth.

Many models present in the literature use simplified equation (127) or describe the fatigue crack growth stochasticity with many random variables (17).

The objective of this section is to propose a comprehensive model able to describe the fatigue crack growth curves and the fatigue threshold region for different stress ratio, accounting also for the stochasticity of the crack growth phenomenon in a simple even though accurate way. This is achieved in two steps. First the influence of the

### 3. EXPERIMENTAL INVESTIGATION ON CRACK GROWTH AND THRESHOLD FOR STRUCTURAL STEELS

---

C	Mn	Si	P	S	$C_{eq}$
$\leq 0.21$	$\leq 1.7$	$\leq 0.5$	$\leq 0.025$	$\leq 0.010$	$\leq 0.54$

**Table 3.1:** Chemical composition of the steels investigated in this work. Chemical components are expressed in terms of percentage by mass.  $C_{eq} = C + \frac{Mn}{6} + \frac{Cr+Mo+V}{5} + \frac{Ni+Cu}{15}$ .

Material	Grade	OD [mm] x WT [mm]
355L	E355 SR	223 x 16.5
355H	E355 SR	120 x 15
410L	E410 SR	270 x 20
410H	E410 SR	170 x 15

**Table 3.2:** Steel grade according to EN 10305-1 (9) and tubes' dimension ( $OD$  is the outer diameter and  $WT$  is the wall thickness).

material properties on the fatigue threshold is investigated, considering that according to the literature the fatigue threshold  $\Delta K_{th}$  is mainly related to the characteristic microstructural domain size  $D$  and to the monotonic or cyclic yield strength  $YS$  or  $\sigma_{yc}$  (see appendix A). Then the stochasticity of fatigue crack growth is experimentally analyzed and a proper simple model to describe it is proposed.

## 3.2 Materials

Four materials, from tubes produced according to EN 10305-1 (9) are selected. The tubes are produced with a cold drawing process, which increases the yield strength of the material through a strain hardening mechanism. Indications regarding the chemical composition of the investigated steels are reported in table 3.1.

Table 3.2 describes the materials in terms of grade and dimension.

### 3.2.1 Microstructural characterization

The characteristic microstructural dimension of the materials  $D$ , namely the ferritic grain size for ferritic-pearlitic steels, and the high angle domain size of bainitic structures, is measured. The ferritic grain size is determined according to the procedure described in ASTM E 112-96 (1) using the lineal intercept method. This same method

Material	D [ $\mu m$ ]
355L	25.2
355H	25.0
410L	11.2
410H	4.7

**Table 3.3:** Average size  $D$  of the characteristic microstructural domain.

Material	$YS[MPa]$	$UTS[MPa]$
355L	500	603
355H	590	705
410L	600	717
410H	720	775

**Table 3.4:** Monotonic tensile properties.

is applied also to EBSD (electron backscattering diffraction) acquisitions to measure the high angle domains of bainitic structures.

Table 3.3 shows the size of the characteristic microstructural domain for each material.

### 3.2.2 Mechanical characterization

The materials' mechanical characterization is aimed at investigating the monotonic tensile properties as well as the cyclic behavior, which is of interest when considering high cycle fatigue crack growth. Additionally, the materials' fracture toughness is of interest for reliability analysis when considering the failure region and the failure mode.

#### 3.2.2.1 Monotonic tensile properties

The monotonic tensile properties are measured according to the standard EN 10002-1 (2). Table 3.4 summarizes the mean value of monotonic tensile yield strength,  $YS$ , and ultimate tensile strength,  $UTS$ .

#### 3.2.2.2 Cyclic behaviour

To investigate the cyclic behavior, strain controlled fatigue tests are carried out according to ASTM E 606 (4). Table 3.5 shows the parameters of the cyclic curves

### 3. EXPERIMENTAL INVESTIGATION ON CRACK GROWTH AND THRESHOLD FOR STRUCTURAL STEELS

---

Material	$E[MPa]$	$H[MPa]$	$n$	$\sigma_{yc}[MPa]$
355L	190150	812	0.12	396
355H	192742	693	0.07	450
410L	198889	1197	0.15	480
410H	198633	1221	0.14	520

**Table 3.5:** Monotonic tensile properties

interpolated with the Ramberg-Osgood expression, reported in equation 3.1, as well as the cyclic yield stress  $\sigma_{yc}$ , which is referred to a 0.2% residual strain.

$$\epsilon = \frac{\sigma_a}{E} + \left(\frac{\sigma_a}{H}\right)^{\frac{1}{n}} \quad (3.1)$$

where  $\sigma$  is the stress,  $\epsilon$  is the strain,  $E$  is the elastic modulus,  $H$  and  $n$  are material's constant.

Figure 3.1 shows the Ramberg-Osgood interpolation of the experimental data.

#### 3.2.2.3 Fracture toughness

Experimental data of fracture toughness previously obtained on compact test (CT) specimens at room temperature (32) are available only for material 355H. The fracture toughness is described using a three-parameter Weibull distribution (165), the cumulative distribution function of which is expressed as:

$$P(K_{mat}) = 1 - \exp \left[ - \left( \frac{K_{mat} - K_{min}}{K_0 - K_{min}} \right)^k \right] \quad (3.2)$$

where  $k$ ,  $K_{min}$  and  $K_0$  are respectively equal to 5,  $28.7MPa\sqrt{m}$  and  $40MPa\sqrt{m}$ , according to the maximum likelihood fitting of the experimental results.

### 3.3 Fatigue crack growth tests

With the aim of investigating the influence of the material properties on the fatigue threshold and the stochasticity of fatigue crack growth, several tests are carried out.

This section describes how the experimental plan is designed, the methodology applied for the tests, the data analysis and the final results.

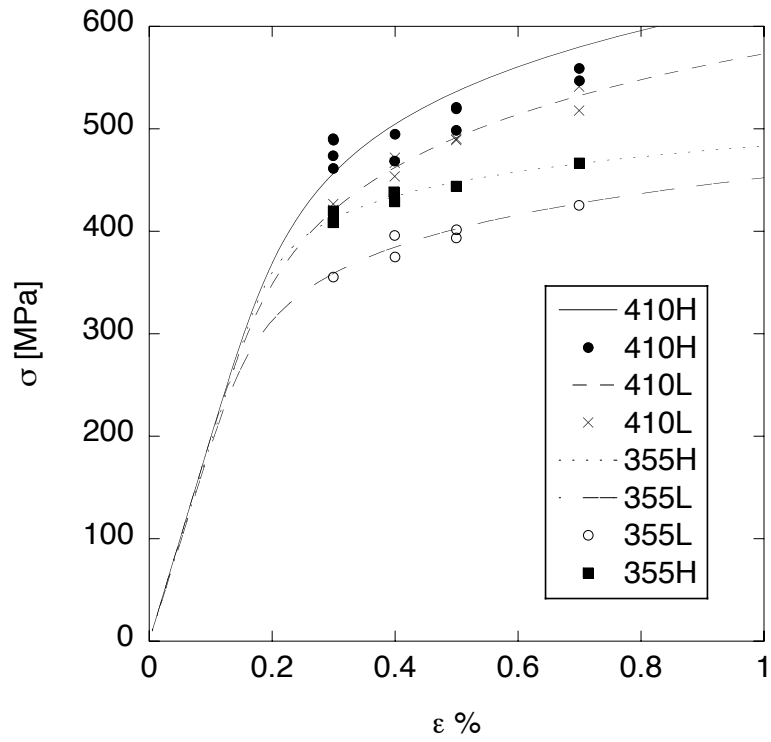


Figure 3.1: Ramberg-Osgood interpolation of the experimental data: stress  $\sigma$  versus strain  $\epsilon$



### 3. EXPERIMENTAL INVESTIGATION ON CRACK GROWTH AND THRESHOLD FOR STRUCTURAL STEELS

---

R	$\Delta$ [MPa $\sqrt{m}$ ]	$\sigma_{dev}$	$n_{replicates}$
0.1	0.4	0.22	4
0.3	0.4	0.22	4
0.7	0.2	0.05	1

**Table 3.6:** Number of replicates for experimental conditions

#### 3.3.1 Design of experiments

An experimental plan is designed with the aim of evaluating differences in the threshold of the four materials described in section 3.2 as well as its variability. Experimental conditions are defined by the material and the applied stress ratio  $R$ . The load ratio of interest for this work are positive and range from  $R = 0.1$  to  $R = 0.7$ .

The method of the operative characteristic curves (95) is used to assess the minimum sample size necessary to discern a significant difference in the experimental output. To this aim the following approximated equation is used:

$$n_{replicates} = \frac{(z_{\frac{\alpha}{2}} + z_{\beta})^2 \cdot \sigma_{dev}^2}{\Delta^2} \quad (3.3)$$

where  $\Delta$  is the quantity that has to be discerned, i.e. the minimum difference that is considered significant,  $\sigma_{dev}$  is the estimated standard deviation of the output quantity,  $z_{\frac{\alpha}{2}}$  and  $z_{\beta}$  are the normal standard variables corresponding to the value of the standard normal cumulative distribution function  $\frac{\alpha}{2}$  and  $\beta$  respectively, being  $\alpha$  the probability of type I error and  $\beta$  the probability of type II error (96),  $n_{replicates}$  is the number of necessary replicates. The required inputs for equation 3.3 are the expected standard deviation of the output,  $\sigma_{dev}$ , and the quantity to be discerned,  $\Delta$ .

The value of  $\sigma_{dev}$  is estimated analyzing a set of available data of fatigue threshold obtained previously on similar materials (22), applying the Fischer test (96). The value of  $\Delta$  is set evaluating a significant wall thickness reduction as a function of the fatigue threshold for non propagating conditions for the maximum design value of the stress, using available data for steel grade E355 SR. Table 3.6 shows the values of  $\Delta$ ,  $\sigma_{dev}$  and the estimation of  $n_{replicates}$ .

#### 3.3.2 Test method

Fatigue crack growth tests are carried out according to the standard ASTM E 647 (7) using single edge notched bend (SENB) specimens, obtained from tubes in direction L-C (longitudinal circumferential), produced according to the indication of the standard ASTM E399 (8).

Specimens are pre-cracked using the compression pre-cracking technique (48, 58, 107, 108, 143) . This technique consists in applying constant compressive load cycles in order to generate a naturally non-propagating closure-free crack very similar to natural cracks present in real structures, thus permitting to obtain more realistic threshold values. The length of the pre-crack is influenced by the extension of the monotonic plastic zone created by the stress amplitude of the first compression cycle (16, 18). Figure 3.2 shows a specimen mounted on a resonant test machine during pre-cracking. Figure 3.3 shows the inner surface of a tested specimen where pre-crack is marked with heat tinting. At the sample boundary, where plane stress conditions act, the monotonic plastic zone is larger, thus causing a larger pre-crack.

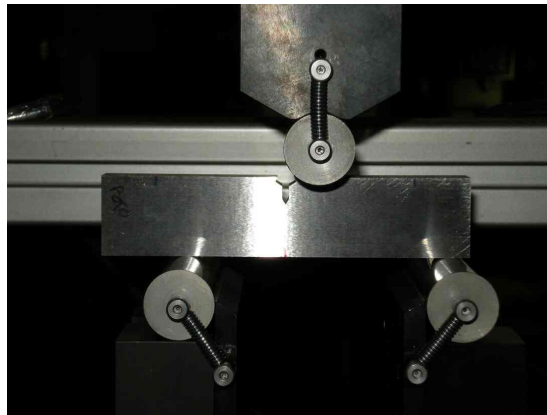


**Figure 3.2: Specimen mounted on a resonant test machine during pre-cracking**

The tests are carried out on a servo-hydraulic machine equipped with a 20 KN load cell and the crack length is assessed with the compliance method mounting a clip on gage.

Fatigue tests are carried either with the compression pre-cracking constant amplitude method (*CPCA*) or with the compression pre-cracking load reduction method (*CPLR*) (27). The first method is used to obtain the crack growth behavior from the

### 3. EXPERIMENTAL INVESTIGATION ON CRACK GROWTH AND THRESHOLD FOR STRUCTURAL STEELS

---

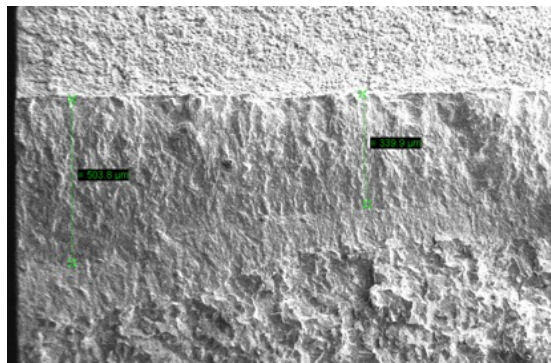


**Figure 3.3:** Inner surface of a tested specimen where precrack is marked with heat tinting. The precrack is larger at the sample boundary where plain stress conditions act.

near threshold region to the Paris region and requires a constant amplitude loading. The second method is applied to evaluate the fatigue threshold and requires both a constant amplitude loading phase as well as a load amplitude reduction phase. The  $\Delta K$  decreasing procedure in the CPLR test program is applied according to the indications reported in (7) in order to reach the fatigue threshold, which is defined as the value of applied  $\Delta K$  which causes a propagation rate of  $10^{-7} \text{ mm/cycle}$ . Figures 3.4 and 3.5 illustrate the two procedures.

Most of the tests are carried out at constant load ratio ( $R=0.1, 0.3$  and  $0.7$ ). Some constant  $K_{max}$  tests, starting from an initial value of the load ratio of  $R=0.7$ , are performed, with the aim of evaluating an additional reduction of the threshold in absence of closure.

The tests are carried out at three different laboratory, namely at *Tenaris Dalmine Research and Development laboratory (TD)*, at *Centro Sviluppo Materiali (CSM)* and at *Politecnico di Milano (PM)*. In order to check the consistency of the data obtained by the different laboratories, one test is carried out applying the same *CPCA* procedure on three samples of the same material in the three laboratories. Figure 3.6 shows that the three Paris curves obtained by the three laboratories are superimposed, thus confirming the consistency of the data.

Figures 3.7 and 3.8 show a specimen mounted on a servo-hydraulic test machine during the test at TenarisDalmine laboratory and at Politecnico di Milano, respectively.

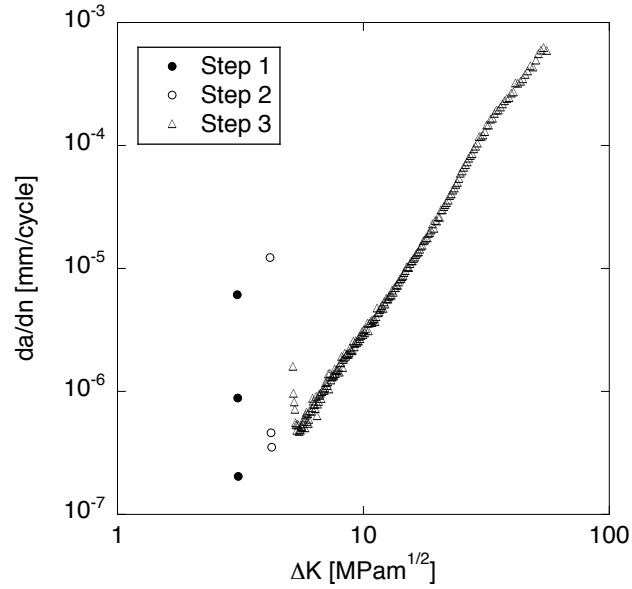


Figure 3.4: *CPCA* experimental procedure: the test is carried out at constant amplitude loading, increasing at each step the applied stress intensity factor until the crack starts growing.

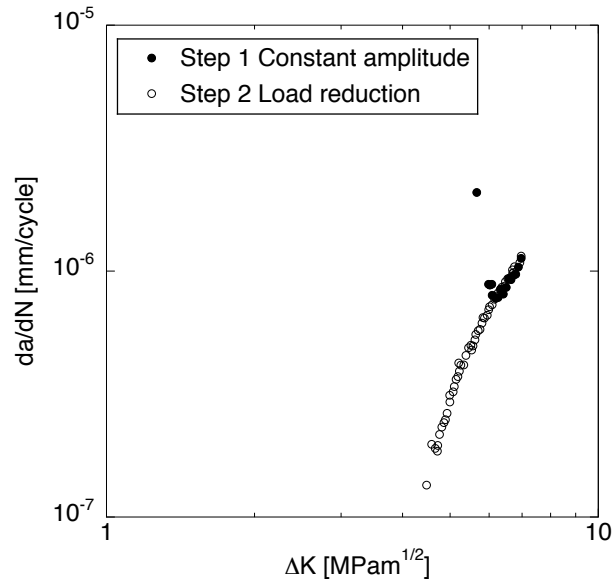
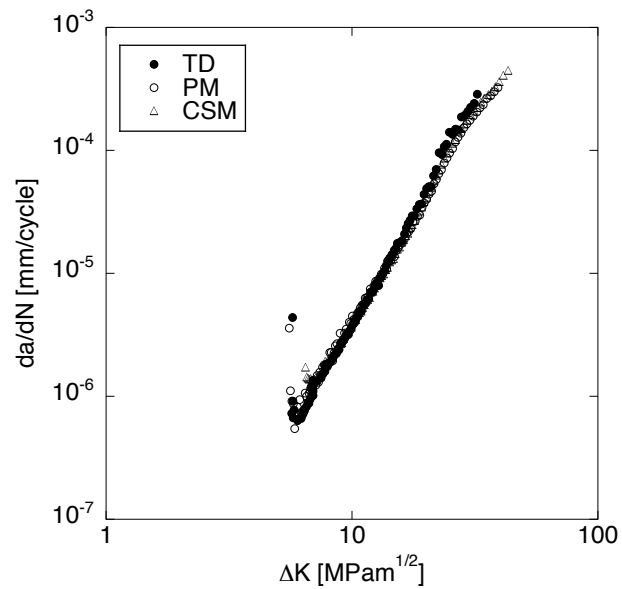


Figure 3.5: *CPLR* experimental procedure: in the first part a constant amplitude load is applied, then a  $\Delta K$  decreasing procedure.

### 3. EXPERIMENTAL INVESTIGATION ON CRACK GROWTH AND THRESHOLD FOR STRUCTURAL STEELS

---



**Figure 3.6:** Three Paris curves obtained applying the same test procedures by the three laboratories: *TenarisDalmine Research and Development laboratory (TD)*, *Centro Sviluppo Materiali (CSM)* and *Politecnico di Milano (PM)*. The data are superimposed.

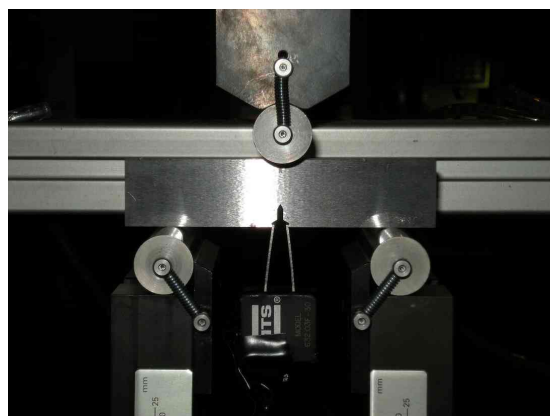


**Figure 3.7:** Specimen mounted on a servo-hydraulic test machine during the tests at TenarisDalmine laboratory.

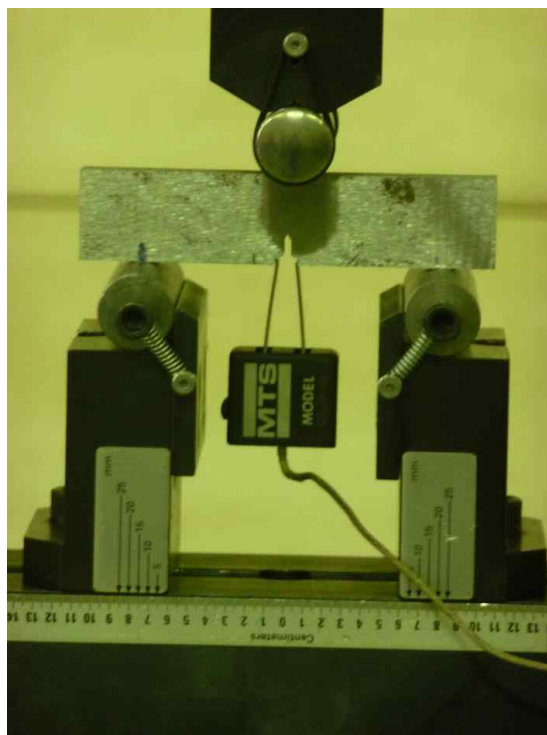


Figure 3.8: Specimen mounted on a servo-hydraulic test machine during the tests at Politecnico di Milano.

### 3. EXPERIMENTAL INVESTIGATION ON CRACK GROWTH AND THRESHOLD FOR STRUCTURAL STEELS

---

#### 3.3.3 Data analysis method

The experimental data are analyzed using the procedure described in the following.

- Raw data (crack length, number of cycles, maximum and minimum applied load) are analyzed and the crack growth curves in terms of  $da/dN$  versus  $\Delta K$  are extracted using the polynomial method suggested by ASTM E 647 (7).
- The fatigue threshold of each material is evaluated at various load ratio as the value of applied  $\Delta K$  which causes a propagation of  $10^{-7}mm/cycle$ , according to ASTM E 647 (7).
- Experimental data are fitted with the Nasgro equation (53) (46) (see Appendix B) using the least square method. First, the best fitting parameters for the relation of  $\Delta K_{th}$  versus  $R$  are obtained for each material, then the best fitting parameters for the relation between the fatigue crack growth rate,  $da/dN$  and  $\Delta K$  are evaluated. The opening stress, i.e. the effect of the plasticity induced crack closure is modeled using the McClung correction, which has been demonstrated to successfully correlate the crack opening stresses for various specimen geometries (87, 88, 89) (see section 4.5 and appendix B).

#### 3.3.4 Test results

Figure 3.9, 3.10, 3.11 and 3.12 show the experimental data for each material and the fitting with the Nasgro equation.

As can be observed in figures 3.9, 3.10, 3.11 and 3.12, the fatigue crack propagation curves rarely cross because tests, showing a low threshold value, tend to show high crack growth rates also in the Paris region. This behavior suggests that the stochasticity of the crack growth is mainly controlled by the variation of the threshold, since the threshold variation creates a fanning effect which reproduces the experimental observations. In other words, it can be stated that the dispersion of the threshold controls the dispersion of fatigue crack growth. For this reason, in the probabilistic model described in sections 5 and 6, the stochasticity of the crack growth is expressed describing the fatigue threshold as a random variable, and considering deterministic all the other parameters of the fatigue crack growth model.

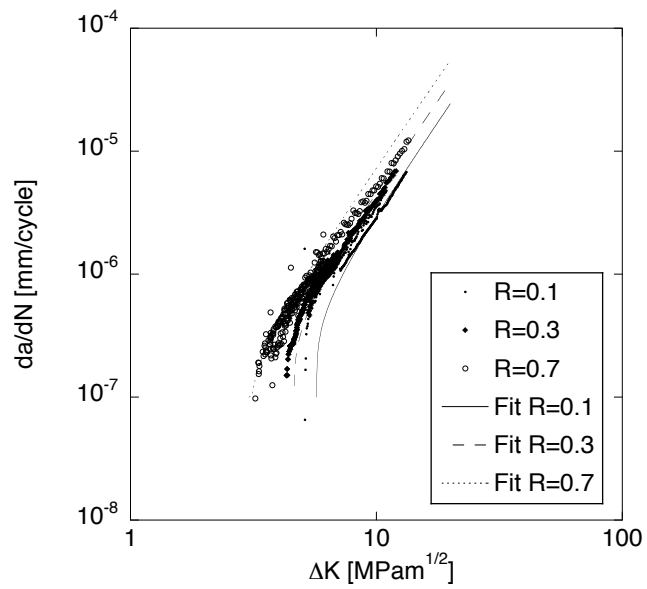


Figure 3.9: Fatigue crack growth experimental data for material 355L and the corresponding fitted Nasgro equation: fatigue crack growth rate  $\frac{da}{dN}$  versus the stress intensification factor range  $\Delta K$ .



### 3. EXPERIMENTAL INVESTIGATION ON CRACK GROWTH AND THRESHOLD FOR STRUCTURAL STEELS

---

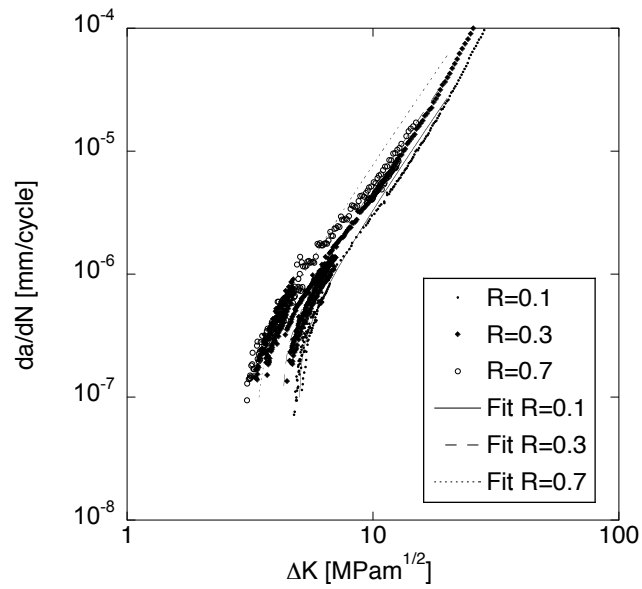


Figure 3.10: Fatigue crack growth experimental data for material 355H and the corresponding fitted Nasgro equation: fatigue crack growth rate  $\frac{da}{dN}$  versus the stress intensification factor range  $\Delta K$ .

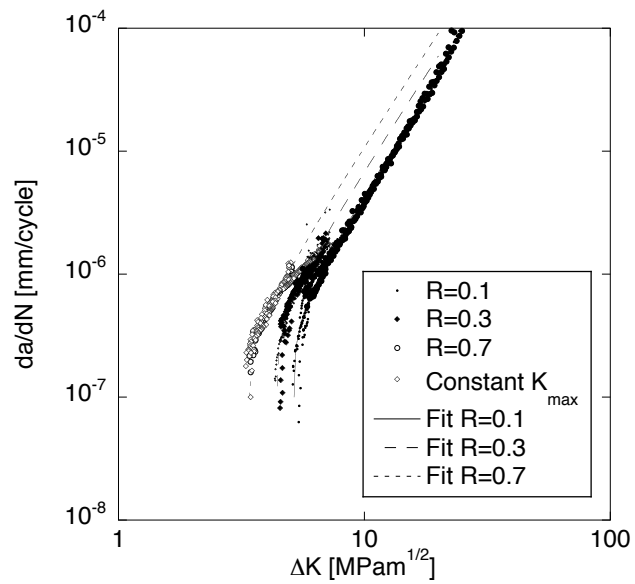


Figure 3.11: Fatigue crack growth experimental data for material 410L and the corresponding fitted Nasgro equation: fatigue crack growth rate  $\frac{da}{dN}$  versus the stress intensification factor range  $\Delta K$ .

### 3. EXPERIMENTAL INVESTIGATION ON CRACK GROWTH AND THRESHOLD FOR STRUCTURAL STEELS

---

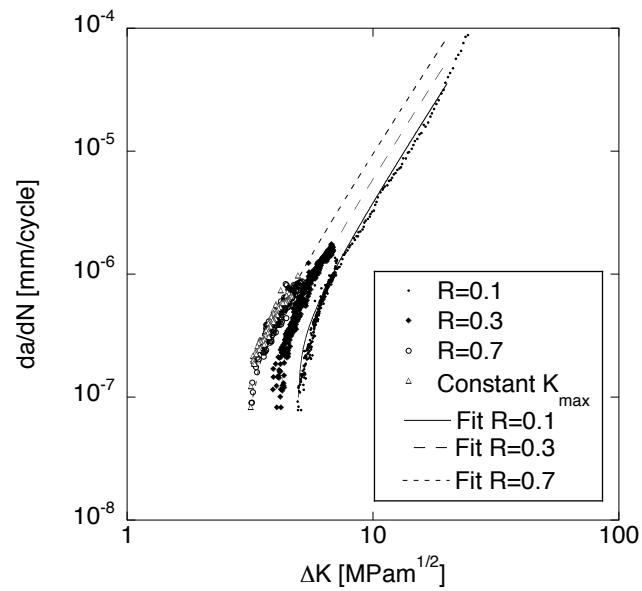
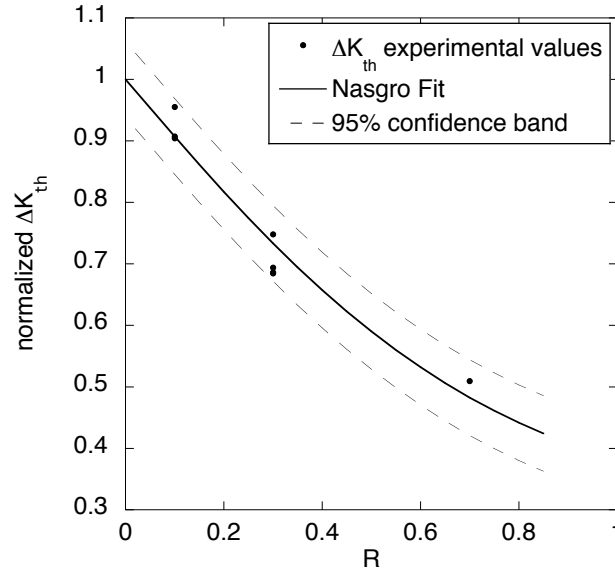


Figure 3.12: Fatigue crack growth experimental data for material E410H and the corresponding fitted Nasgro equation: fatigue crack growth rate  $\frac{da}{dN}$  versus the stress intensification factor range  $\Delta K$ .

### 3.4 Fatigue threshold statistical analysis

Figures 3.13, 3.14, 3.15 and 3.16 show the normalized fatigue threshold,  $\Delta K_{th}$ , versus the load ratio,  $R$ , for the four materials as well as the Nasgro fitting and the 95% confidence band. For confidentiality reasons, the values of  $\Delta K_{th}$  are normalized in respect to the fitted value of  $\Delta K_{th}$  at  $R = 0.1$  for material 355L. In all cases the Nasgro equation fits well the experimental data.



**Figure 3.13:** Normalized fatigue threshold experimental data for material 355L and the corresponding fitted Nasgro equation with its 95% confidence interval.

### 3.4 Fatigue threshold statistical analysis

The fatigue threshold experimental data are statistically analyzed with the aim of assessing differences in the variance or in the mean of the threshold of the four materials at the three load ratio applied during the experiments. The threshold of each material at a given load ratio is assumed normal distributed. Twelve groups of experimental data are considered, each containing the threshold data of a material at a given load ratio. The following statistical tests are applied:

- Bartlett's test to assess the equality of the variance (20) (137);
- One-way ANOVA and a multiple comparison procedure based on Tukey's test to assess the difference of the mean (11) (95).

### 3. EXPERIMENTAL INVESTIGATION ON CRACK GROWTH AND THRESHOLD FOR STRUCTURAL STEELS

---

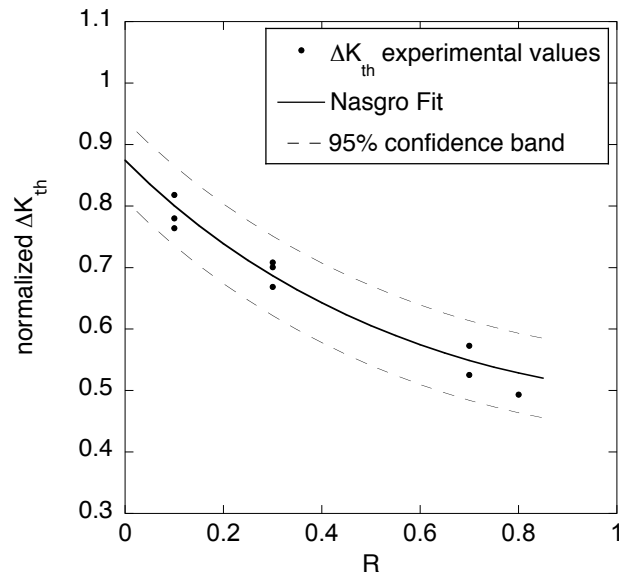


Figure 3.14: Normalized fatigue threshold experimental data for material 355H and the corresponding fitted Nasgro equation with its 95% confidence interval.

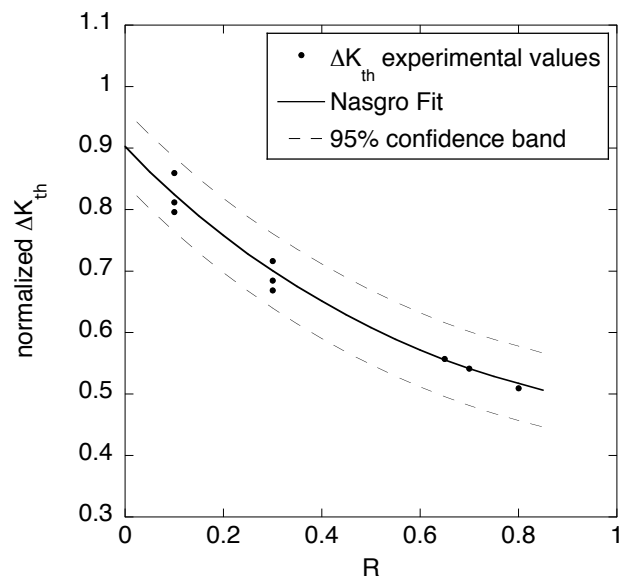
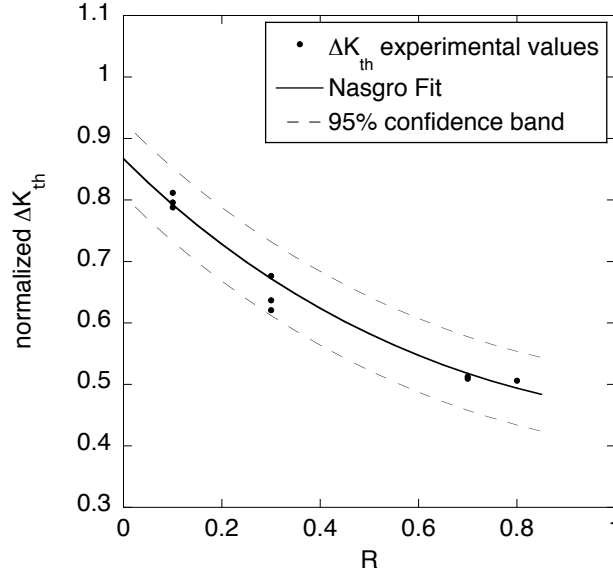


Figure 3.15: Normalized fatigue threshold experimental data for material 410L and the corresponding fitted Nasgro equation with its 95% confidence interval.



**Figure 3.16:** Normalized fatigue threshold experimental data for material 410H and the corresponding fitted Nasgro equation with its 95% confidence interval.

### 3.4.1 Equality of the variance

Bartlett’s test is used to assess if different sample set have identical variance, assuming that they are normal distributed. According to this test, all the threshold groups have the same standard deviation, namely  $0.17 \text{ MPa}\sqrt{m}$ , with a probability (p-value) of 0.83.

### 3.4.2 Equality of the mean

The one-way ANOVA tests the equality of the means of two or more samples containing mutually independent observations, assuming that i) all sample populations are normally distributed, ii) all sample populations have equal variance, iii) all observations are mutually independent. Table 3.7 shows the results of the ANOVA, reporting the probability (p-value) that the samples have the same mean for each of the three values of the applied load ratio. The data at  $R=0.1$  are unlikely to have the same mean, while the likelihood increases for  $R=0.3$  and for  $R=0.7$ .

The multiple comparison procedure, permits to evaluate which material shows a different threshold than the others at the same load ratio. Figure 3.17 shows the

### 3. EXPERIMENTAL INVESTIGATION ON CRACK GROWTH AND THRESHOLD FOR STRUCTURAL STEELS

R	p-value
0.1	$9.66 \cdot 10^{-4}$
0.3	$8.89 \cdot 10^{-2}$
0.7	$1.11 \cdot 10^{-1}$

**Table 3.7:** ANOVA: probability that the samples at R=0.1, R=0.3 and R=0.7 have the same mean

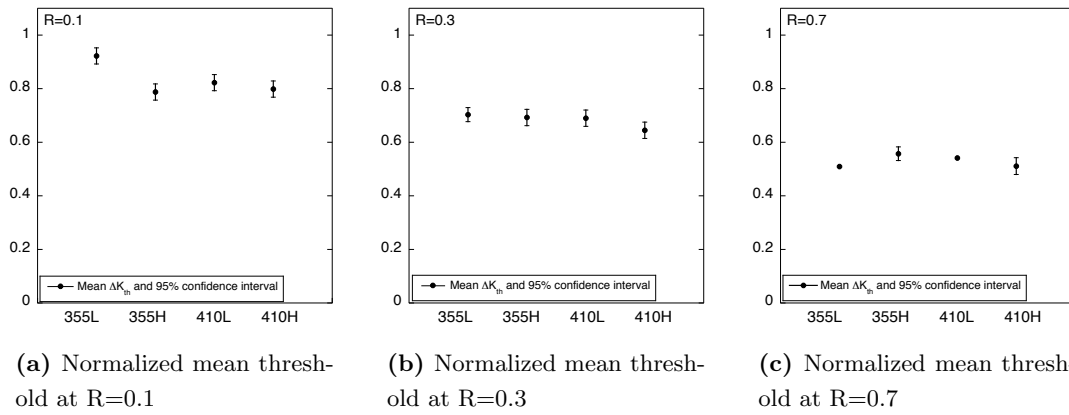


**Figure 3.17:** Multiple comparison procedure: the normalized mean values of the threshold and its 95% confidence interval for each load ratio for the four investigated materials.

normalized mean values of the threshold and their 95% confidence interval for each material at each load ratio.

According to ANOVA and the multiple comparison procedure it can be stated that:

- at R=0.1 material 355L has a different threshold than the other materials.
- at R=0.3 and R=0.7 no statistically significant difference in the threshold of the four materials can be stated, even if material 410H at R=0.3 is likely to have a lower threshold than the others. As explained in appendix A, when the load ratio increases, the threshold tends to reach its asymptotic intrinsic value in absence of closure. Since the closure level is proportional to the load ratio and to the microstructural domain size, considering that material 410H has the smallest characteristic microstructural dimension,  $D$ , it is reasonable to infer that its threshold decreases faster than that of the other materials as the load ratio increases.

## 3.5 Crack paths, crack closure and microstructure in the threshold region

### 3.4.3 Pooled data analysis

Based on the results obtained in the previous analysis of the separate groups, the pooled data are analyzed in order to assess their normality, to evaluate the significant difference of the threshold at  $R = 0.1$  and to evaluate the pooled standard deviation.

Assuming that at  $R=0.1$  the fatigue thresholds of material 355H, 410L and 410H are from the same population, and that at  $R=0.3$  and at  $R=0.7$  the data of all materials are from the same population, the statistical analysis is accomplished as follows:

- the Lilliefors test (77) is applied to evaluate the normality of the population, considering that the test can be applied to a minimum group of four data. In all cases the normality of the data is confirmed with a 99% significance level.
- applying a z-test (96) to the pooled data, it can be stated that the difference between the threshold of E355L and the other materials at  $R=0.1$  is  $0.5 \text{ MPa}\sqrt{m}$  with a 95% significance level. At  $R \geq 0.3$  no difference in the mean fatigue threshold of the four materials can be detected.
- applying the Bartlett's test on the pooled data, the standard deviation of the groups appears to be the same and it is equal to  $0.2 \text{ MPa}\sqrt{m}$ .

According to the statistical analysis on the pooled fatigue threshold data, the material mechanical and microstructural properties in the explored range do not influence significantly the fatigue threshold, except in the case of one material, which shows a higher threshold than the others and offers therefore more conservative conditions. Therefore, considering that most of the fatigue life is spent in the near threshold region, they are also not expected to exert a significant influence on the reliability.

## 3.5 Crack paths, crack closure and microstructure in the threshold region

With the aim of investigating the relation between fatigue crack growth and microstructure for the chosen materials, the crack paths are observed using the optical microscope.

Crack branching and tortuosity are caused by the microstructural features that the crack encounters while it grows, while second phase particles or inhomogeneities may



### 3. EXPERIMENTAL INVESTIGATION ON CRACK GROWTH AND THRESHOLD FOR STRUCTURAL STEELS

---

stop the crack propagation (75) and (149). The observation of crack paths offers an insight in the fatigue behavior of the materials, connecting the experimental threshold data with the microstructural characteristics. Samples of each material tested at each load ratio, subjected to the load reduction, namely  $\Delta K$  decreasing test procedure, are polished and etched in order to observe the crack paths. The main remarks related to the observations of the crack paths are the following:

- Material 355L, which has a low yield strength, shows crack deviations and branching along the entire crack path at any load ratio (see figure 3.18).
- Material 355H and 410L show also crack deviations, especially at  $R = 0.1$  and  $R = 0.3$ , but branching in this case is absent (figure 3.19);
- Crack paths of materials 355L, 355H and 410L show deviations located most of the times at grain boundaries and cracks mainly stop at grain boundaries or at pearlite islands (figure 3.20);
- Material 410H, having a bainitic structure, shows path deviations at  $R=0.1$ , while at higher load ratio values, the path seems not to be influenced by the microstructure (see figure 3.21).

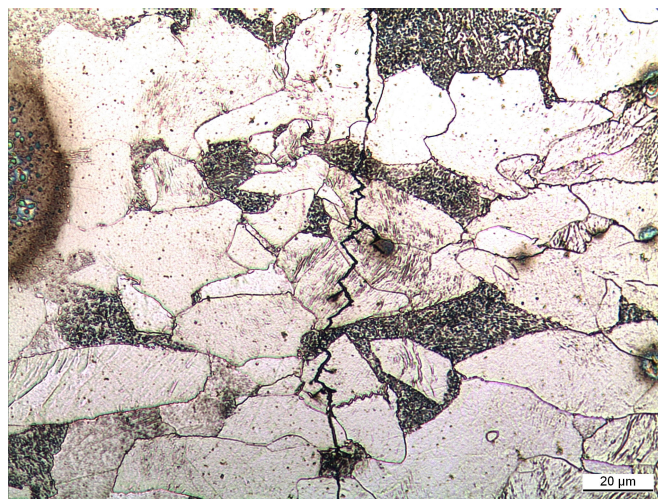


**Figure 3.18: Crack path observed with the optical microscopy: deviations and branching (material 355L).**

### 3.5 Crack paths, crack closure and microstructure in the threshold region

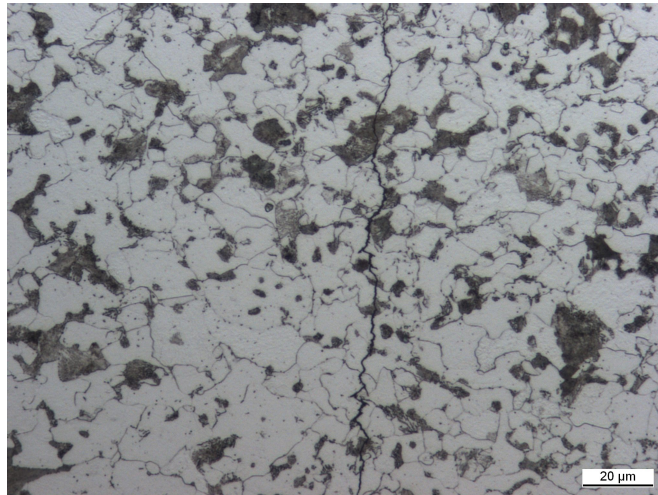


Figure 3.19: Crack path observed with the optical microscopy: deviations are evident (material 410L)

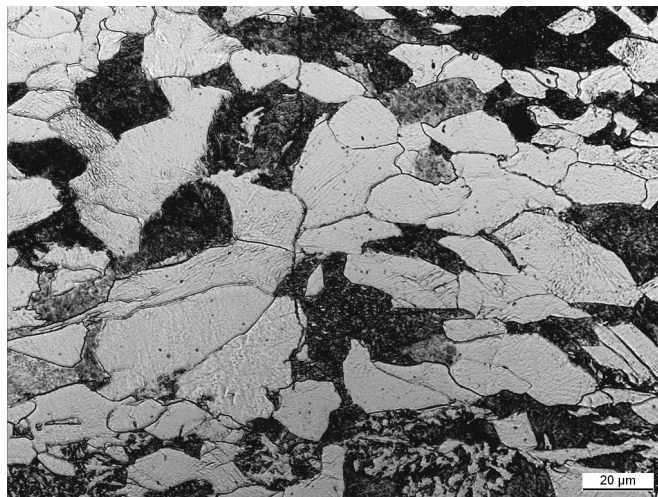
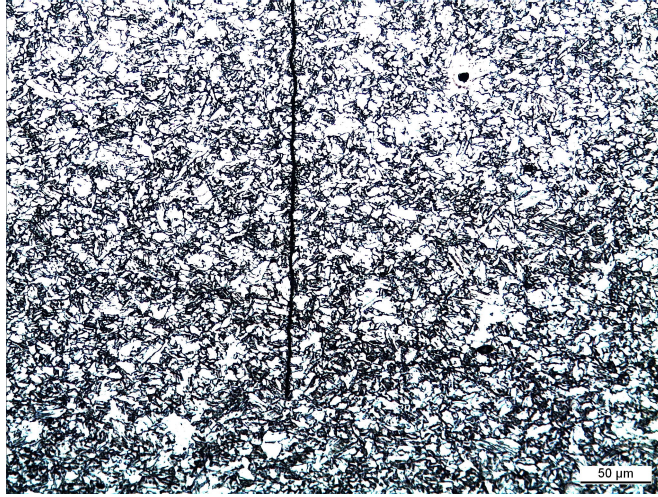


Figure 3.20: Crack path observed with the optical microscopy arresting at a pearlite island (material 355H).

### 3. EXPERIMENTAL INVESTIGATION ON CRACK GROWTH AND THRESHOLD FOR STRUCTURAL STEELS

---



**Figure 3.21: Crack path observed with the optical microscopy: no influence of the microstructure (material 410H).**

These observations suggest that crack paths are more easily subjected to the influence of the microstructural features in low yield materials, when branching and deviations are more often observed. Cracks in high yield strength structures are less affected by the microstructural features.

### 3.6 Discussion

The results shown in figures 3.9, 3.10, 3.11 and 3.12 show that the stochasticity of the crack growth requires the application of a random variable model, while a model based purely on a random process approach would be insufficient (see considerations on probabilistic fatigue crack growth in sections 2.5). Similar considerations can be done observing figures 3.13, 3.14, 3.15 and 3.16.

A random variable description of the threshold combined with a proper model for the closure, which describes the dependence of the fatigue threshold with the stress ratio, allows an exhaustive description of the fatigue crack growth behavior. The dependence of the fatigue threshold on the stress ratio can be well fitted using the Nasgro model and expressing the plasticity induced closure as a function of  $\frac{k_{max}}{k_{flow}}$  (see Appendix B), where  $k_{flow}$  is expressed as a function of the cyclic yield strength. This approach has already been implemented in (32), where it has been successfully applied to describe the experimental data related to fatigue threshold of small and long cracks.

These experimental observations are the starting point for the fatigue crack growth model algorithm presented in section 4.5 and for the random variable definition described in section 5.3.

## 3.7 Concluding remarks

In this chapter the influence of the material properties on the fatigue threshold and the stochastic fatigue crack growth behavior of four different materials are investigated by performing several fatigue crack growth tests.

According to the statistical analysis on the fatigue threshold data, the material mechanical and microstructural properties in the explored range exert a moderate influence on the fatigue threshold at low stress ratio, while at higher stress ratio no significant difference between the fatigue threshold of the investigated materials can be detected.

The fatigue crack growth tests provide evidence that the stochasticity of the crack growth is mainly controlled by the dispersion of the threshold. For this reason in the probabilistic models for fatigue crack growth described in section 5 and 6, the only parameter of the crack growth equation assumed as a random variable is the threshold. The threshold variation with the stress ratio can be well modeled by using the cyclic yield strength to describe the plasticity induced closure. Based on experimental evidence, the overall fatigue crack growth behavior at various load ratio can be successfully described applying the Nasgro model for the fatigue crack growth and for the threshold, randomizing the threshold and describing the closure as a function of the cyclic yield stress.

The observation of the crack paths provides an insight on the interaction between microstructure and crack growth in the near threshold region: crack paths are more easily subjected to the influence of the microstructural features in low yield materials, while cracks in high yield strength structures are less affected by the microstructural features.

### **3. EXPERIMENTAL INVESTIGATION ON CRACK GROWTH AND THRESHOLD FOR STRUCTURAL STEELS**

---

## 4

# Case study: description of the adopted models

### 4.1 Introduction

When dealing with reliability of components subjected to variable amplitude fatigue loading, the following input models are necessary:

- a model for initial crack size, if initial cracks are present, alternatively a model for the crack nucleation;
- a structural integrity model to evaluate the stress intensity factor at the crack tip;
- failure criteria and the corresponding limit state functions;
- a fatigue crack growth equation;
- a model for the variable amplitude fatigue load;
- a probabilistic model for the reliability evaluation.

This section introduces the case studied in this work and is dedicated to the description of the models used in the reliability evaluation reported in the following. The adopted models of the load are not described here, but separately in sections 5 and 6.

## 4. CASE STUDY: DESCRIPTION OF THE ADOPTED MODELS

### 4.2 Case study

This work focuses on tubular components and the case studied addresses tubes for hydraulic cylinders produced from cold drawn seamless steel tubes. These tubes are subjected to cyclic variable amplitude internal pressure during their service life. The manufacturing process introduces some imperfections on the external surface of the tubes, from which cracks may grow.

Based on experimental observations described in section 5.2, surface flaws are modeled as shallow semi-elliptical surface imperfections, characterized by the depth,  $a$ , and the semi-length,  $c$  (13, 15).

Figure 4.1 shows a sketch of a pipe containing a semi-elliptical surface flaw subjected to internal pressure.

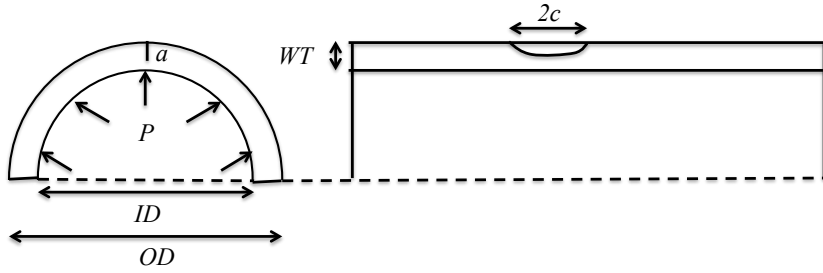


**Figure 4.1: Transversal and longitudinal sections of the tube subjected to internal pressure,  $P$ . On the external surface an initial flaw characterized by the depth  $a$  and the semi-length  $c$  is present. The geometry of the tube is defined by the outer diameter,  $OD$ , the wall thickness,  $WT$ , and the inner diameter,  $ID$ .**

### 4.3 Model for the pre-existing flaws distribution and POD model

In the application considered in this case study, pre-existing surface imperfections due to the manufacturing process are assumed to be present on the tubes' surface and their initial depth is modeled as a random variable for the purpose of reliability evaluation. The distribution of pre-existing flaws' depth,  $f'(a_0)$ , is determined during an experimental activity, described in section 5.2 and published in (13). The depth of initial

surface imperfections,  $a_0$ , on tubular components is limited by application of non destructive tests (NDT). Therefore the probability of detection,  $POD$  (see 2.2.1), is taken into account and it is modeled as a lognormal cumulative distribution function (166) (60), as reported in equations 4.1, 4.2 and 4.3:

$$POD(a_0) = \Phi\left(\frac{\ln(a_0) - \theta}{\rho}\right) \quad (4.1)$$

$$\rho^2 = \ln\left[1 + \left(\frac{\sigma_{POD}}{\mu_{POD}}\right)^2\right] \quad (4.2)$$

$$\theta = \ln(\mu_{POD}) - \frac{1}{2}\rho^2 \quad (4.3)$$

where  $\theta$  and  $\rho$  are the parameters of the lognormal distribution, related to the mean,  $\mu_{POD}$ , and the standard deviation,  $\sigma_{POD}$ , according to equations 4.2 and 4.3.

## 4.4 Structural integrity model

Two structural integrity models are implemented, with the aim of evaluating the applied stress intensity factor for surface semi-elliptical flaws during fatigue loading. In the first model, the hoop stress is assumed constant through the cylinder wall and the stress intensity factor is evaluated according to the solution for a semi-elliptical surface crack in a flat plate (16, 106). In the second model, the membrane and the bending components of the stress are taken into account and the stress intensity factor is evaluated according to the solution for external semi-elliptical surface cracks in cylindrical vessels (69).

The solution for a semi-elliptical surface crack in a flat plate offers conservative though reasonable results, is easier to implement and requires less computational time. For this reason, it is applied in the reliability evaluations presented in sections 5 and 6. In the following, the equations for the two models are reported.

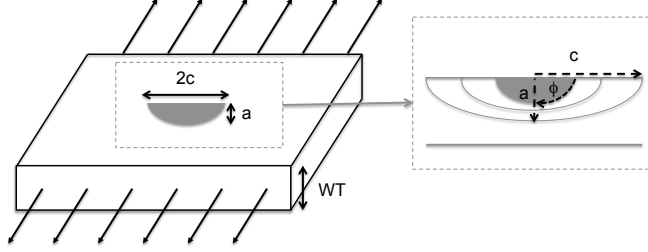
### 4.4.1 Semi-elliptical surface cracks in flat plates

Figure 4.2 shows a scheme of the model of a semi-elliptical surface crack in a flat plate.

The stress is considered constant along the wall thickness according to the approximated equation of the hoop stress for a thin-walled cylinder subjected to internal



#### 4. CASE STUDY: DESCRIPTION OF THE ADOPTED MODELS



**Figure 4.2: Scheme of the model of a semi-elliptical surface crack in a flat plate: membrane stress  $\sigma_m$  and bi-dimensional fatigue crack growth.**

pressure (33)

$$\sigma = \frac{P \cdot ID}{2 \cdot WT} \quad (4.4)$$

where  $P$  is the internal pressure,  $ID$  and  $WT$  are the internal diameter and the wall thickness of the tube. The stress intensity factor,  $K$ , is calculated as (16):

$$K = \beta_x \cdot \sigma \cdot \sqrt{\pi a} \quad (4.5)$$

where  $\beta$  is the boundary correction factor,  $\sigma$  is the applied stress,  $a$  is the crack depth and  $c$  is the crack semi-length. The boundary correction factor is obtained according to the stress intensity solution for a semi-elliptical surface crack in a flat plate (106), and it is a function of various geometrical parameters:

$$\beta_x = f\left(\frac{a}{c}, \frac{a}{WT}, \frac{c}{L}, \phi\right) \quad (4.6)$$

where  $L$  is the length of the component,  $\phi$  is a parametric angle equal to 0 degrees when referred the  $c$  direction, equal to 90 degrees when referred to the  $a$  direction.

#### 4.4.2 Semi-elliptical external surface cracks in thick tubes

This model considers the membrane and the bending components of the stress. The hoop stress throughout the tube wall is evaluated with the equation for thick-walled cylinders subjected to internal pressure (33):

$$\sigma(r) = \frac{P \cdot R_i^2}{R_o^2 - R_i^2} - \frac{R_i^2 \cdot R_o^2 \cdot P}{r^2 \cdot (R_o^2 - R_i^2)} \quad (4.7)$$

where  $R_o$  and  $R_i$  are the outer and the inner radius respectively,  $r$  is the radius, ranging from  $R_i$  to  $R_o$ ,  $P$  is the internal pressure. The value of the external pressure is

## 4.5 Fatigue crack growth algorithm and Nasgro equation

---

assumed equal to zero. The membrane and the bending stress components, indicated as  $\sigma_m$  and  $\sigma_b$  respectively, are obtained as:

$$\sigma_m = \frac{\sigma_{max} + \sigma_{min}}{2} \quad (4.8)$$

$$\sigma_b = \frac{\sigma_{max} - \sigma_{min}}{2} \quad (4.9)$$

where the maximum value of the stress is obtained on the inner surface,  $\sigma_{max} = \sigma(ID/2)$ , and the minimum value on the outer surface,  $\sigma_{min} = \sigma(OD/2)$ .

The applied stress intensity factor is evaluated according to the solution reported in (69) for external semi-elliptical surface cracks in cylindrical vessels:

$$K = \sqrt{\pi a} \sum_{i=0}^3 \sigma_i f_i\left(\frac{a}{WT}, \frac{2c}{a}, \frac{R_i}{WT}\right) \quad (4.10)$$

where the stress components,  $\sigma_i$ , are determined by fitting the stress as:

$$\sigma(u) = \sum_{i=0}^3 \sigma_i \left(\frac{u}{a}\right)^i \quad 0 < u < a \quad (4.11)$$

The functions  $f_i$  are given in (69) for the stress intensity factor in direction of  $a$  and of  $c$ .

## 4.5 Fatigue crack growth algorithm and Nasgro equation

The fatigue crack growth algorithm is implemented according to the general two-dimensional model with variable amplitude loading described in section 2.4.2.4.

The Forman-Mettu model (46), otherwise called Nasgro equation (47, 53) is used. According to this model, the threshold as a function of the load ratio  $R = \frac{K_{min}}{K_{max}}$  ( $K_{max}$  and  $K_{min}$  are the maximum and the minimum stress intensity factors in a fatigue cycle) is expressed as:

$$\Delta K_{th,R} = \frac{\Delta K_{th,0}}{\left[ \frac{1-f}{(1-A_0)(1-R)} \right]^{1+C_{th}R}} \quad (4.12)$$

where  $\Delta K_{th,0}$  is the fatigue threshold range at  $R = 0$ ,  $C_{th}$  is a fitted model parameter,  $A_0$  is a function of the maximum stress and of the constraint (see equation B.3 in appendix B) and  $f$  is the Newman's crack opening function, accounting for the plasticity induced crack closure using the Newman model (103), originally defined as

## 4. CASE STUDY: DESCRIPTION OF THE ADOPTED MODELS

---

$f = \frac{\sigma_o}{\sigma_{max}}$ , where  $\sigma_o$  is the crack opening stress. Based on the experimental observations chapter 3, the effect of the plasticity induced crack closure is modeled using the McClung correction (87), which has been demonstrated to successfully correlate the crack opening stresses for various specimen geometries (see also section 3.6 and (32)).

The fatigue crack growth rate is expressed as:

$$h_x = \frac{dx}{dn} = C \left[ \left( \frac{1-f}{1-R} \right) \Delta K \right]^m \cdot \frac{\left( 1 - \frac{\Delta K_{th,R}}{\Delta K} \right)^p}{\left( 1 - \frac{K_{max}}{K_{mat}} \right)^q} \quad (4.13)$$

where  $x$  is the crack length, either  $a$  or  $c$ ,  $n$  is the number of cycles,  $R$  is the load ratio,  $C$ ,  $m$ ,  $p$  and  $q$  are fitting parameters,  $\Delta K$  is the range of the stress intensity factor,  $\Delta K_{th,R}$  is the fatigue threshold at load ratio  $R$ , defined in equation 4.12,  $K_{max} = \frac{\Delta K}{(1-R)}$  is the maximum stress intensity factor,  $K_{mat}$  is the fracture toughness of the material.

Further details on the model and the numerical values used in this work can be found in appendix B.

## 4.6 Failure evaluation

### 4.6.1 Failure criteria

Two failure criteria are considered (see also section 2.6.2):

1. leakage, i. e. stable crack growth until the crack depth reaches a critical crack size (critical crack size failure, *CCSF*);
2. crack driving force failure condition (*CDF*) i.e. when the applied crack driving force exceeds the fracture resistance of the material (165), which accounts for both plastic collapse and unstable crack growth.

The *CDF* assessment is implemented according to the indications reported in (165). The criterion is based on the evaluation of the ligament yielding factor

$$L_r = \frac{\sigma_{ref}}{YS} \quad (4.14)$$

where  $\sigma_{ref}$  is the so called *reference stress* and  $YS$  is the yield stress.

Failure by plastic collapse is encountered when  $L_r \geq L_{rmax}$ , where  $L_{rmax}$  is the plastic collapse limit:

$$L_{rmax} = \frac{YS + UTS}{2 \cdot R_{el}} \quad (4.15)$$

where  $UTS$  indicates the ultimate tensile stress and  $R_{el}$  is the elastic limit.

Unstable crack growth is encountered when  $J \geq J_{mat}$ , where

$$J = J_e \cdot f(L_r)^{-2} \quad (4.16)$$

$$J_e = \frac{K_{a,max}^2}{E(1 - \nu^2)} \quad (4.17)$$

$$J_{mat} = \frac{K_{mat}^2}{(1 - \nu^2)} \quad (4.18)$$

with  $J$  the J-integral,  $J_e$  the elastic component of  $J$ ,  $K_{a,max}$  the highest value of  $K$  in direction  $a$  during a stress cycle,  $E$  the elastic modulus and  $\nu$  the Poisson's ratio,  $K_{mat}$  the fracture toughness of the material in terms of  $K$  and  $J_{mat}$  the corresponding fracture toughness in terms of  $J$ .

The expression for  $f(L_r)$  is the following

$$f(L_r) = (1 + 0.5L_r^2)^{-0.5} [0.3 + 0.7 \cdot \exp(-\mu L_r^6)] \quad 0 \leq L_r \leq 1 \quad (4.19)$$

$$f(L_r) = f(L_r = 1) \cdot L_r^{\frac{n-1}{2n}} \quad 1 \leq L_r \leq L_{rmax} \quad (4.20)$$

where

$$\mu = \min\left[\frac{0.001E}{YS}; 0.6\right] \quad (4.21)$$

$$n = 0.3\left(1 - \frac{YS}{UTS}\right) \quad (4.22)$$

When considering semi-elliptical surface cracks in flat plates,  $L_r$  is evaluated according to (165) as:

$$L_r = \frac{\sigma}{(1 - \zeta) \cdot YS} \quad (4.23)$$

$$\zeta = \frac{a \cdot c}{WT(c + WT)} \quad (4.24)$$

Being the expression for  $\zeta$  valid only when the length of the component,  $L$ , is larger than  $WT + c$  ( $WT$  is the pipe's wall thickness).

When considering external semi-elliptical surface cracks in thick tubes,  $L_r$  is evaluated as (69):

$$L_r = \frac{\sigma_r}{YS} = \frac{g(\zeta) \frac{\sigma_b}{3} + \sqrt{g^2(\zeta) \frac{\sigma_b^2}{9} + (1 - \zeta)^2 \sigma_m^2}}{(1 - \zeta)^2 YS} \quad (4.25)$$

## 4. CASE STUDY: DESCRIPTION OF THE ADOPTED MODELS

---

$$g(\zeta) = (1 - 20\zeta^3) \left(\frac{a}{2c}\right)^{0.75} \quad (4.26)$$

where  $\zeta$  is defined in equation 4.24,  $\sigma_b$  and  $\sigma_m$  are the bending and membrane components of the stress, respectively.

### 4.6.2 Proposed algorithm for the evaluation of the limit state function

In the previous section 2.6.2 the limit state function for fatigue crack growth is defined according to equation 2.36. In practice, the direct evaluation of the limit state function according to this equation can lead to numerical problems. In particular, the number of cycles to failure  $N_{fail}(X)$  can become very large or even infinite if the fatigue threshold  $\Delta K_{th}$  is never exceeded. To remediate these numerical problems, it is often convenient to modify the formulation to:

$$g(X) = \{min[N_{fail,1}(X), N_{fail,2}(X), N_{fail,3}(X), N_{stop}] - N\} \cdot \{1 - min[0, (\Delta K_{max} - \Delta K_{th})]\} \quad (4.27)$$

which can be rewritten as:

$$g(X) = \{N_{min} - N\} \cdot \{1 - min[0, (\Delta K_{max} - \Delta K_{th})]\} \quad (4.28)$$

Here  $N_{stop}$  is the maximum number of cycles up to which the fatigue crack growth is evaluated. Obviously, it must be  $N_{stop} > N$ .  $\Delta K_{max}$  is the maximum stress intensity factor in  $N_{stop}$  cycles and  $\Delta K_{th}$  is the fatigue threshold. When using the mean approximation (paragraph 2.4.2.3 and 2.4.2.4),  $\Delta K_{max}$  and  $\Delta K_{th}$  are replaced by their expected values  $E_{\{\Delta\sigma\}\{R\}}[\Delta K_{max}]$  and  $E_{\{\Delta\sigma\}\{R\}}[\Delta K_{th}]$ .

The term  $\{1 - min[0, (\Delta K_{max} - \Delta K_{th})]\}$  accounts for the possibility that the fatigue threshold  $\Delta K_{th}$  is never exceeded and the crack does not propagate. The term has value 1 if crack propagation occurs, and a value larger than 1 when no crack propagation occurs. The term  $(\Delta K_{max} - \Delta K_{th})$  ensures that the limit state function is not constant in the non-propagation case, which is relevant for avoiding numerical problems in structural reliability methods.

Figure 4.3 shows a sketch of the function  $g(X)$ , defined according to equations 4.27. It is worth noticing that when propagation occurs the function  $g(X)$  is not continuous,

but it is defined at steps of  $b$  cycles, with  $b$  the length of the blocks used to carry out the fatigue crack growth evaluation (see section 2.4.2.4).

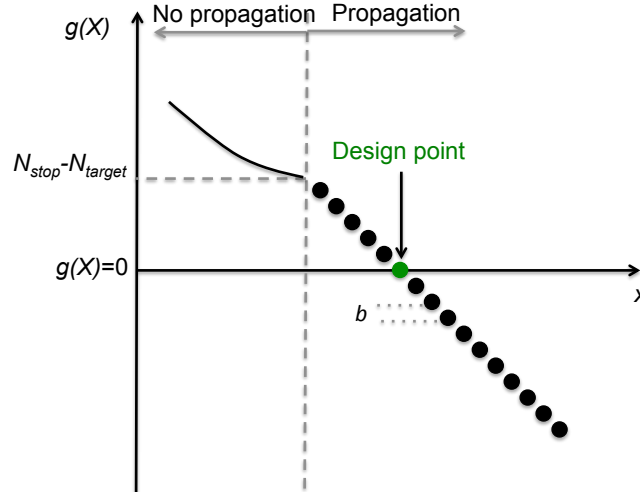


**Figure 4.3:** 2-D Sketch of the limit state function  $g(X)$  defined according to equation 4.27.  $g(X)$  is plotted against one generic component of the vector  $X$  of the input random variables, exemplarily assuming that increasing  $x$  increases the probability of failure.

Figure 4.4 shows a scheme of the different cases that can be encountered when evaluating the crack propagation and the failure conditions: no propagation, propagation without failure, failure by leakage or by the crack driving force condition.

In the flow chart of figure 4.5, an algorithm for evaluating  $N_{min}$  (equations 4.27 and 4.28) is shown. This algorithm applies the block approximation of section 2.4.2.4 for two-dimensional crack growth evaluation under variable amplitude loading.

## 4.7 Verification

The crack growth algorithm evaluation and the failure criteria is tested using the commercial software AFGROW (12) and full scale tests data on tubes with artificial notches of 0.3 mm depth obtained by electro discharge machining (EDM) (32) tested at  $R = 0.1$ . The integration of equations 4.13 for the two crack growth directions,  $a$  and  $c$ , is done using blocks of  $b = 10^4$  number of cycles. Figure 4.6a shows the results obtained using the model of a centre semi-elliptical surface flaw on a plate subjected to pure tension stress. Figure 4.6b shows the results obtained using the model of an external

#### 4. CASE STUDY: DESCRIPTION OF THE ADOPTED MODELS

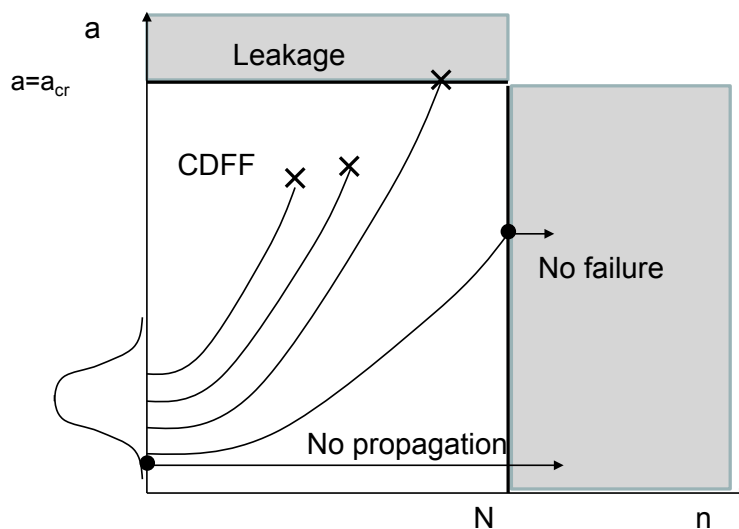


**Figure 4.4:** Scheme of the different cases that can be encountered when evaluating the crack propagation and of the possible failure conditions: no propagation, propagation without failure in  $N$  cycles, failure by leakage (*CCSF*) or by the crack driving force condition (*CDDF*).

semi-elliptical surface flaw on a thick pipe.

The life prediction obtained with the crack growth model and with AFGROW are in good agreement in both cases. The model of a semi-elliptical surface flaw in a flat plate subjected to uniform stress offers more conservative predictions than the thick pipe model. Additionally, the former model permits to achieve faster computational times, being  $\beta_x$  (equation 4.6) expressed analytically, while the latter model requires the numerical interpolation of multi-variables geometry numerical functions to obtain the appropriate values of the weight functions  $f_i$ , (equation 4.10). The life prediction obtained with the crack growth model are also in good agreement with the full scale tests. In all cases the predicted curve is within the 90% scatter band of the experimental data. The model of a semi-elliptical surface crack in a thick pipe (figure 4.6b) delivers a slightly unconservative prediction, which can be justified by the fact that the model assumes that initial surface flaws behave like long crack, and does not consider any nucleation time. The model of a semi-elliptical surface crack in a flat plate (figure 4.6a) offers reasonable conservative results.

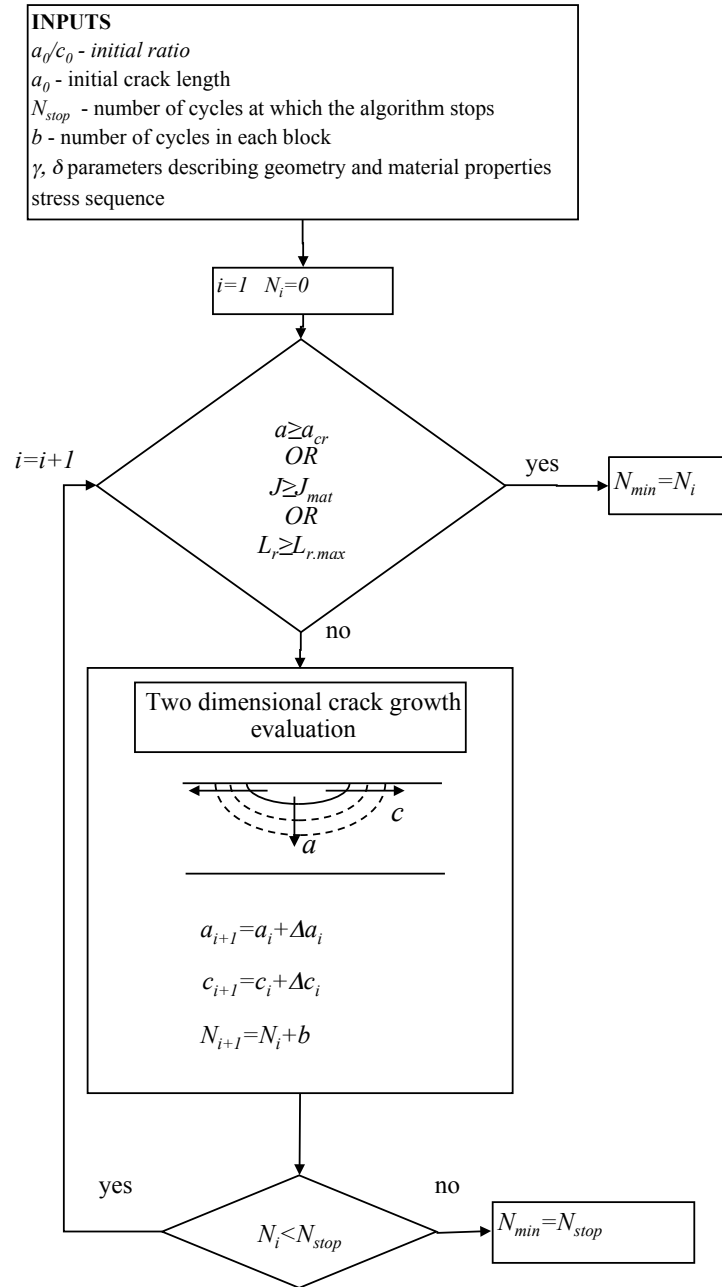
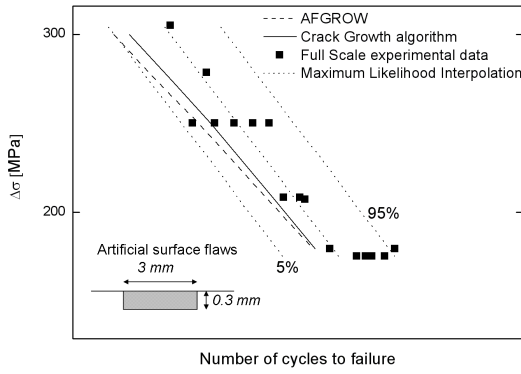


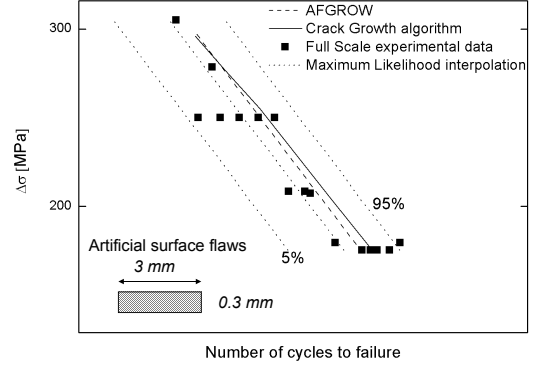
**Figure 4.5:** Flow chart of the algorithm used to calculate the number of cycles to failure,  $N_{fail}$ , necessary for the evaluation of the limit state function. The failure criteria are implemented according to equations 2.30 and 2.31. The crack growth is evaluated according to equations 2.6 and 2.7



## 4. CASE STUDY: DESCRIPTION OF THE ADOPTED MODELS



(a) Semi-elliptical surface crack in a flat plate



(b) Semi-elliptical surface crack in a thick pipe

**Figure 4.6:** Full scale test data (32) (cylinders with 0.3 mm EDM notches ) with their maximum likelihood interpolation and its 90% scatter band compared with the present crack growth model prediction and AFGROW evaluation (13). For confidentiality reasons no quantitative data concerning the number of cycles to failure can be disclosed.

### 4.8 Probabilistic model

The probabilistic models presented in this study are based on the experimental observation that undetected surface flaws below the NDT threshold can grow under fatigue loads, spending most of their life in the near threshold region, in which the fatigue crack growth has a stochastic behavior. The models evaluate the crack growth under variable amplitude loading using the previously described algorithm for the evaluation of the limit state functions (section 4.6.2).

Being the case studies focused on tubes for hydraulic cylinders, which are components having a moderate length (1 to 3 m on average), the average number of imperfections present in a component must also be taken into consideration when calculating the probability of failure. In the case study herein presented experimental data show that not all components contain a flaw, as the density of surface flaws is small compared to the average surface of a hydraulic cylinder. Therefore the probability of a flaw to be present in the component must be considered in order to avoid an overestimation of the probability of failure. Thus, the final probability of failure,  $P_f$  has to be calculated

according to equation 4.29:

$$P_f = Pr\{F|flaw\} \cdot Pr\{flaw\} + Pr\{F|noflaw\} \cdot Pr\{noflaw\} \quad (4.29)$$

where  $Pr\{flaw\}$  and  $Pr\{noflaw\}$  are respectively the probability of having a flaw in a components or not;  $Pr\{F|flaw\}$  and  $Pr\{F|noflaw\}$  are the probability of failure respectively when a flaw is present or absent.

The distribution of the flaw size is experimentally obtained. In section 5.2) the experimental results are derscribed and it is demonstrated that the flaw size does not depend on the tube dimension. No inference regarding the surface flaw density are given. For the sake of simplicity, in the following numerical calculations it is assumed  $Pr\{F|noflaw\} = 0$  and  $Pr\{flaw\} = 1$ . Being actually  $Pr\{flaw\} < 1$ , the the results are conservative. T

## 4.9 Validity and limits of the models

Two main assumptions are formulated when establishing the input models for the reliability evaluation. One is the existence of initial surface flaws behaving like long cracks. This hypothesis is reasonable and conservative. It permits to neglect the cracks nucleation phase and the short crack behavior. The other main assumption is the absence of retardation effects due to overloads and other load interaction effects. This hypothesis permits to simplify the fatigue crack growth model and it is reasonable as long as high cycle fatigue is considered and as long as the the stress can be described with a stationary ergodic random process. In the case for example of a constant stress sequence with sporadic overloads, the retardation effects should not be neglected.

## 4.10 Concluding remarks

The fatigue crack growth presented in this chapter is based on the Forman-Mettu model and on the fatigue crack growth experiments presented in chapter 3. The algorithm predicts successfully the full scale experimental results and its prediction corresponds to the AFGROW commercial software prediction.

The proposed algorithm for the evaluation of the limit state function considers three different failure criteria according to the most state of the art assessment method for

#### **4. CASE STUDY: DESCRIPTION OF THE ADOPTED MODELS**

structure containing flaws. The limit state function for a finite fatigue life is smartly built: it is always finite and monotonic in respect to each variable. These features avoid numerical problems when the failure domain is explored.

The proposed fatigue crack growth algorithm as well as the limit state function defining the failure domain are key requirements for the reliability evaluation presented later in this work. Their innovative implementation represents a distinct and unique feature of the reliability evaluation methods developed in this study, because they permit to take into account any kind of randomly generated stress sequence and uses a comprehensive and validate fatigue crack growth model as well as a state of the art failure evaluation approach.

## 5

# Fracture mechanics based fatigue reliability under variable amplitude loading: random variable approach

## 5.1 Introduction

Manufacturing process, service conditions and material properties are factors to be considered when designing structural components subjected to fatigue. Exemplarily, in this work tubular components, produced according to the standard EN10305-1 (9) and EN10297-1 (3) are considered. For these products, non-destructive tests (NDT) are optional and their flaw acceptance level is at the discretion of the manufacturer. Typically, values between 0.3 mm and 10 percent of the wall thickness (10% WT) are adopted as NDT threshold value. The case study analyzes tubular components used for the hydraulic cylinders application. During their service life, they are subjected to variable amplitude internal pressure and no inspections are planned. Therefore, the distribution of initial flaws, the applied service loads, the material fracture toughness, the fatigue threshold and the characteristic crack growth curve are key parameters to be considered for a safe design.

This chapter proposes a reliability assessment method implemented with a random variable approach and with a fracture mechanics based fatigue crack growth model,

## 5. FRACTURE MECHANICS BASED FATIGUE RELIABILITY UNDER VARIABLE AMPLITUDE LOADING: RANDOM VARIABLE APPROACH

---

which is used to investigate the influence of simplified approaches on the reliability evaluation, assessing the most important factors influencing the prediction of fatigue life under variable amplitude loads .

The random variable approach takes into account the stochasticity of the fatigue crack growth, randomizing the fatigue threshold according to the experimental data presented in paragraph 3.3.4, and the fracture toughness variability (see paragraph 3.2.2.3). The random variable approach is used also to describe the variability of the initial flaw depth, the distribution of which is evaluated with the experimental activity presented in the first part of this section.

The case study herein tackled is based on service stress measurements of hydraulic cylinders of earthmoving machines (paragraph 5.4).

### 5.2 Experimental assessment of the distribution of initial surface flaws depth

Some imperfections may be present on the surface of cold drawn tubes due to the manufacturing process. Their maximum depth is limited by the threshold of non-destructive tests. According to experimental observations, there are two different populations of surface discontinuities: one having a characteristic depth of one order of magnitude lower than the NDT threshold, as shown in figure 5.1, another having a characteristic depth of the same order of magnitude as the non-destructive tests threshold. Flaws with a depth of the same order of magnitude of the NDT threshold can be detrimental for the behavior of tubes subjected to fatigue, since they are able to propagate, although their depth is smaller than the NDT threshold. Figure 5.2a shows a flaw on the surface of a tube, figure 5.2b shows a scanning electron microscopy (SEM) image of a longitudinal section of a surface flaw of depth of approximately  $150\mu m$ .

#### 5.2.1 Methodology

With the aim of assessing the statistical distribution of the largest initial surface flaws, an extensive experimental activity on cold drawn and stress relieved tubes (15) produced according to (9) (3), is carried out. Tubes previously subjected to eddy current NDT with a threshold set at 5% of the wall thickness are inspected using magnetic powder. The length of detected flaws is measured using a pocket rule, as shown in

## 5.2 Experimental assessment of the distribution of initial surface flaws depth

---

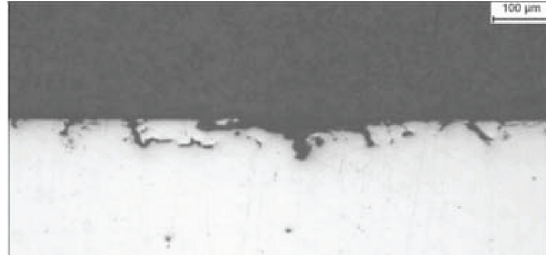
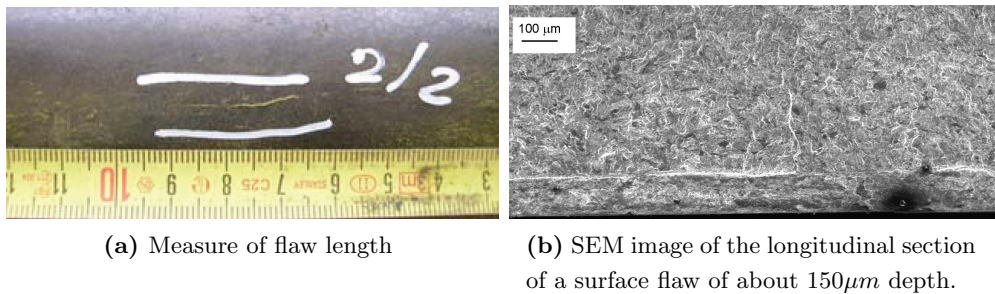


**Figure 5.1:** SEM image of the longitudinal section of micro-defects (13).



(a) Measure of flaw length

(b) SEM image of the longitudinal section of a surface flaw of about  $150\mu m$  depth.

**Figure 5.2:** Surface flaws of the same order of magnitude as the NDT threshold (13).

figure 5.2a, while their depth is measured with a micrometer gauge after grinding the surface of the tube and measuring the depth of the ground surface.

The experimental data are analyzed with the aim of assessing whether different data sets can be described with the same distribution. The parameters of each data set are estimated with the maximum likelihood method. Then the simultaneous confidence interval test and the likelihood ratio test are applied to the data (101, 102). Finally, the parameters are also estimated for the set of the pooled data.

### 5.2.2 Experimental results

Several tubes from seven production batches, with different diameter and wall thickness, are inspected, the total examined surface is  $363m^2$ . Table 5.1 summarizes the geometry of the tubes from each examined batch as well as the total examined surface.

Some tubes do not contain any flaw detectable with magnetic particles, while some contain more than one. All examined surface discontinuities have a ratio  $\frac{a}{c}$  ( $a$  is the flaw's depth and  $c$  is the flaw's semi-length) lower than 0.1, which means they are long and shallow longitudinal flaws, having a shape similar to a semi-ellipse.

## 5. FRACTURE MECHANICS BASED FATIGUE RELIABILITY UNDER VARIABLE AMPLITUDE LOADING: RANDOM VARIABLE APPROACH

---

lot #	OD [mm]	WT [mm]	Examined surface [m <sup>2</sup> ]
1	125	12.5	86
2	130	15	33
3	150	10	63
4	185	12.5	48
5	160	12.5	63
6	185	17.5	42
7	225	17.5	28
Total			363

**Table 5.1:** Geometry of the inspected tubes.

As suggested by (34), the depths of flaws are usually described with a Weibull or a lognormal distribution. Figure 5.3 shows the lognormal, the Weibull and the largest extreme value distribution (LEVD) probability papers of lots 1, 2 and 3, which have a sufficiently large number of samples, as well as the probability paper of the pooled data, in which the flaw depth is expressed as percentage of the tubes wall thickness. A LEVD distribution, the cumulative distribution function of which is reported in equation 5.1, is chosen to describe the depth of surface flaws, since it is the most suitable to experimental data, according to the Kolgomorov-Smirnov test (52). Its CDF is:

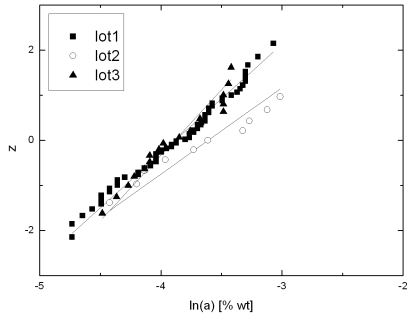
$$F(a) = \exp \left[ -\exp \left( -\frac{a - \lambda}{\delta} \right) \right] \quad (5.1)$$

The simultaneous confidence interval test (96) is applied in order to evaluate the dependence of the LEVD maximum value estimates of  $\lambda$  and  $\delta$  on the tube wall thickness or diameter. Figure 5.4 shows the simultaneous confidence interval test, where  $\lambda$  and  $\delta$  are normalized with respect to the pooled data best fitting  $\bar{\lambda}$  and  $\bar{\delta}$ . The confidence intervals overlap and no dependence of the parameters  $\lambda$  and  $\delta$  on the batch or on the tubes outer diameter and wall thickness is observed. Therefore, flaws from different batches can be described with the same parameters  $\bar{\lambda}$  and  $\bar{\delta}$ .

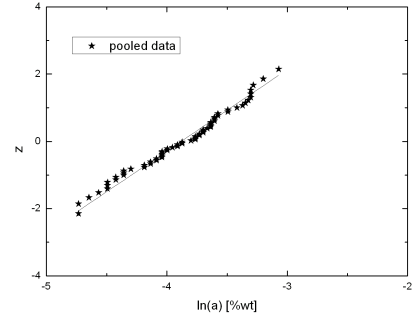
Alternatively the maximum likelihood ratio test is used to assess the equality of the parameters  $\lambda$  and  $\delta$  for the batches 1, 2 and 3. The same conclusions as above are obtained.

## 5.2 Experimental assessment of the distribution of initial surface flaws depth

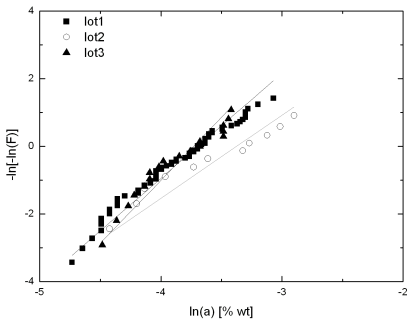
---



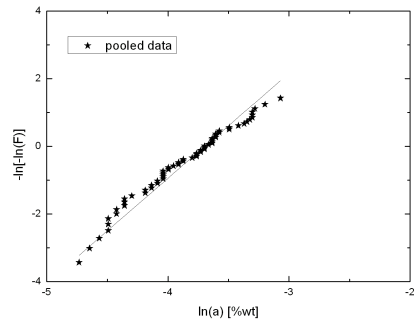
(a) Lognormal probability paper for lots 1, 2, 3



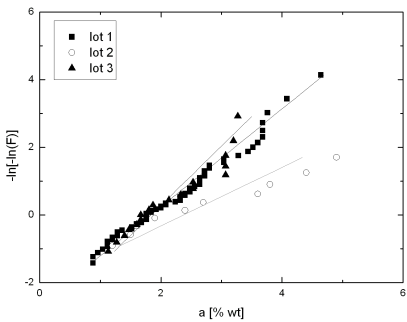
(b) Lognormal probability paper for the pooled data



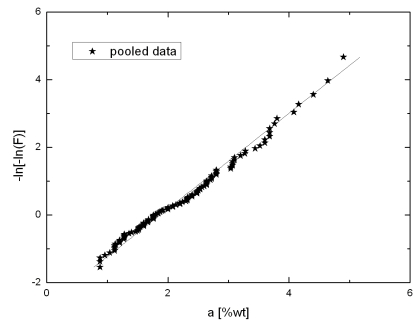
(c) Weibull probability paper for lots 1, 2, 3



(d) Weibull probability paper for the pooled data



(e) LEVD probability paper for lots 1, 2, 3



(f) LEVD probability paper for the pooled data

**Figure 5.3:** Lognormal, Weibull and LEVD probability papers of the crack depth,  $a$ , expressed as percentage of tube wall thickness (for confidentiality reasons no absolute values can be disclosed) (13).



## 5. FRACTURE MECHANICS BASED FATIGUE RELIABILITY UNDER VARIABLE AMPLITUDE LOADING: RANDOM VARIABLE APPROACH

---

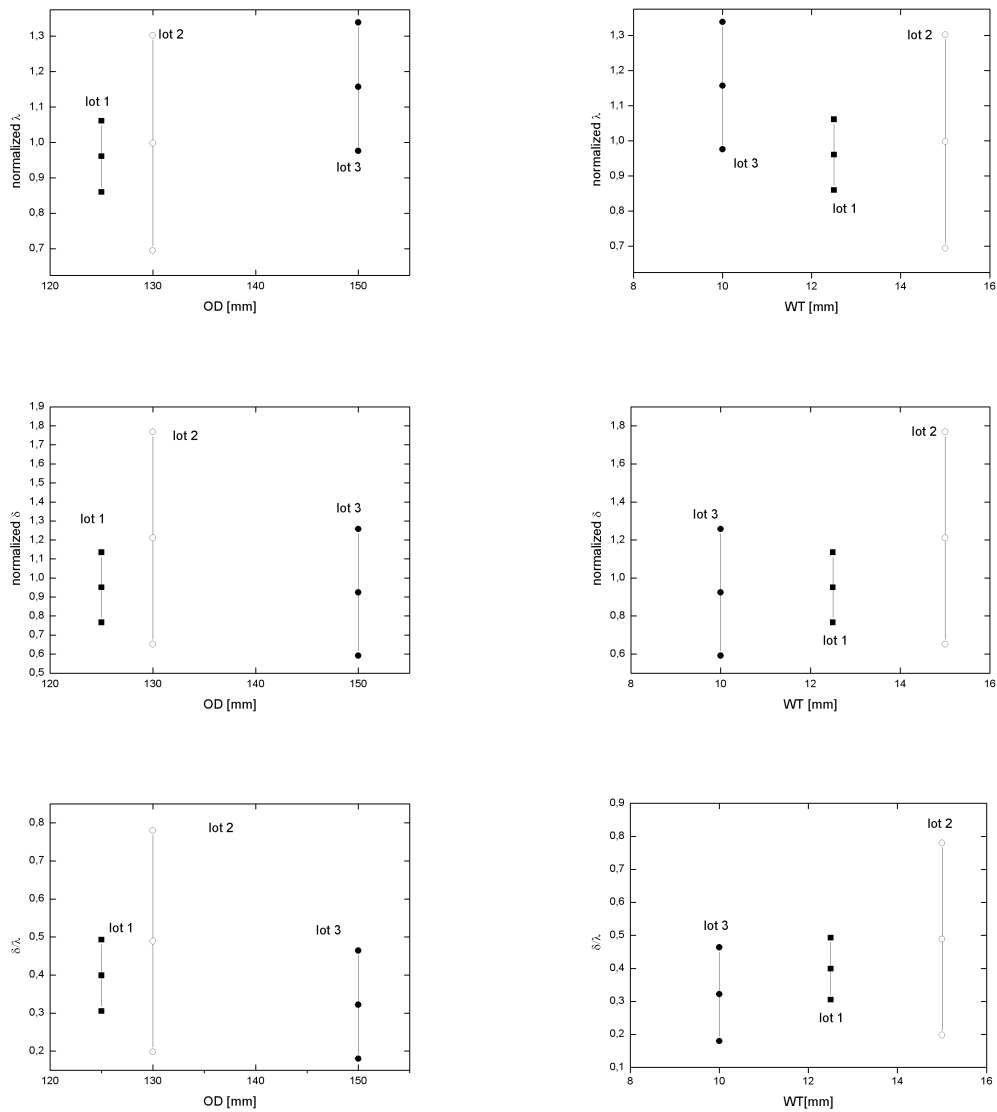


**Figure 5.4:** Simultaneous confidence interval tests:  $\frac{\lambda}{\lambda}$ ,  $\frac{\delta}{\delta}$  and  $\frac{\lambda}{\delta}$  versus outer diameter and wall thickness (13).

### 5.3 Reliability assessment method

The reliability assessment method presented in this section is based on the definition of the limit state function given in 2.6.1 and on the corresponding algorithm for its evaluation described in 4.6.2, in which  $N_{stop} = N$ , that is the fatigue crack growth is evaluated for a number of cycles correspondent to the service life. The latin hypercube Monte Carlo method (see paragraph 2.7.1) is used for the evaluation of the probability of failure, given the probabilistic model described in 4.8.

The fatigue crack growth is assessed according to the procedures indicated in paragraphs 2.4.2.4 and 4.5, given a stress sequence extracted randomly from its spectrum (see further paragraph 5.4.1). The Nasgro equation is applied (see section 4.5), which parameters are deduced from the experimental results presented in paragraph 3 and are available in appendix B.

Three random variables are considered in the model: the initial flaw's depth,  $a_0$ , the fatigue threshold,  $\Delta K_{th,0}$ , and the material fracture toughness,  $K_{mat}$ .

The distribution of initial flaw's depth is experimentally obtained, as described in section 5.2. According to experimental observations, surface flaws are modeled as shallow semi-elliptical surface imperfections, characterized by the depth,  $a$ , and the semi-length,  $c$ . The initial value of the ratio  $\frac{a}{c}$  is assumed fixed and equal to 0.1. The probability of detection and the posterior flaw distribution are modeled as described in section 4.3. Figure 5.5 shows an example of the probability density function before,  $f'(a_0)$ , and after,  $f''(a_0)$ , the non-destructive tests as well as the curve of the probability of detection of the NDT, where  $\mu_{POD}$  is fixed at 5% WT.

$K_{mat}$  is modeled with a Weibull distribution, as described in section 3.2.2.3.

$\Delta K_{th,0}$  is a normal distributed random variable (23) since, according to the experimental data presented in chapter 3. The dispersion of propagation lifetimes appears to be controlled by the dispersion of the threshold and the uncertainty in the fatigue crack growth rate can be described by the uncertainty in the threshold (see comments in paragraphs 3.3.4). Notice that according to the experimental data on the investigated materials the fatigue threshold has a smaller coefficient of variation than the other random variables.

The structural integrity model of a semi-elliptical surface crack in a flat plate subjected to tension loading is used (see section 4.4.1), since it delivers more conservative

## 5. FRACTURE MECHANICS BASED FATIGUE RELIABILITY UNDER VARIABLE AMPLITUDE LOADING: RANDOM VARIABLE APPROACH

---

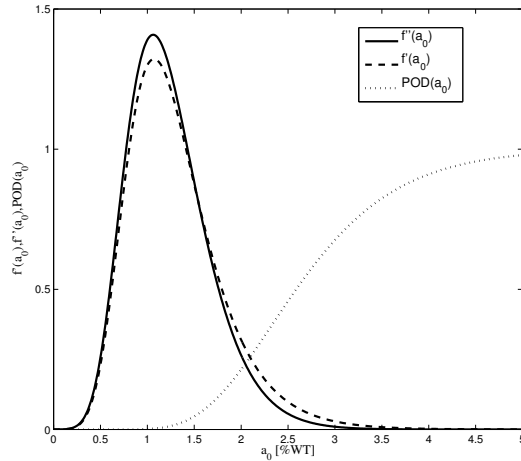


**Figure 5.5:**  $f'(a_0)$ ,  $f''(a_0)$  and  $POD(a_0)$ , where  $a_0$  is expressed as percentage of the tube wall thickness (for confidentiality reason no quantitative information can be disclosed) (13).

results and permits to achieve faster computational times (section 4.7). This model can be applied, assuming that the crack growth evaluation and the failure criteria verified in section 4.7 are valid also in cases of variable amplitude loads.

### 5.4 Case Study

The case study presented in this section is related to tubular components for hydraulic cylinders, produced from cold drawn tubes made of the material 355H (see chapter 3 and appendix B for the details on material's properties).

#### 5.4.1 Service stress measurements

Stress measurements are conducted on excavators' hydraulic cylinders to estimate service stress spectra. Selected histories are joined and extrapolated to 360 working hours. The Peak Over Threshold method is used to extrapolate these histories (113). Stress spectra extrapolated with the Rainflow method (10) from experimental measurements are shown in figure 5.6.

Assuming that a cylinder has a service life of 20.000 hours (8 hours per day, for 250 days a year for 10 years), the corresponding service life,  $N$ , is obtained for each loading

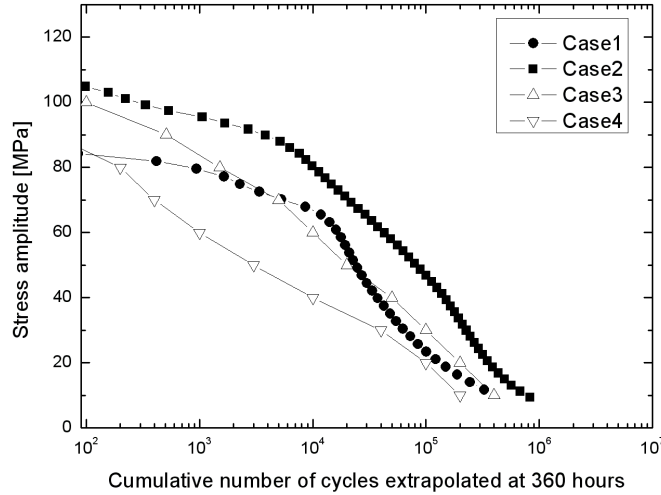


**Figure 5.6:** Stress spectra measured on earth moving machines extrapolated to 360 working hours (13).

	Case 1	Case 2	Case 3	Case 4
Service	Stone loading & soil digging		Soil digging	
$\Delta\sigma_{max}$ [MPa]	84	138	110	100
$N$	$1.8 \cdot 10^7$	$4.6 \cdot 10^7$	$2 \cdot 10^7$	$1.1 \cdot 10^7$

**Table 5.2:** Case studies of service stress measurements

condition. Table 5.2 summarizes the kind of service, the maximum applied stress range,  $\Delta\sigma_{max}$  and the service life,  $N$ , for each spectrum presented in figure 5.6.

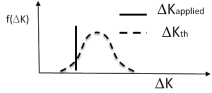
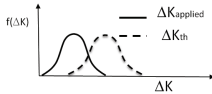
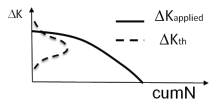
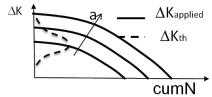
#### 5.4.2 Approaches for the evaluation of the probability of failure

The probability of failure for the four stress cases described in table 5.2 is evaluated using the following approaches:

- A simplified semi-probabilistic approach, assuming a fixed initial flaw depth equal to 5%WT, which is a common NDT acceptance level, and assuming that the condition for failure is the propagation of the initial flaw. Referring to the algorithm for the evaluation of the limit state function in section 4.6.2, this corresponds to setting  $N = \infty$ .

## 5. FRACTURE MECHANICS BASED FATIGUE RELIABILITY UNDER VARIABLE AMPLITUDE LOADING: RANDOM VARIABLE APPROACH

---

Approach	Scheme	Initial flaw	Failure condition
a) Simplified semi-probabilistic model		5% WT	Crack propagation
b) Simplified probabilistic model		LEVD distributed	Crack propagation
c) Semi-probabilistic model with crack propagation		5% WT	$N_{min} < N$
d) Probabilistic model		LEVD distributed	$N_{min} < N$

**Figure 5.7:** Approaches adopted to evaluate the probability of failure (13).

- b. A simplified probabilistic approach, considering randomly distributed initial flaws and assuming that the condition for failure is the propagation of the initial flaw ( $N = \infty$ ).
- c. A semi-probabilistic approach, assuming a fixed initial flaw depth equal to 5%WT, evaluating the crack growth with the algorithm described in section 4.5, the condition for failure with the limit state function given in equation 2.33 and the algorithm described in section 4.6.2.
- d. A fully probabilistic approach, considering randomly distributed initial flaws, evaluating the condition for failure with the algorithm described in section 4.6.2.

Summarizing, the failure condition for approaches *a* and *b* is the propagation of the initial flaw, while the failure condition for approaches *c* and *d* is the leakage or the failure by crack driving force condition before  $N$  cycles.

Figure 5.7 summarizes the approaches adopted to evaluate the probability of failure.

### 5.4.3 Results and discussion

Figure 5.8 shows the results evaluated for the four cases described in table 5.2 using the approaches described in paragraph 5.4.2. The probability of failure is evaluated

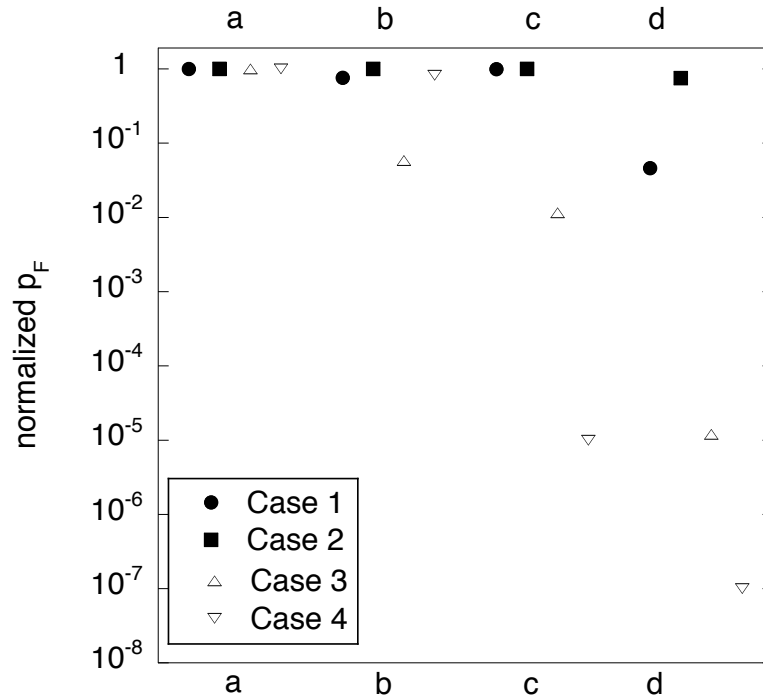


**Figure 5.8:** Probability of failure for the various approaches. The probability of failure is normalized with respect to the highest value.

assuming that each component contains one flaw and that the stress spectra have a constant load ratio equal to 0.1. Furthermore, the probability of failure is normalized with respect to the highest value.

The probability of failure obtained with approach *d* is considered the most accurate result, used as a reference.

The probability of failure obtained assuming a fixed initial flaw depth equal to 5% WT is lower or equal than that evaluated considering the distribution of initial flaws, since on average the flaws are smaller than 5% WT.

For Case 2, which has the most demanding spectrum, the use of the different approaches does not make any significant difference in the evaluation of the probability of failure. However, a higher difference can be obtained for Case 1, which has a lower maximum stress and a spectrum with a quite flat shape. Results for Case 3 and Case

## 5. FRACTURE MECHANICS BASED FATIGUE RELIABILITY UNDER VARIABLE AMPLITUDE LOADING: RANDOM VARIABLE APPROACH

---

4 depend much more strongly on the adopted approach.

The great overestimation of the probability of failure obtained for Cases 3 and 4, when adopting simplified approaches, is due to the fact that, when steep spectra with moderate maximum stress values are applied, only the largest flaw propagate under a small portion of the spectrum. Therefore, especially in these cases, it is essential to take into account the distribution of initial flaws as well as the crack growth under the variable amplitude stress, in order to obtain an accurate estimation of the reliability of the component.

It is also worth noticing that the probability of failure obtained with approach d is not directly related to the maximum applied stress, but it depends also on the spectrum shape and on the service life. For example, Case 1, having a flat spectrum, has a higher probability of failure than Case 3, which has a spectrum with a steep shape, even though Case 1 has a lower maximum applied stress.

### 5.5 Concluding remarks

This chapter presents a large experimental activity to measure the distribution of the initial flaw depth on the surface of tubes. It shows that the depth distribution is independent from the tubes dimension.

A reliability assessment method is also presented in this chapter. The method, according to experimental observations, adopts a fracture mechanics fatigue crack growth algorithm and a random variable probabilistic approach. The random variable approach takes into account the stochasticity of the fatigue crack growth, randomizing the fatigue threshold the variability of the initial flaw depth, the distribution of which is evaluated with the experimental activity presented in the first part of this section.

A distinct feature of the methods is the description of initial flaw size with a random variable approach based on experimental data, while often the maximum size of the flaws, corresponding to the non-destructive tests threshold, or an equivalent flaw size, is adopted (82). Another innovative aspect is the reliability evaluation algorithm itself, which have unique features, which are not present in any commercial software. It permits to take into account any kind of randomly generated stress sequence and uses a comprehensive and validate fatigue crack growth model as well as a state of the art failure evaluation approach.

## 5.5 Concluding remarks

---

The reliability is assessed for four case studies derived from real service spectra measurements on hydraulic cylinders of earth moving machines.

The probability of failure is then compared with the results obtained with simplified approaches.

The comparison of the results shows that generally a correct life assessment of components subjected to variable amplitude fatigue loads has to be carried out considering the distribution of initial flaws and the crack growth under randomly applied load spectra. The shape of the spectrum is a key factor. Simplified hypothesis, such as fixed initial flaw size or the assumption that crack propagation implies failure, may lead to a large overestimation of the probability of failure, especially in cases of medium or high maximum applied stresses.



**5. FRACTURE MECHANICS BASED FATIGUE RELIABILITY  
UNDER VARIABLE AMPLITUDE LOADING: RANDOM VARIABLE  
APPROACH**

---

## 6

# Fracture mechanics based fatigue reliability under variable amplitude loading: random process model

## 6.1 Introduction

The results of chapter 5 show that for a correct life assessment of components subjected to variable fatigue loads the stochasticity of the inputs and the shape of the stress spectrum is a key factor.

This chapter proposes a model of the load, which permits representing different types of service histories, by modeling the load as a Markov random process having a variable correlation length. Advanced reliability evaluation methods, such as subset simulation (19) and first order reliability method (54, 121), are applied, in order to avoid the large computational effort required by the Monte Carlo simulation method. To assess the fatigue reliability under variable amplitude loading, time discretization is combined with the subset simulation, which allows handling the resulting large number of random variables. Results are then compared with those obtained with the first order reliability method for approximations of the time-variant loading (14).

Additionally this chapter investigates the influence of the failure criteria on the reliability evaluation. Two classes of failure modes are investigated: (*i*) one defined

## 6. FRACTURE MECHANICS BASED FATIGUE RELIABILITY UNDER VARIABLE AMPLITUDE LOADING: RANDOM PROCESS MODEL

---

by the crack reaching a critical crack size and *(ii)* one caused by plastic collapse or by unstable crack growth. Results show that the failure criteria are also an important issue in the frame of fatigue reliability analysis. While the failure mode itself is a significant factor for an applied design, its influence on the reliability evaluation is not easily predictable.

### 6.2 Markov process model of the load

A gaussian copula type model for fatigue load processes, which is simultaneously a Markov process, is described in the following. This model is applied later in this chapter for numerical investigations, because it has the advantage that the dependence structure is represented by a single parameter. For simplicity, only the stress range is modeled as a random process  $\{\Delta\sigma\}$ , the stress ratio  $R$  is assumed to be constant and its value is  $R = 0.1$ . The marginal distribution of  $\Delta\sigma$  is defined through its cumulative distribution function (CDF)  $F_{\Delta\sigma}$ . Let  $\Delta\sigma(n)$  be defined through a transformation  $T'$  from a standard Normal variate  $V(n)$  as:

$$\Delta\sigma(n) = T'(V(n)) = F_{\Delta\sigma}^{-1}(\Phi(V(n))) \quad (6.1)$$

where  $\Phi$  is the standard normal CDF and  $F_{\Delta\sigma}^{-1}$  is the inverse CDF of  $\Delta\sigma(n)$ . If it is imposed that  $V(n_i)$  and  $V(n_j)$  have the joint Normal distribution, then the corresponding pair of stress ranges  $\Delta\sigma(n_i)$  and  $\Delta\sigma(n_j)$ , defined through the transformation in equation 6.1, are said to follow the gaussian copula. The autocovariance function of the process  $\{\Delta\sigma\}$  is described through an autocovariance function  $K_{VV}$  of the underlying standard Normal process  $\{V\}$ , which is here assumed to be of the exponential type with correlation length  $z$ :

$$K_{VV}(\Delta n) = Cov[V(n), V(n + \Delta n)] = exp\left(-\frac{\Delta n}{z}\right) \quad (6.2)$$

The process  $\{\Delta\sigma\}$  does not have the same autocorrelation function as the underlying Gaussian process  $\{V\}$ , however, the difference between the two is generally small.  $K_{\Delta\sigma\Delta\sigma}(\Delta n)$  is obtained from  $K_{VV}(\Delta n)$  by means of the Nataf transformation (80). It can be shown that with the exponential autocovariance function, the process  $\{V\}$  has the Markovian property (152):

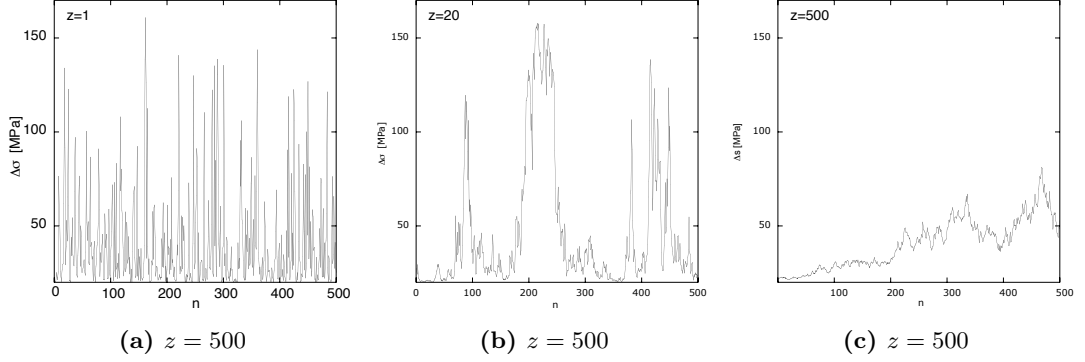


**Figure 6.1:** Randomly generated sequences of the stress range  $\Delta\sigma$ , with identical marginal distribution and varying correlation length  $z$ .

$$F_V[V(n_j)|V(n_{j-1}), V(n_{j-2}), ..Vn_1] = F_V[V(n_j)|V(n_{j-1})] \quad (6.3)$$

Consequently, also the process  $\{\Delta\sigma\}$  is a Markov process:

$$F_V[\Delta\sigma(n_j)|\Delta\sigma(n_{j-1}), \Delta\sigma(n_{j-2}), ..\Delta\sigma n_1] = F_{\Delta\sigma}[\Delta\sigma(n_j)|\Delta\sigma(n_{j-1})] \quad (6.4)$$

With this model, the dependence structure is characterized solely by the correlation length  $z$ . To illustrate the effect of  $z$ , figure 6.1 shows three different realizations of stress range processes  $\{\Delta\sigma\}$  with identical marginal distribution but varying correlation length.

### 6.2.1 Discretization of the fatigue load process into blocks

For practical purposes, it is computationally advantageous to approximate the random load sequence by blocks of cycles with constant amplitude and stress ratio. Such blocks can be defined from the original fatigue load process  $\{\Delta\sigma\}$  by dividing the sequence of cycles  $\{n_1, n_2, \dots, n_j, \dots, n_{tot}\}$  into blocks of  $b$  cycles. Each block  $i$  is characterized by a stress range  $\Delta\sigma_i$  that is equal to the value of the stress cycle at the mid-point of the block  $\Delta\sigma_i = \Delta\sigma_{(i-\frac{1}{2}) \cdot b}$ . Unlike the blocks of the Gassner sequence, or similar deterministic load sequences, the loading blocks obtained with this method still represent a random process. The resulting stress range process has the same marginal distribution  $F_{\Delta\sigma}$  as the original one. The autocovariance function of the block approximation of  $\Delta\sigma$  is:

## 6. FRACTURE MECHANICS BASED FATIGUE RELIABILITY UNDER VARIABLE AMPLITUDE LOADING: RANDOM PROCESS MODEL

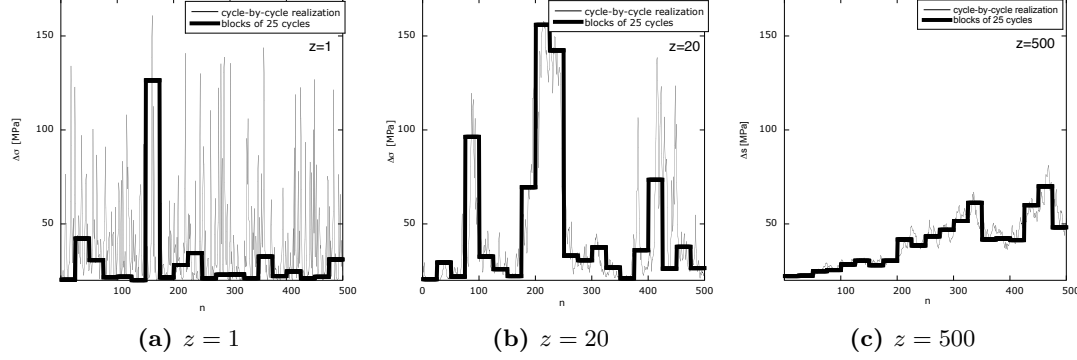


**Figure 6.2:** Approximated load sequences built as blocks of length  $b = 20$  cycles, superimposed on the load sequences shown in figure 6.1. The value of  $\Delta\sigma$  at each block is equal to the mid-point value of the original random process at each block.

$$K_{\check{\Delta}\sigma\check{\Delta}\sigma}(\Delta n) = K_{\Delta\sigma\Delta\sigma}(k \cdot b) - \frac{\Delta n - k \cdot b}{b} [K_{\Delta\sigma\Delta\sigma}(k \cdot b) - K_{\Delta\sigma\Delta\sigma}((k+1) \cdot b)] \quad (6.5)$$

with  $k = \text{floor}(\frac{\Delta n}{b})$ .

The error in the covariance is small as long as the correlation length is much larger than the block size,  $z \gg b$ . Figure 6.2 exemplarily illustrates the stress range block sequence corresponding to the realizations of the stress ranges shown in figure 6.1, with a block length  $b = 20$  cycles. It can be observed that the approximation becomes better with increasing correlation length  $z$ .

### 6.2.2 Generation of a Markov process load sequence for reliability analysis

To solve the structural reliability problem formulated in equation 2.29, the multidimensional integral in the space of  $X$  is rewritten to an integral in standard normal space:

$$p_F(N) = \int_{\Omega_F(N)} f_X(x) dx = \int_{G(U,N) \leq 0} \phi_n(u) du = \int_{G(U,N) \leq 0} \phi(u_1) \phi(u_2) \dots \phi(u_n) du_1 du_2 \dots du_n \quad (6.6)$$

where  $U = [U_1; \dots; U_n]$  are uncorrelated standard normal random variables,  $\Phi_n$  is the  $n$ -variate uncorrelated standard normal PDF, and  $G(U, N)$  is the limit state function

in the space of U-variables. Underlying equation 6.6 is the equality  $Pr\{g(X, N) \leq 0\} = Pr\{G(U, N) \leq 0\}$ . In order to determine  $G(U, N)$  from  $g(X, N)$ , a probability-conserving transformation  $T$  from  $U$  to  $X$  is required (35, 91, 121):

$$G(U, N) = g(T(U), N) \quad (6.7)$$

Due to the large number of random variables used to represent the discrete load process  $\Delta\sigma_1, \dots, \Delta\sigma_l$ , an efficient procedure is required for this transformation. The Markovian property of the process  $\Delta\sigma_1, \dots, \Delta\sigma_l$  (see equation 6.4), facilitates the application of the Rosenblatt transformation for this purpose (57, 121). First, the random variables  $U_1, \dots, U_l$  are transformed into the correlated standard normal random variables  $V_1, \dots, V_l$  sequentially:

$$V_1 = F_{V_1}^{-1} \cdot (\Phi(U_1)) = U_1 \quad (6.8)$$

$$V_2 = F_{V_2}^{-1} \cdot (\Phi(U_2|V_1)) = \frac{U_2 - \mu_{V_2|V_1}}{\sigma_{V_2|V_1}} \quad (6.9)$$

$$V_3 = F_{V_3}^{-1} \cdot (\Phi(U_3|V_1, V_2)) = F_{V_3}^{-1} \cdot (\Phi(U_3|V_2)) = \frac{U_3 - \mu_{V_3|V_2}}{\sigma_{V_3|V_2}} \quad (6.10)$$

$$V_l = \frac{U_l - \mu_{V_l|V_{l-1}}}{\sigma_{V_l|V_{l-1}}} \quad (6.11)$$

The conditional mean and standard deviation of  $V_l$  given  $V_{l-1}$  are:

$$\mu_{V_l|V_{l-1}} = V_{l-1} \cdot \rho \quad (6.12)$$

$$\sigma_{V_l|V_{l-1}} = \sqrt{1 - \rho^2} \quad (6.13)$$

where the correlation coefficient  $\rho$  is equal to the covariance between  $V_{l-1}$  and  $V_l$ , defined following equation 6.2. Due to the stationarity of the load process,  $\rho$  is equal for all  $l$ . Finally,  $\Delta\sigma_1, \dots, \Delta\sigma_l$  are obtained from  $V_1, \dots, V_l$  through the marginal transformation defined in equation 6.1.

## 6. FRACTURE MECHANICS BASED FATIGUE RELIABILITY UNDER VARIABLE AMPLITUDE LOADING: RANDOM PROCESS MODEL

---

### 6.2.3 Variable amplitude stress for numerical investigation

The gaussian copula type stress amplitude process is characterized by its CDF  $F_{\Delta\sigma}(\Delta\sigma)$  and by the correlation length  $z$ . In the subsequent calculations three  $F_{\Delta\sigma}(\Delta\sigma)$  are considered: two empirical and one analytical CDF, which are depicted in figure 6.3. The two empirical ones,  $C1$  and  $C2$ , are obtained from service stress measurements on hydraulic cylinders of earth moving machines (13) and correspond to Case1 and Case 3 of table 5.2. The analytical one,  $CW$ , is a 3-parameters Weibull with the same mean and standard deviation as  $C1$ .

Table 6.1 summarizes the statistical properties of the three load sequences: the maximum stress range value,  $\Delta\sigma_{max}$ , the service life,  $N$ , the mean and the standard deviation of the stress range,  $\mu_{\Delta\sigma}$  and  $\sigma_{\Delta\sigma}$ . The correlation length  $z$  is varied to investigate its effect on the reliability.

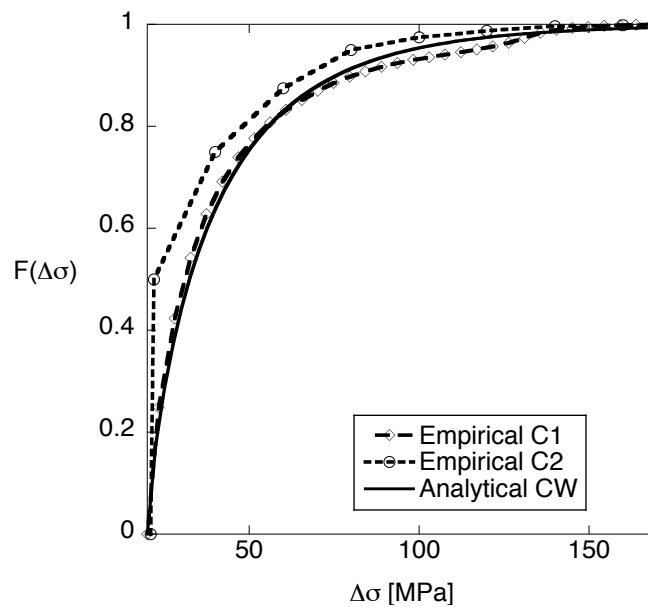


**Figure 6.3:** Cumulative distribution CDF of the three applied load models.

### 6.3 Innovative solutions for the reliability evaluation

---

	<i>C1</i>	<i>C2</i>	<i>CW</i>
$\Delta\sigma_{max}$ [MPa]	84	110	$\infty$
$N$	$1.8 \cdot 10^7$	$2 \cdot 10^7$	$1.8 \cdot 10^7$
$\mu_{\Delta\sigma}$ [MPa]	42	34	42
$\sigma_{\Delta\sigma}$ [MPa]	28	23	28

**Table 6.1:** Properties of the three applied load models: maximum stress range  $\Delta\sigma_{max}$ , number of fatigue cycles during the service life  $N$ , mean of the stress range  $\mu_{\Delta\sigma}$ , and standard deviation  $\sigma_{\Delta\sigma}$ .

### 6.3 Innovative solutions for the reliability evaluation

In chapter 5 the reliability evaluation is carried out using the latin hypercube Monte Carlo simulation method (see section 2.7.1). This section presents advanced solutions for the evaluation of the fatigue reliability.

The reliability assessment described in the following are based on the definition of the limit state function presented in section 2.6.1 and on the corresponding algorithm for its evaluation described in section 4.6.2.

As in the previous chapter (see section 5.3), three random variables are considered: the initial flaw size,  $a_0$ , the fatigue threshold,  $\Delta K_{th,0}$ , and the material fracture toughness,  $K_{mat}$ . Notice that the material fracture toughness is relevant only if the crack driving force failure criterion is considered (see section 4.6.1 for the description of the failure criteria). The structural integrity model of a semi-elliptical surface crack in a flat plate subjected to tension loading is applied (see section 4.4.1). The block length,  $b$ , used for the simulations is  $10^4$  or smaller.

Three approaches to the reliability evaluation are implemented, which correspond to different models of the stress range process:

- *Random process approach* (RP): the load is modeled as a Markov process (see sections 2.3.2 and 6.2) with various correlation lengths and the reliability is evaluated with a subset simulation algorithm (see section 2.7.3). In the implemented algorithm, the constants  $o_i$  defining the intermediate failure events are chosen such that  $P(E_i|E_{i-1}) = 10^{-1}$ , and 500 samples are generated at each intermediate simulation step. Therefore, in each step  $N_{stop}$  (see paragraph 4.6.2) is chosen in order to reach a  $10^{-1}$  probability of failure. The load sequences are generated



## 6. FRACTURE MECHANICS BASED FATIGUE RELIABILITY UNDER VARIABLE AMPLITUDE LOADING: RANDOM PROCESS MODEL

---

applying the method proposed in section 6.2.2. The results obtained with subset simulation are verified for the stress model  $C1$  against a Monte Carlo simulation, as shown in Appendix C.

- *Random variable approach* (RV): the load is modeled as a random variable and the first order reliability method (FORM, see section 2.7.2) as well as Monte Carlo simulation (MCS, see section 2.7.1) are applied. Modeling the load as a random variable is equivalent to a Markov process with infinite correlation length.
- *Mean approximation approach* (MA): the mean approximation is applied (see section 2.4.2.3 and 2.4.2.4) and the reliability is evaluated with FORM. Since the mean approximation does not consider interdependency among stress cycles, it is equivalent to a random process with correlation length zero  $z = 0$ .

### 6.4 Results - critical crack size failure criterion

In this section, the results obtained for the critical crack size failure criterion are reported. The results obtained when considering also the crack driving force failure criteria are presented in paragraph 6.5.

Figures 6.4 show the plots of the probability of failure,  $p_F$ , versus the correlation length  $z$  of the stress range process  $\{\Delta\sigma\}$  with CDF  $C1$ ,  $C2$ ,  $CW$  and for the different reliability evaluation approaches RP, RV and MA. Results for  $z = 1, 10^3, 10^5, 10^7, 10^9$  are obtained describing the load as Markov random process and applying a subset simulation algorithm (SuS RP). Results for  $z = \infty$  refer to the case of the load described as a random variable and solved with Monte Carlo simulation or with first order reliability method (MCS RV and FORM RV). Results for  $z = 0$  are obtained applying the mean approximation with respect to the stress process and solving with FORM (FORM MA).

It can be observed from figure 6.4 that the correlation length  $z$  of the stress range process has a strong effect on the resulting reliability. When the CDF  $C2$  is applied, which is the one with the highest reliability, the probability of failure varies by four orders of magnitude, from  $10^{-6}$  to  $10^{-2}$ ! The highest probability of failure occurs for values of  $z$  close to the service life time. For  $z \geq 10^7$ , the probability of failure decreases again until it reaches the value corresponding to the random variable case ( $z = \infty$ ).

## 6.4 Results - critical crack size failure criterion

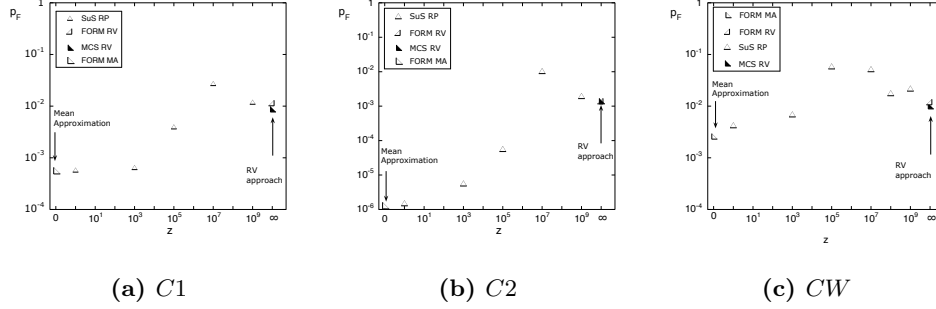


**Figure 6.4:** Probability of failure  $p_F$  versus correlation length of the stress range process  $z$  corresponding to the three models:  $C1$ ,  $C2$ ,  $CW$ . Results for  $z = 1, 10^3, 10^5, 10^7, 10^9$  are obtained describing the load as Markov random process and applying a subset simulation algorithm (SuS RP). Results for  $z = \infty$  refer to the case of the load described as a random variable and solved with Monte Carlo simulation or with first order reliability method (MCS RV and FORM RV). Results for  $z = 0$  are obtained applying the mean approximation with respect to the stress process and solving with FORM (FORM MA).

Values of  $z$  in the range  $10^6 - 10^7$  correspond to cases with a few distinct service conditions during the service life. These are the most unfavorable cases, since they imply a high probability of enduring a high load level during an extended time period. Shorter correlation lengths correspond to a single service condition with randomly varying stress ranges. In these cases, lower failure probabilities are observed because the mixing of the stress ranges decreases the actual uncertainty in the loading (law of large numbers). Finally, for  $z \geq 10^7$ , the probability of having a high load level during lifetime decreases, and therefore the probability of failure slightly decreases.

There is a good agreement between the results obtained describing the load as a random process with a high correlation length ( $z = 10^9$ ) and applying a random variable approach. The probability of failure obtained applying the mean approximation is close to the one obtained with the load modeled as a random process with a short correlation length ( $z = 1$ ). It should be noted that the correlation length  $z = 1$  refers to the specification of the stress process; however, due to the block approximation in the fatigue crack growth evaluation, the correlation length of the simulated stress process is larger than the specified  $z = 1$  (see comments in section 6.2.1). This effect is relevant only for the small correlation lengths, i.e.  $z = 1$  and  $z = 10^3$ . It can also explain

## 6. FRACTURE MECHANICS BASED FATIGUE RELIABILITY UNDER VARIABLE AMPLITUDE LOADING: RANDOM PROCESS MODEL

---

the slight difference in figures 6.4a and 6.4c between the  $p_F$  calculated with the mean approximation and with a random process with correlation length  $z = 1$ .

The probability of failure of case  $CW$  is slightly higher than that of  $C1$ , even though the two correspond to stress range processes with the same mean and standard deviation. The difference between the results can be explained by the fact that in the case of  $CW$  the distribution of the stress ranges is analytically defined and has no upper limit, which implies a heavier tail of the distribution. The effect of the two different distribution forms can also be observed in figure 6.5, which compares the mean approximation for cases  $C1$  and  $CW$ . Figure 6.5a shows the expected value of the fatigue crack growth rate  $E[\frac{da}{dn}] = h'_a(a, \frac{a}{c}, \delta, \gamma)$  (equations 2.25) as a function of the crack length  $a$  (see paragraph 2.4.2.4). The expected value of the fatigue crack growth rate evaluated with  $CW$  is higher than that evaluated with  $C1$ . Fig. 6.5b shows the crack depth  $a$  versus the number of fatigue cycles  $n$  applying the mean approximation with respect to the stress distributions  $C1$  and  $CW$  at the design point  $u^*$  of the FORM solution for case  $C1$ . It is observed that the analytical Weibull distribution  $CW$  leads to a lower number of cycles to failure, which is in agreement with the differences in the probabilities of failure observed between figures 6.4a and 6.4c.

Figure 6.4 shows that the correlation of the load sequence has a significant influence on the fatigue reliability. To better understand the reasons for this effect, it is helpful to look at some realizations of the crack growth process for different values of the correlation length  $z$ . In figure 6.6a, random realizations of the crack growth with a stress range correlation length  $z = 1$  are shown for two different values of the initial crack size  $a_0$ . In 6.6b, random realizations of the crack growth are shown for the case where the stress range is a random variable ( $z = \infty$ ). Comparing the results for  $z = 1$  and  $z = \infty$  shows the effect of a small correlation length: the randomness of the stress range process essentially disappears due to the law of large numbers. Therefore, the resulting randomness is much smaller in this case, and the reliability is significantly higher. This is also confirmed by FORM sensitivity results shown later.

In figure 6.7 random realizations of the crack growth are shown for correlation length  $z = 10^7$ , together with the underlying load sequences. This value of  $z$  is of the same order of magnitude as the service life, and it is the value with the highest failure probability (figure 6.4). It can be clearly observed how the stress range processes correspond to a few distinct service conditions during the service life. This implies a

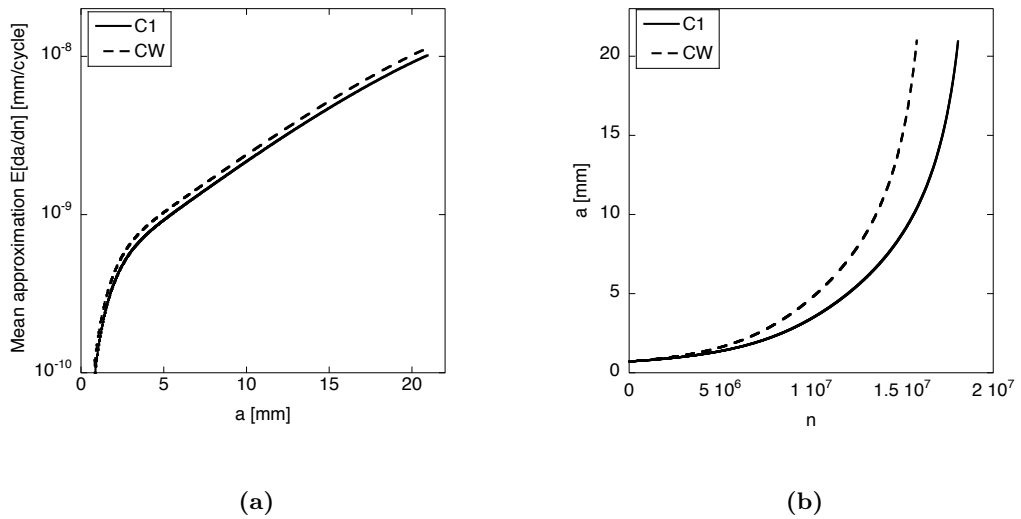
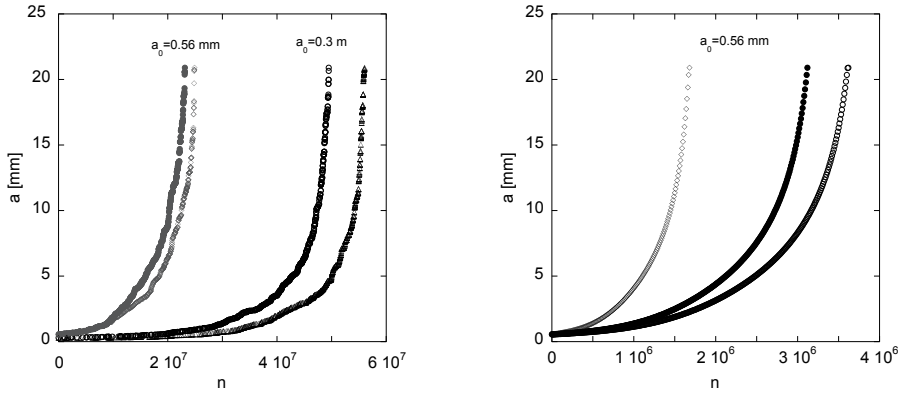


**Figure 6.5:** Mean approximation for cases  $C1$  and  $CW$ : (a) expected value of the fatigue crack growth rate  $E[\frac{da}{dn}] = h'_a(a, \frac{a}{c}, \delta, \gamma)$  as a function of the crack length  $a$ ; (b) crack depth  $a$  versus the number of fatigue cycles  $n$  calculated with the mean approximation at the design point  $u^*$  of the FORM solution for case  $C1$ .

## 6. FRACTURE MECHANICS BASED FATIGUE RELIABILITY UNDER VARIABLE AMPLITUDE LOADING: RANDOM PROCESS MODEL

---



(a) The stress range is a random process with CDF  $C1$  and correlation  $z = 1$ .

(b) The stress range is fixed:  $\Delta\sigma = 113, 135, 170 MPa$ .

**Figure 6.6:** Crack depth  $a$  versus number of fatigue cycles  $n$  with initial crack depth  $a_0 = 0.0003$  m or  $a_0 = 0.00056$  m and fixed fatigue threshold.

high probability of enduring a high stress range level during an extended time period, which leads to fast growth of the crack.

### 6.4.0.1 FORM sensitivity analysis

The FORM algorithm provides sensitivity factors  $\alpha_i$  that describe the influence of the random variables on the failure probability (paragraph 2.7.2). Table 6.2 and 6.3 show the FORM sensitivity factors  $\alpha_i$  for the random variable approach (corresponding to  $z = \infty$ ) and the mean approximation approach (corresponding to  $z = 0$ ). In the random variable approach, the most influent variables are the stress range  $\Delta\sigma$  and the initial value of the flaw depth  $a_0$ , while the fatigue threshold  $\Delta K_{th}$  has little influence on the reliability due to its small coefficient of variation (see section 5.3). The negative sign of  $\alpha_{\Delta K_{th}}$  indicates that a decrease in the value of  $\Delta K_{th}$  leads to a decrease in reliability. With the mean approximation approach, the only two random variables are  $\Delta K_{th}$  and the initial crack depth  $a_0$ . As seen from table 6.2, the reliability is determined mainly by the latter.

## 6.4 Results - critical crack size failure criterion

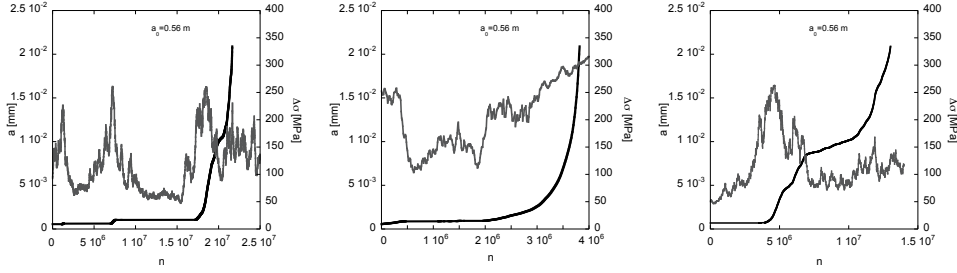


**Figure 6.7:** Crack depth (black) and stress range (gray) versus number of cycles with initial crack depth  $a_0 = 0.56$  mm and fixed fatigue threshold. The crack growth is evaluated for realizations of the stress range modeled as a random process with a correlation  $z = 10^7$  based on the empirical *C1*. Three randomly generated load histories are exemplarily shown.

	C1	C2	CW
$\alpha_{\Delta\sigma}$	0.83	0.89	0.72
$\alpha_{\Delta K_{th}}$	-0.04	-0.01	-0.036
$\alpha_{a_0}$	0.56	0.44	0.68

**Table 6.2:** FORM sensitivity analysis for the random variable approach

	C1	C2	CW1
$\alpha_{\Delta K_{th}}$	-0.18	-0.03	-0.036
$\alpha_{a_0}$	0.98	0.99	0.99

**Table 6.3:** FORM sensitivity analysis for the mean approximation approach

## 6. FRACTURE MECHANICS BASED FATIGUE RELIABILITY UNDER VARIABLE AMPLITUDE LOADING: RANDOM PROCESS MODEL

---

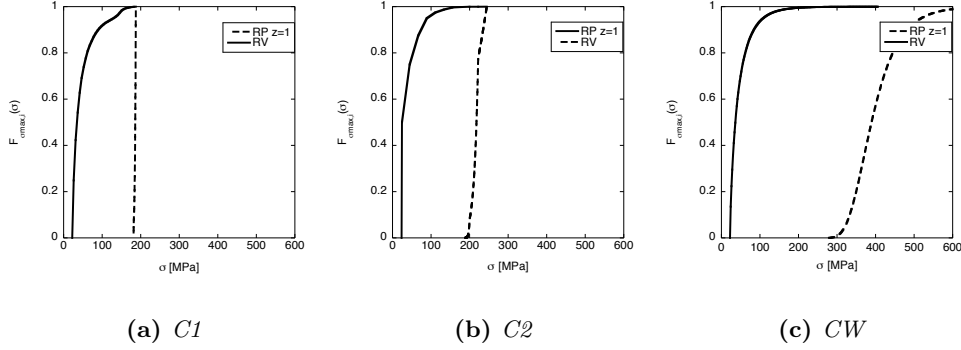


**Figure 6.8:** CDF of the maximum stress range in a block of  $b = 10^4$  number of cycles for the random variable model of the stress range and for the random process model with correlation length ( $z = 1$ ).

### 6.5 Results - Critical crack size failure and crack driving force failure criteria

Following section 2.6.3, the crack driving force failure criteria are considered for the two limit cases:

- RV: the stress range is a random variable ( $z = \infty$ , assumption of full correlation);
- RP: the stress range is a random process with correlation length  $z = 1$  (assumption of no correlation).

The reliability computations are performed with a block size of  $b = 10^4$ . For the RP case, the CDF of  $\sigma_{max,i}$ , the maximum stress during  $b$  cycles, is evaluated following equation 2.37, and it is shown in figure 6.8 together with the CDF for case RV. In the RV case, the maximum stress is constant throughout the entire service life and the CDF is independent of  $b$ . For load models C1 and C2, the maximum stress in RP case is essentially equal to the upper limit of the stress distribution  $\sigma_{UL}$ . For load model CW, where stress ranges follow the Weibull distribution, the stress distribution has no upper limit and high values of  $\sigma_{max,i}$  are expected.

Figure 6.9 shows the probability of failure  $p_F$  versus correlation length  $z$  calculated by applying either the critical crack size failure criterion alone or in combination with

## 6.5 Results - Critical crack size failure and crack driving force failure criteria

---

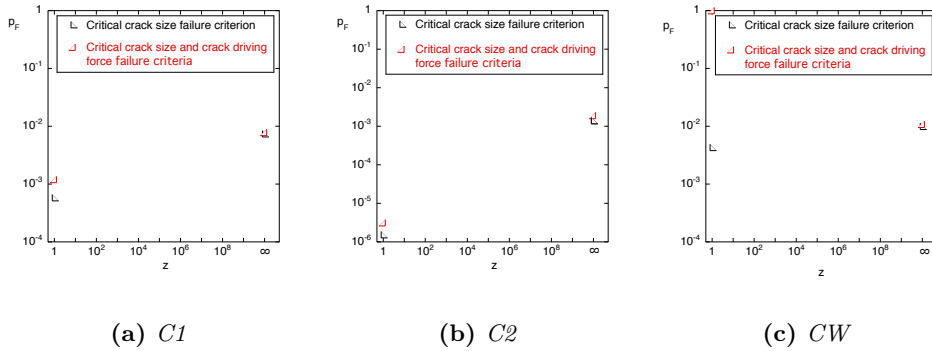


**Figure 6.9:** Probability of failure versus correlation length  $z$  when applying either the critical crack size failure criterion alone or in combination with the crack driving force failure criteria. For  $z = 1$ , results are computed with SuS; for  $z = \infty$ , the MCS is applied.

the crack driving force failure criteria. The results show that the crack driving force failure criteria have a significant influence on the reliability only for load model CW and no correlation ( $z = 1$ ). In this case, the probability of failure is close to one, which is not surprising when looking at the CDF of  $\sigma_{max,i}$  in figure 6.8c. Since a total of over  $10^3$  load blocks occur during the service life, these maximum stresses would lead to failure even without the presence of a crack. In all other cases shown in figure 6.9, the reliability is only slightly influenced by the crack driving force failure criteria. For  $z = \infty$  there is no effect (the differences are due to the variability of the MCS).

To understand the effect of the crack driving force failure criteria in the case of a random process model with a correlation length  $z \geq 1$ , some additional considerations are necessary. Figure 6.10 shows the empirical CDF of the maximum stress in a block, for the RV case and for the RP case with  $z = 1$  and  $z = 10^7$  (load model *C1*). The resulting CDF of case  $z = 10^7$  is in-between the CDFs of the other two cases, which is to be expected given that those are the limit cases.

Figure 6.11 depicts the empirical distributions of the crack depth  $a$  that causes failure according to the crack driving force failure criteria. These distributions correspond to the three CDFs of the maximum stresses given in figure 6.10. The critical crack depth applied in the critical crack size failure criterion is 21 mm. The mean crack depth at which the crack driving force failure occurs is close to the critical crack size



## 6. FRACTURE MECHANICS BASED FATIGUE RELIABILITY UNDER VARIABLE AMPLITUDE LOADING: RANDOM PROCESS MODEL

---

criterion in all cases: it is 19 mm for the random variable load model, 18 mm and 15 mm for the random process models with  $z = 10^7$  and  $z = 1$  respectively. Therefore, the crack driving force failure criteria are reached just slightly before the critical crack size criterion, in particular since the crack growth rate increases strongly with crack size (see figures 6.6 and 6.7).

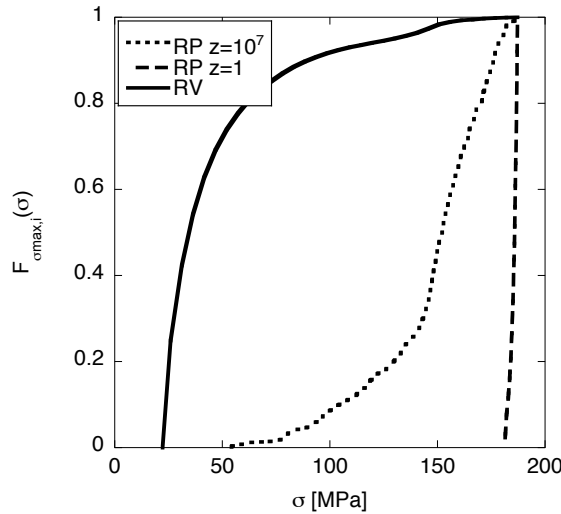


**Figure 6.10:** CDF of the maximum stress for the random variable case (RV) and for the random process case with  $z = 1$  ( $RP z = 1$ ) and  $z = 10^7$  ( $RP z = 10^7$ ), evaluated for the load model  $C1$  with blocks of  $b = 10^4$  cycles.

From the above observations it follows that if the effect of the crack driving force failure criteria is small already for  $z = 1$ , it is reasonable to assume that it will be low also for values of  $z \geq 1$ . This is the case for load models  $C1$  and  $C2$ . If the effect of the crack driving force failure criteria is significant for  $z = 1$ , additional computations, such as a cycle-by-cycle evaluation may become necessary.

### 6.6 Discussion

The results of the numerical investigation point to the importance of accurately modeling the characteristics of the stress range process, in particular its correlation structure. In reliability analysis of structural components subject to fatigue, it has generally been assumed that the fatigue stress cycles are either fully correlated or uncorrelated. The

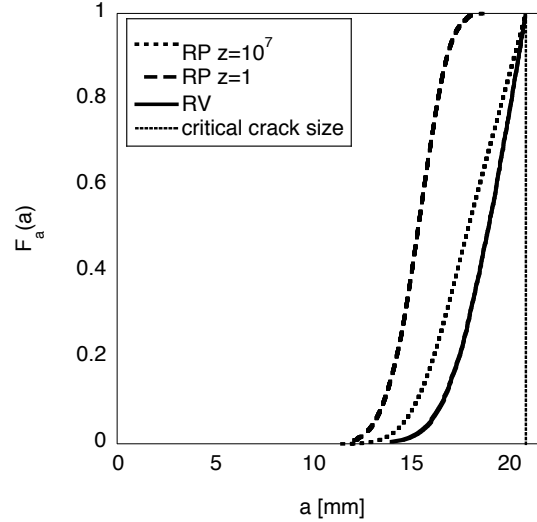


**Figure 6.11:** CDF of the critical crack size for the crack driving force failure criteria for the random variable case (RV) and for the random process case with  $z = 1$  ( $RP z=1$ ) and  $z = 10^7$  ( $RP z = 10^7$ ), evaluated for the load model *C1* with blocks of  $b = 10^4$  cycles.

results shown in figure 6.4 demonstrate that both these assumptions can overestimate the reliability. They indicate that the highest probability of failure occurs when the correlation length of the stress range process is of the same order of magnitude as the service life. This corresponds to structures that are subjected to a few distinct service conditions or mission types over their life-time. In these situations, the assumption of uncorrelated fatigue stress cycles leads to predictions of the probability of failure that may be several orders of magnitude too low. As shown in this chapter, effective methods for considering the correlation structure of the stress range process in reliability analysis exist when using fracture mechanics based fatigue models. When applying S-N models, however, this effect cannot be accounted for.

For the specific case study investigated in this work, unstable crack growth, as represented by the crack driving force failure criteria, has only a limited effect on the reliability. A similar behavior is expected in many structures subject to high-cycle fatigue. The effect can be appraised by determining the probability distribution of the crack size at which unstable crack growth occurs (figure 6.11). If it can be ruled out that unstable crack growth plays a significant role, the reliability assessment is greatly

## 6. FRACTURE MECHANICS BASED FATIGUE RELIABILITY UNDER VARIABLE AMPLITUDE LOADING: RANDOM PROCESS MODEL

---

simplified, as it becomes sufficient to assess the critical crack size failure criterion. However, even if unstable crack growth has a limited effect on the reliability, it may still be necessary to consider it in case that not only the probability of failure but also the failure mode is of relevance. This can be the case for example in pipelines and pressure vessels where one needs to distinguish between failure by leakage and failure by burst.

### 6.7 Concluding remarks

The work presented in this section provides an insight on the importance of the load model and its influence on the simulated load histories, on the crack growth and on the reliability evaluation.

Random processes with varying correlation lengths are successfully applied to describe various types of fatigue loading, corresponding to different mission types. Alternatively, in order to reduce the computational effort, the fatigue crack growth is evaluated applying a mean approximation of the random stress process or the stress range is treated as a random variable. These simplified methods provide a good estimation of the reliability which applies in some cases, such as:

- when the load is totally uncorrelated (mean approximation)
- when the load can be assumed totally correlated (random variable)

For the first time a fatigue reliability evaluation is approached applying a time discretization of the Markov stress process with subset simulation method and a mean approximation of the stress process is applied and solved with the first order reliability method (FORM).

The results show that the correlation length of the load process has significant influence on the estimated reliability; the probability of failure can vary up to several orders of magnitude for the same marginal probability distribution of stress amplitudes. These observations point out to the importance of an accurate modeling of the fatigue load processes. Also the selection of the failure criteria appears to have a different effect depending on how the maximum load is modeled. All failure modes must however be included to allow assessing the consequences of failure.

# 7

## Conclusions

In this thesis a damage tolerant approach is adopted to evaluate the reliability evaluation of structures subjected to variable amplitude fatigue stress.

To this aim three key steps are identified: *(i)* the modeling of stochastic fatigue crack growth for fatigue life estimation, *(ii)* the modeling of variable amplitude stress sequences, *(iii)* the reliability estimation. For each step innovative solutions are implemented.

The fatigue life estimation *(i)* is based on the Forman-Mettu model, which describes accurately all the phases of the fatigue crack growth process. The stochasticity of the fatigue crack growth phenomenon is investigated by means of many fatigue crack growth experiments, in which the fatigue threshold and the fatigue crack growth curves are obtained. The plasticity induced crack closure is accounted for through the cyclic yield stress. A comprehensive model to describe the fatigue crack growth curves and the fatigue threshold for different stress ratio, accounting also for the stochasticity of the crack growth phenomenon, is successfully implemented and verified with full scale tests as well as with a commercial software (32). The behavior of the experimental fatigue crack growth curves suggests that the stochasticity of the crack growth is mainly controlled by the variation of the threshold, since the threshold variation creates a fanning effect which reproduces the experimental observations (13). This work shows that the stochasticity of the fatigue crack growth can be described simply with only one random variable. So far usually multiple correlated random variables have been used to describe the stochasticity of the fatigue crack growth, implying the assessment

## 7. CONCLUSIONS

---

of the distribution of each variable as well as the correlation between them. This last procedure is more complex and can easily lead to erroneous estimations which can affect the life-time evaluation. The use of one random variable simplifies the statistical assessment and reduces the approximation in the models, thus limiting bias in the results coming from erroneous assumptions.

The modeling of the variable amplitude stress sequences (*ii*) is implemented with Markov processes, characterized by a cumulative density function and by a correlation length. This model permits to describe various types of fatigue loading, corresponding to different mission types. The Markov process model offers a limited computational time for the sequence generation and an ease of implementation. Additionally it permits to define analytically and uniquely the stress model, which can then be reproduced for numerical analysis or laboratory tests. Results show that the correlation structure of the stress range process has a significant influence on the estimated reliability. The probability of fatigue failure varies by several orders of magnitude for different correlation lengths. So far, studies regarding fatigue under variable amplitude loading have been focused on the load interaction effects, but have not explicitly described the influence of the stress sequence on the fatigue crack growth. The present thesis shows that, even if load interaction effects due to plasticity are neglected, the structure of the stress sequence has a tremendous effect on reliability evaluation (14).

The reliability estimation (*iii*) is implemented with the traditional Monte Carlo method and, for the first time, combining a time discretization of the Markov stress process with subset simulation method. Additionally a mean approximation and a random variable approach for the stress are combined with first order reliability method to explore approximated solutions with faster computational time. Numerical investigations are presented in this work using the Monte Carlo simulation method and the new methods proposed in this thesis in relation to the case study of tubular parts loaded with internal pressure carrying initial semi-elliptical surface flaws. They are used to investigate which factors have the most significant influence in the reliability evaluation, how these factors affect the reliability and when approximated approaches can be applied.

Results show that the initial flaws depth and the stress model are the factors which exert the most significant influence on the reliability evaluation when variable amplitude fatigue loading are applied (13, 14). Simplified conservative approaches, which assume a fixed initial flaw depth or which do not properly take into account the fatigue crack growth under variable amplitude stress, may lead to an erroneous estimation of the probability of failure, especially when the stress distribution have a large standard deviation and a high upper tail. The numerical investigations show also that the failure criteria may exert an influence on the reliability depending on the model adopted for the stress (14).

For stress range processes that are ergodic and have limited correlation, the mean approximation of the stress is suitable; for constant stress ranges, the random variable model is applicable; in all other cases, the load block model in combination with the subset simulation provides a practical tool for assessing the reliability (14).

It is therefore recommended to accurately define the distribution of the initial flaws depth, as well as the distribution and the correlation of the stress. The possibility to apply any approximation should be accurately evaluated, based on experimental evidence and designers should be aware of the error to which the adopted approximation can lead in terms of reliability estimation. All the failure modes should also be included, unless it can be clearly demonstrated that neglecting some of them does not affect the reliability evaluation.

## 7.1 Validity and limits of the results

The assessments presented in the work are based on the following assumptions: *(i)* initial surface flaws, behaving like long cracks, are present on the components' surface, *(ii)* the variability of the load can be described by the variability of its amplitude, while the load ratio is assumed constant, *(iii)* retardation and acceleration effects due to load interaction can be neglected.

The first assumption *(i)* permits to neglect the nucleation phase of cracks as well as the short crack behavior. However, inclusion of crack nucleation and small crack growth into the reliability analysis would be straightforward, by combining the crack growth model with a crack nucleation model and a small crack growth model.

## 7. CONCLUSIONS

---

The second assumption (*ii*) is introduced for simplicity, in order to focus the analysis on the variability of the stress amplitude. In analogy to the stress ranges, the stress ratios can be modeled through a random process, and can be included in the reliability analysis. Additional work would be necessary to determine the characteristics of such a stress ratio process, which would be correlated to the stress range process.

The presented crack growth model also does not include retardation and acceleration effects due to load interaction (*iii*). Their effect is considered marginal when random stress sequences described by a sufficiently large number of cycles in respect to the service life are applied, since retardation and acceleration effects on average cancel out. These effects can be included without the need for modifying the presented reliability evaluation methods. The representation of the load interaction effects will however be affected by the block approximation of the stress range process.

### 7.2 Future work

Further work should be dedicated to the investigation of the fatigue crack growth stochastic behavior in the negative stress ratio domain, since the experiments carried out in this work refer only to positive stress ratio, i.e. to cases when the maximum and the minimum stress have the same sign. In the case of negative stress ratio, the contribution of plasticity induced closure might need a modified description, which can not be foreseen based on the available results.

Further work should also be devoted to investigate more accurately the effects of the failure criteria on the reliability, depending on the adopted model of the stress and on its correlation structure. In this respect it would be useful to dedicate further research to the development of a model for the maximum stress in a block approximation approach. The maximum stress model should be based on real service measurements and should be applicable to any measured stress sequence. This would allow a proper evaluation of the failure modes accounting for unstable crack growth and plastic collapse. Additionally, the influence of the failure criteria on the reliability evaluation needs to be further investigated, since its dependence on the stress process is complex and require further analysis.

## Appendix A

# Influence of mechanical properties and microstructural features on the fatigue threshold of steels

### A.1 Introduction

Fatigue threshold is defined as the applied stress intensity factor,  $\Delta K$ , which makes the crack propagation rate lower than  $10^{-7}$  mm/cycle. It is measured experimentally according to the standard ASTM E-647-08 (7). Many studies have been carried out since more than 20 years on the fatigue threshold for long cracks, which is a parameter of great importance when designing a structure subjected to fatigue loads. Some studies describe experimental observations and apply empirical models (75, 117). Others propose theoretical models based on energy considerations, dislocation dynamics and crack tip plasticity (79, 118, 126, 148). The objective of this annex is to offer to the reader an overview on the literature on the influence of mechanical and microstructural features on the fatigue threshold of steels. To this aim, the closure mechanisms have to be introduced first.



## A. INFLUENCE OF MECHANICAL PROPERTIES AND MICROSTRUCTURAL FEATURES ON THE FATIGUE THRESHOLD OF STEELS

---

### A.2 Closure mechanisms and their influence on the fatigue threshold

The mechanism of closure reduces the effective stress intensity factor applied to the crack, because it causes the crack to open at an applied stress level,  $S_{open}$ , higher than the minimum applied stress,  $S_{min}$ . Figure A.1 shows the effect of closure in the cyclic stress acting on the crack: the applied stress is  $\Delta\sigma = \sigma_{max} - \sigma_{min}$ , but the effective stress is  $\Delta\sigma_{eff} = \sigma_{max} - \sigma_{open}$ . Different mechanisms, which impede the growth of cracks under constant amplitude loading, are described in the following paragraphs. Various mechanisms can act at the same time and it is difficult to evaluate accurately the individual contributions (144).

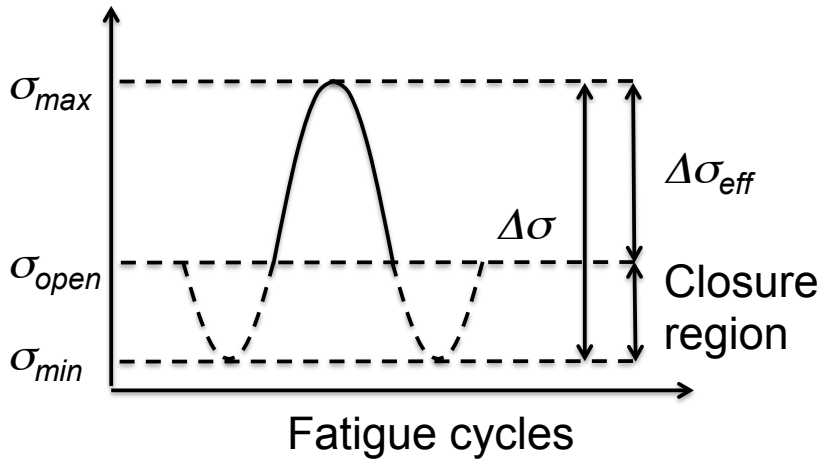


**Figure A.1:** Crack closure: the applied stress is  $\Delta\sigma = \sigma_{max} - \sigma_{min}$ , but the effective stress is  $\Delta\sigma_{eff} = \sigma_{max} - \sigma_{open}$ . The crack tip opens at  $\sigma_{open}$ .

#### A.2.1 Plasticity induced closure

Linear elastic fracture mechanics assumes that only the field ahead of the crack tip determines the crack growth. Experiments by Elber (40) have shown that crack growth is also influenced by the nature of crack face contact. The propagation of a fatigue crack under constant amplitude loading gives rise to a wake of plastically deformed material.

The plasticity induced crack closure can be described with the strip yield model, which was firstly proposed by Dugdale and Barenblatt (16). The model assumes a

## A.2 Closure mechanisms and their influence on the fatigue threshold

slender plastic zone at the crack tip with a closure stress equal to the material yield strength.

### A.2.2 Oxide induced closure

Oxide induced crack closure is due to surface oxidation during fatigue loading. The oxidation of the freshly formed fracture surface is mostly caused by moist atmosphere. In the near threshold region, that is for a low stress intensity factor,  $\Delta K$ , and at low stress ratio  $R$  oxide layer is continuously broken and reformed, thus leading to the formation of an oxide layer 20 times thicker than the freshly formed one. Oxide induced crack closure is promoted by high temperature, moisture containing environments, low  $R$  and low  $\Delta K$  levels, high cyclic frequencies, low strength and coarse grain microstructures (144).

### A.2.3 Roughness induced closure

In the near threshold regime a cristallographic fracture process is promoted, producing a faceted fracture morphology. An increase in crack closure is due to the tortuous crack path induced by the cristallographic growth in conjunction with mixed mode sliding and mismatch between the crack face asperities. Roughness induced closure is also caused by crack deflection and consequently surface roughness created when the crack encounters a grain boundary or a second phase (68, 148, 149). Measuring surface roughness on the specimen fracture surface is a method to evaluate the amount of roughness induced closure and to compare the behaviour of various materials (29, 66). In the near threshold region roughness induced closure is the prevalent mechanism of closure, and prevails over plasticity induced closure (62). Roughness induced closure is strictly related to the microstructure and provides an explanation for the effects of microstructure on fatigue threshold (126, 144, 156).

### A.2.4 Measurement of closure

Closure can be measured through the measurement of the compliance (7), which is the slope of the displacement versus force curve. Figure A.2 shows a graph of the displacement versus the applied load in presence of closure. The shape of the graph

## A. INFLUENCE OF MECHANICAL PROPERTIES AND MICROSTRUCTURAL FEATURES ON THE FATIGUE THRESHOLD OF STEELS

---

suggests that the crack does not close completely until zero load and that there is a transition region in which the closure level changes continuously.

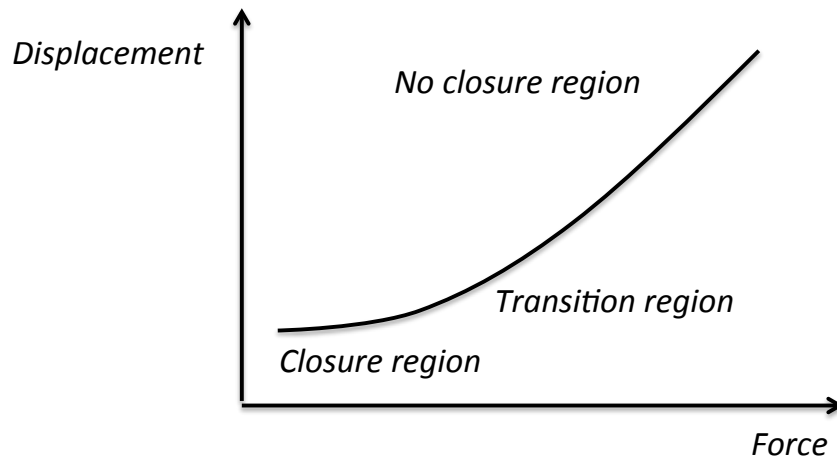


**Figure A.2:** Scheme of the displacement versus the applied force in presence of closure.

### A.3 Parameters influencing the threshold

Experimental observations have shown that the near threshold region is affected by stress ratio, microstructural features and mechanical properties. The Paris region is not influenced by these parameters (79, 126, 148). The reason for this behavior is that the crack tip opening displacement and the crack tip plastic zone size in the near threshold region are of the same order of magnitude as the microstructural features, while in the Paris region they are much larger than the characteristic microstructural dimension.

#### A.3.1 Influence of stress ratio

Closure is active at low stress ratio, while its effect is reduced at high stress ratio (26, 28, 128, 132). This explains the experimental observation of a threshold's strong dependance on the stress ratio,  $R$ : the fatigue threshold decreases as the stress ratio increases. This trend is observed for values of  $R$  within a certain range, which is about  $-2 \leq R \leq 0.7$ , depending on the material. Outside this range threshold values tend to

### A.3 Parameters influencing the threshold

---

be constant. Commonly it is considered that closure is absent for stress ratio above 0.5-0.7, depending on material microstructure and properties. The dependance of closure with stress ratio can be expressed as (144):

$$\frac{K_{opening}}{K_{max}} = f(R) \quad (A.1)$$

Where  $f(R)$  depends on the material and on the testing conditions.

The dependance of the threshold on the stress ratio has been modeled with various simple empirical relations, such as (26, 75, 134):

$$\Delta K_{th,R} = A - BR \quad (A.2)$$

$$\Delta K_{th,R} = D(1 - R)^\gamma \quad (A.3)$$

Where A, B, D and  $\gamma$  are empirical constants. According to the Nasgro equation, the threshold is modeled as (53):

$$\Delta K_{th,R} = \frac{\Delta K_{th,0}}{\left[ \frac{1-f}{(1-A_0)(1-R)} \right]^{1+C_{th}R}} \quad (A.4)$$

Where  $R$  is the stress ratio,  $f$  is a closure function,  $A_0$  is a constant used in the formulation of  $f$ ,  $\Delta K_{th0}$  is the threshold at  $R=0$ ,  $\alpha$  is the crack length,  $C_{th}$  is an empirical constant. These equations are valid in a limited range of  $R$ , usually for  $-2 < R < 0.7$ . Outside this range the threshold tends to be constant and a lower or an upper bound of the threshold have to be considered. The value of  $R$  at which the threshold reaches its minimum value as well as the threshold sensitivity with  $R$  are influenced by the microstructure (70). For example, low yield strength materials or large grain size materials are more sensitive to  $R$  changes than materials with a high yield strength or a fine structure.

#### A.3.2 Influence of microstructural domain size and yield strength

Both roughness and plasticity induced closure depend on microstructural characteristic size and material yield properties, thus causing the  $\Delta K_{th}$  to be dependent on these characteristics (147). According to considerations based on crack closure mechanisms, an increase in the threshold is obtained when the mean free path, which corresponds to

## A. INFLUENCE OF MECHANICAL PROPERTIES AND MICROSTRUCTURAL FEATURES ON THE FATIGUE THRESHOLD OF STEELS

---

the characteristic microstructural domain size, increases and when the yield strength decreases (29, 125).

Many authors have observed that at the threshold the size of the plastic zone at the crack tip equals the size of the characteristic microstructural domain (29), (168). Plasticity induced closure increases as the plastic zone size at the crack tip increases (118), thus being higher for low yield strength materials and for materials with a large characteristic microstructural dimension, which is grain size for ferritic steels (29) (148), high angle domain size for martensitic or bainitic steels (168) and pearlite colony size for eutectoidic steels (39). The morphology of the microstructure exerts an influence on the extension of the plastic zone size, as shown in (68).

Experimental results show that the dependence of the threshold with the the yield strength varies for different types of microstructures: the threshold increases with yield strength for ferritic structures and decreases for martensitic or bainitic structures (148). This result reflects the fact that yield strength is not an independent factor affecting the threshold. Yield strength depends on characteristic microstructural dimension (for example for ferritic steels grain size and yield strength are related by the well known Hall-Petch relation), dislocation density and precipitates.

### A.3.3 Influence of microstructural inhomogeneities and second phases

The crack propagation rate is also influenced by the microstructural dishomogeneities. For example grain boundaries retard the crack growth rate.

Crack branching and tortuosity are other phenomena related to the microstructural features that the crack encounters while it grows and they slow the crack propagation rate. A tortuous crack path and branching for example create micro and macro roughness. For example in (75) it is shown that in ferritic-pearlitic steels, the roughness induced closure is strongly influenced by the distance between pearlitic lamellae.

During  $\Delta K$  decreasing tests, it is often observed that the crack stops propagating when it encounters a second phase particle or an inhomogeneities. For example the crack stops in correspondence with the interface between ferrite and pearlite.

### A.4 Intrinsic and extrinsic threshold concept

The threshold value in absence of closure is often called intrinsic component of the threshold of the material. The intrinsic component, according to most of the models, is described through considerations based on the energy necessary for dislocation movement to permit the crack to advance. These models result in an intrinsic threshold dependent on elastic modulus (149), parameters describing the crystal lattice (magnitude of the Burger vector) and texture (Taylor factor) (28, 156). The extrinsic component of the threshold is mainly due to closure and can be observed at low values of  $R$ . The extrinsic component is affected by material microstructural features, such as the characteristic size of the microstructural domain (grain size, packet size, prior austenitic grain size, pearlitic interlamellar spacing, pearlite colony size), which represents the mean free path that a crack encounters without being deviated by microstructural inhomogeneities (39, 125, 126, 148, 168). The extrinsic component is also affected by microstructural morphology (68) and by the monotonic or cyclic yield strength, which determines the extension of the plastic zone size at the crack tip. The intrinsic threshold is independent from yield stress and varies in a limited range for various steels. The extrinsic threshold shows a strong dependence on stress ratio and for high stress ratio shows highly scattered values for various steels.

### A.5 Two parameters threshold representation

Recently some authors have proposed a two-parameters threshold concept. According to their observations, both  $K_{max}$  and  $\Delta K$  must be higher than their threshold value to permit the crack growth (79, 131, 154). According to (131) closure effects are absent and the phenomena attributed to closure can be explained with a unified  $\Delta K - K_{max}$  threshold approach. This approach, which refuses the concept of closure, is however rejected by some scientists (59).

### A.6 Factors affecting the fatigue threshold

Summarizing, the main factors affecting the threshold, as reported in the previous paragraph, are: the characteristic microstructural domain, the yield stress and the stress ratio. However, it must be underlined that the yield stress is dependent on the

## **A. INFLUENCE OF MECHANICAL PROPERTIES AND MICROSTRUCTURAL FEATURES ON THE FATIGUE THRESHOLD OF STEELS**

---

characteristic microstructural domain, because one of the strengthening mechanisms in steel is grain size refinement, (the others are dislocation density increase, second phase particles and solid solution (117)).

## Appendix B

# Fatigue crack growth model: Nasgro equation

The Forman-Mettu equation (46), also called Nasgro equation (47, 53), provides a model for the fatigue threshold,  $\Delta K_{th}$ , shown in equation B.1, and for the crack growth rate,  $\frac{dx}{dn}$ , shown in equation B.2.

The threshold variation with stress ratio is described as:

$$\Delta K_{th,R} = \frac{\Delta K_{th,0}}{\left[ \frac{1-f}{(1-A_0)(1-R)} \right] (1 + C_{th}R)} \quad (\text{B.1})$$

where  $\Delta K_{th,0}$  is the fatigue threshold range at stress ratio  $R = 0$ ,  $C_{th}$  is a fitting parameter,  $A_0$  is a function of the maximum stress and of the constraint (see equation B.3).  $f$  is Newman's crack opening function (103), originally defined as  $f = \frac{\sigma_0}{\sigma_{max}}$ , with  $\sigma_0$  the crack opening stress. This function accounts for the plasticity induced closure, which is the main source of closure.

The fatigue crack growth rate is expressed as:

$$h_x = \frac{dx}{dn} = C \left[ \left( \frac{1-f}{1-R} \right) \Delta K \right]^m \cdot \frac{\left( 1 - \frac{\Delta K_{th,R}}{\Delta K} \right)^p}{\left( 1 - \frac{K_{max}}{K_{mat}} \right)^q} \quad (\text{B.2})$$

where  $x$  is the crack length, either  $a$  or  $c$ ,  $N$  is the number of cycles,  $R$  is the stress ratio,  $C$ ,  $m$ ,  $p$  and  $q$  are fitting parameters,  $\Delta K$  is the range of the stress intensity factor,  $\Delta K_{th,R}$  is the fatigue threshold at stress ratio  $R$ , defined in equation B.1,  $K_{max} = \frac{\Delta K}{(1-R)}$  is the maximum stress intensity factor,  $K_{mat}$  is the fracture toughness of the material.



## B. FATIGUE CRACK GROWTH MODEL: NASGRO EQUATION

---

Parameter	Value
C	$1.33 \cdot 10^{-11} \text{MPa}\sqrt{m}$ with $\frac{da}{dN}$ in $\frac{mm}{cycle}$
m	2.85
p	0.3
q	0.01
$C_{th}$	0.48

**Table B.1:** Forman-Mettu equation parameters

The opening stress due to plasticity induced closure is a function of the stress ratio  $R$ , of the stress state, defined by the constraint  $\alpha$  and of the ratio  $\frac{\sigma_{max}}{\sigma_{flow}}$ .

The Newman's crack opening function  $f$  is originally defined as follows.

$$A_0 = (0.825 - 0.34 \cdot \alpha + 0.05 \cdot \alpha^2) \cdot [\cos(\frac{\pi}{2} \frac{\sigma_{max}}{\sigma_{flow}})]^{(\frac{1}{\alpha})} \quad (\text{B.3})$$

$$A_1 = (0.415 - 0.071 \cdot \alpha) \cdot \frac{\sigma_{max}}{\sigma_{flow}} \quad (\text{B.4})$$

$$A_2 = 1 - A_0 - A_1 - A_3 \quad (\text{B.5})$$

$$A_3 = 2A_0 + A_1 - 1 \quad (\text{B.6})$$

$$f = \max\{R, A_0 + A_1R + A_2R^2 + A_3R^3\} \quad (\text{B.7})$$

Usually the opening stress is expressed as a function of  $\frac{\sigma_{max}}{\sigma_{flow}}$ , as reported in equations B.3 and B.4. In this work the opening stress is expressed as a function of the normalized stress intensity parameter,  $K_{max}/K_{flow}$  ( $K_{flow} = \sigma_{flow} \cdot \sqrt{\pi a}$  and  $K_{max} = \beta_x \cdot \sigma_{max} \cdot \sqrt{\pi a}$ ), which has been demonstrated to successfully correlate the crack opening stresses for various specimen geometries (87) (88) (89). The flow stress is assumed equal to the cyclic yield stress:  $\sigma_{flow} = \sigma_{yc}$ .

The reliability evaluations presented in sections 5 and 6 are carried out applying the values of the parameters reported in table B.1, and using the mechanical properties in table B.2, which refer to material 355H (see section 3.2).

---

Parameter	Value	
Yield strength	$YS[MPa]$	590
Cyclic yield strength	$\sigma_{yc}[MPa]$	350
Ultimate tensile strength	$UTS[MPa]$	705
Elastic modulus	E [MPa]	210.000
Poisson's ratio	$\nu$	0.3

**Table B.2:** Mechanical properties

## **B. FATIGUE CRACK GROWTH MODEL: NASGRO EQUATION**

## Appendix C

# Verification of the subset simulation algorithm

Figure C.1 shows the probability of failure  $p_F$  versus the correlation length  $z$  of the random process of the stress referred to the empirical cumulative distribution function of the stress  $C1$  (figure 6.3). The results obtained with the subset simulation algorithm are consistent with the 95% confidence band of the *MCS* simulations.

### C. VERIFICATION OF THE SUBSET SIMULATION ALGORITHM

---

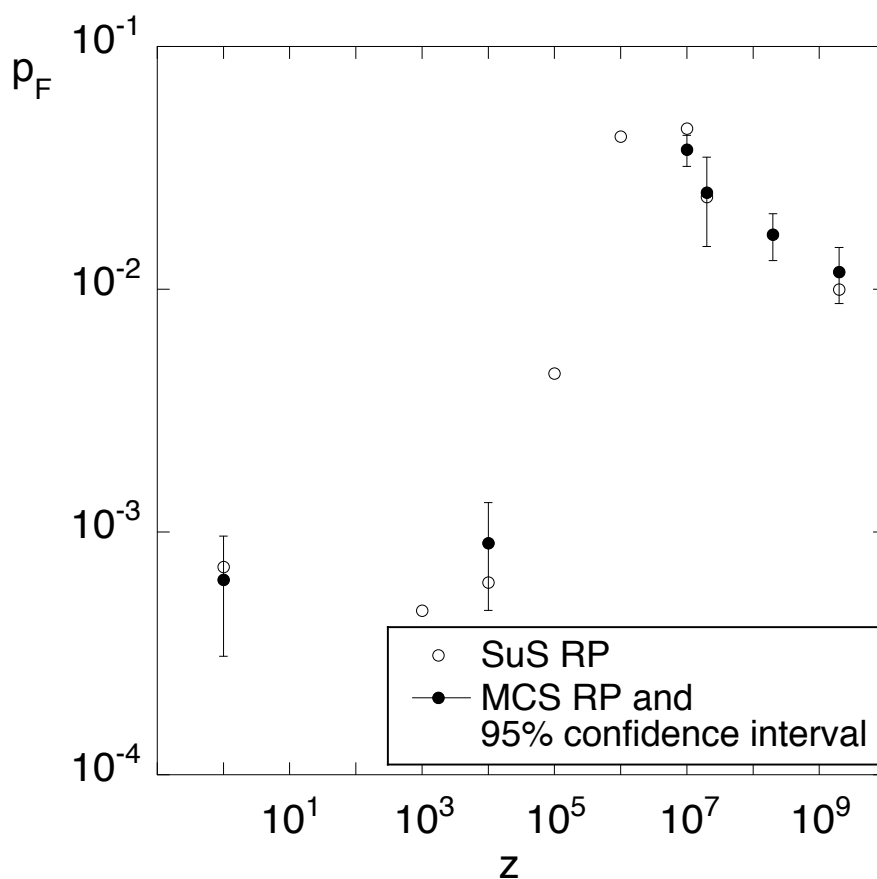


Figure C.1: Probability of failure versus correlation length of the stress random process, having cumulative distribution function  $CDF_1$ , obtained applying subset simulation method (*SuS RP*) and Monte Carlo simulation method (*MCS RP*). The results are obtained considering the critical crack size failure condition and evaluating the fatigue crack growth using  $b = 10^4$  cycles for each block.

# References

- [1] (1996). ASTM E112 Standard test methods for determining average grain size. 36
- [2] (2001). EN 10002-1 Tensile testing of metallic materials. Method of test at ambient temperature. 37
- [3] (2003). EN 10297-1 Seamless circular steel tubes for mechanical and general engineering purposes. Technical delivery conditions. Non alloy and alloy steel tubes. 75, 76
- [4] (2004). ASTM E606 Standard practice for strain controlled fatigue testing. 37
- [5] (2005). BS 7910 Guide to methods for assessing the acceptability of flaws in metallic structures. 18
- [6] (2005). Eurocode 3 Design of steel structures - part 1-9: Fatigue. 5
- [7] (2008). ASTM E647 Standard test method for measurement of fatigue crack growth rates. 10, 13, 41, 42, 46, 111, 113
- [8] (2009). ASTM E399 Standard test method for linear-elastic plane-strain fracture toughness  $K_{IC}$  of metallic materials. 41
- [9] (2010). EN 10305-1 Steel tubes for precision applications. Technical delivery conditions. Seamless cold drawn tubes. xv, 36, 75, 76
- [10] (2011). ASTM E1049-85 Standard practices for cycle counting in fatigue analysis. 15, 17, 82
- [11] (2011). *Matlab User's Manual R2011b*. The MathWorks. 51
- [12] AFGROW (2010). Fracture mechanics and fatigue crack growth analysis software tool. <http://www.afgrow.net/>. 25, 69
- [13] ALTAMURA, A. & BERETTA, S. (2012). Reliability assessment of hydraulic cylinders considering service loads and flaw distribution. *International Journal of Pressure Vessels and Piping*, **98**, 76–88. xi, 22, 62, 72, 77, 79, 80, 82, 83, 84, 94, 107, 109
- [14] ALTAMURA, A. & STRAUB, D. (2012). Fracture mechanics based fatigue reliability under variable amplitude loading: review and solutions, manuscript submitted to Engineering Fracture Mechanics. 89, 108, 109
- [15] ALTAMURA, A., BERETTA, S. & DESIMONE, H. (2009). In-service reliability of hydraulic cylinders' housings. In *ICF12 - 12<sup>th</sup> International conference on fracture*, Ottawa, Ontario Canada. 62, 76
- [16] ANDERSON, T. (1995). *Fracture mechanics: fundamentals and applications*. CRC Press, Boca raton, 2<sup>nd</sup> edn. 41, 63, 64, 112
- [17] ANNIS, C. (2003). Probabilistic life prediction isn't as easy as it looks. In W. Johnson & E. B.M. Hillberry, eds., *Probabilistic aspects of life prediction, ASTM STP-1450*, ASTM International, West Conshohocken, PA. 7, 26, 28, 35
- [18] ASWATH, P., SURESH, S., HOLM, D. & BLOM, A. (1988). Load interaction effects on compression fatigue crack growth in ductile solids. *Journal of Engineering Materials and Technology*, **110**, 282–285. 41
- [19] AU, S. & BECK, J. (2001). Estimation of small failure probabilities in high dimensions by subset simulation. *Probabilistic Engineering Mechanics*, **16**, 263–277. 34, 89
- [20] BARTLETT, M.S. (1937). Properties of sufficiency and statistical tests. *Proceedings of The Royal Society of London. Series A, Mathematical and Physical Sciences*, **160**, 268–282. 51
- [21] BAYLAC, G. & KOPLEWICZ, D. (2004). EN 13445 Un-fired pressure vessels background to the rules in part 3 design. Tech. rep., Union de Normalization de la Mécanique. 5
- [22] BERETTA, S. (2004). Defect tolerance of mechanical components obtained from tubes. Tenaris internal report, Politecnico di Milano. 40
- [23] BERETTA, S. & CARBONI, M. (2006). Experiments and stochastic model for propagation lifetime of railway axles. *Engineering Fracture Mechanics*, **73**, 2627–2641. 35, 81
- [24] BIRNBAUM, Z. & SAUNDERS, S. (1968). A probabilistic interpretation of miner's rule. *SIAM Journal of Applied Mathematics*, **16**, 637–652. 9
- [25] BOLJANOVIĆ, S. & MAKSIMOVIĆ, S. (2011). Analysis of the crack growth propagation under mixed-mode loading. *Engineering Fracture Mechanics*, **78**, 1565–1576. 19
- [26] BULLOCH, J. (1994). Fatigue threshold in steels – mean stress and microstructure influences. *International Journal of Pressure Vessels and Piping*, **58**, 103–127. 114, 115
- [27] CARBONI, M., PATRIARCA, L. & REGAZZI, D. (2010). Determination of  $\Delta K_{th}$  by compression pre-cracking in a structural steel. *Journal of ASTM International*, **6**, 1–13. 41
- [28] CHAN, K. (2004). Variability of large crack fatigue crack growth thresholds in structural alloys. *Metallurgical and Materials Transactions A*, **35**, 3721–3735. 114, 117
- [29] CHAPETTI, M. (2005). Fatigue crack propagation behaviour in ultra fine grain low carbon steel. *International Journal of Fatigue*, **27**, 235–243. 15, 113, 116

## REFERENCES

---

- [30] CHEN, C., LIU, C., CHEN, J., YU, A. & HSU, H. (2008). The effects of material variations on aircraft inspection schedules based on stochastic crack growth model. *International Journal of Fatigue*, **30**, 861–869. 27
- [31] CHIAKI, I. & MISAWA, T. (1988). A stochastic model for fatigue crack propagation with random propagation resistance. *Engineering Fracture Mechanics*, **31**. 27
- [32] CRISTEA, M., BERETTA, S. & ALTAMURA, A. (2012). Fatigue limit assessment on seamless tubes in presence of inhomogeneities: experimental small vs. full scale testing. *International Journal of Fatigue*, **41**, 150–157. xi, 38, 58, 66, 69, 72, 107
- [33] DAVOLI, P., VERGANI, L., BERETTA, S., GUAGLIANO, M. & BARAGETTI, S. (2007). *Costruzione di macchine 1*. McGraw Hill. 64
- [34] DILLSTROM, P. (2000). ProSINTAP a probabilistic program implementing the SINTAP assessment procedure. *Engineering Fracture Mechanics*, **67**, 647–668. 78
- [35] DITLEVSEN, O. & MADSEN, H. (1996). *Structural reliability methods*. John Wiley & Sons. 29, 93
- [36] DOLINSKI, K. (1986). Stochastic loading and material inhomogeneity in fatigue crack propagation. *Engineering Fracture Mechanics*, **25**. 28
- [37] DONALD, J. & PARIS, P. (1999). An evaluation of  $\Delta K_{eff}$  estimation procedures on 6061-t6 and 2024-t3 aluminium alloys. *International Journal of Fatigue*, **21**. 20
- [38] EL-HADDAD, M.H., SMITH, K.N. & TOPPER, T.H. (1979). Fatigue crack propagation of short crack. *Journal of Engineering Materials and Technology*, **101**, 42–47. 11
- [39] EL-SHABASY, A.B. & LEWANDOWSKI, J. (2003). Effects of load ratio,  $R$ , and test temperature on fatigue crack growth of fully pearlitic eutectoid steel (fatigue crack growth of pearlitic steel). *International Journal of Fatigue*, **26**, 305–309. 14, 116, 117
- [40] ELBER, W. (1970). Fatigue crack closure. *Journal of Engineering Fracture Mechanics*, **2**. 15, 112
- [41] ELBER, W. (1971). The significance of crack closure. In *ASTM/STP 486*. 15
- [42] ENGESVIK, K.M. (1981). Analysis of uncertainties in the fatigue analysis of welded joints. Tech. rep., The university of Trondheim - The Norwegian Institute of technology. 26
- [43] FASH, J., CONLE, F. & MINTER, G. (1989). Analysis of irregular loading histories for the SAE biaxial fatigue program. In G. Leese & D.Socie, eds., *Multiaxial fatigue: analysis and experiments*, vol. AE-14, 33–59, Society of Automotive Engineers, Warrendale, PA. 16
- [44] FATEMI, A. & YANG, L. (1998). Cumulative fatigue damage and life prediction theories: a survey of the state of the art for homogeneous materials. *International Journal of Fatigue*, **20**, 9–34. 9
- [45] FETT, T. & MUNZ, D. (1997). Stress intensity factors and weight functions. In *Computational Mechanics Publications*, Southampton. 18
- [46] FORMAN, R. & METTU, S. (1992). Behavior of surface and corner cracks subjected to tensile and bending loads in a Ti-6Al-4V alloy. In H. Ernst, A. Saxena & D. McDowell, eds., *Fracture Mechanics: Twenty-Second Symposium*, vol. I of *ASTM STP 1131*, 519–546, American Society for Testing and Materials. 46, 65, 119
- [47] FORMAN, R., SHIVAKUMAR, V., METTU, S. & NEWMAN, J. (2000). Fatigue crack growth computer program NASGRO - version 3.0. Tech. rep., NASA, Johnson Space Center, Houston, Texas. 25, 65, 119
- [48] FORTH, S., NEWMAN, J. & FORMAN, R. (2003). On generating fatigue crack growth thresholds. *International Journal of Fatigue*, **25**, 9–15. 41
- [49] GASSNER, E. (1939). Festigkeitsversuche mit wiederholter Beanspruchung im Flugzeugbau (Strength tests under repeated loading for aeronautical engineering). *Luftwissen*, **6**, 61–64. 15, 22
- [50] GASSNER, E. (1954). Betriebsfestigkeit, eine Bemessungsgrundlage für Konstruktionsteile mit statistisch wechselnden Betriebsbeanspruchungen. *Konstruktion*, **6**, 97–104. 16
- [51] GDOUTOS, E. & HATZITRIFON, N. (1987). Growth of three-dimensional cracks in finite thickness plates. *Engineering Fracture Mechanics*, **26**, 883–895. 19
- [52] HALDAR, A. & MAHADEVAN, S. (2000). *Probability, reliability and statistical methods in engineering design*. John Wiley & Sons, Inc., New York. 78
- [53] HARTER, J.A. (2006). AFGROW users guide and technical manual. Tech. rep., US air force research laboratory technical report AFRL-VA-WP-TR-2006-XXXX, Air vehicle directorate, 2790 D Street, Ste 504. 46, 65, 115, 119
- [54] HASOFER, A. & LIND, N. (1974). An exact and invariant first order reliability format. *Journal of Engineering Mechanics*, **100**, 111–121. 33, 89
- [55] HEAD, A. (1953). The growth of fatigue cracks. *Philosophical Magazine*, **44**, 925–938. 16
- [56] HEULER, P. & KLÄTSCHKE, H. (2005). Generation and use of standardised load spectra and load-time histories. *International Journal of Fatigue*, **27**, 974–990. 6, 16
- [57] HOHENBICHLER, M. & RACKWITZ, R. (1981). Non-normal dependent vectors in structural safety. *Journal of Engineering Mechanics*, **107**, 1227–1238. 93
- [58] HOLM, D., BLOM, A. & SURESH, S. (1986). Growth of cracks under far-field cyclic compressive loads: numerical and experimental results. *Engineering Fracture Mechanics*, **23**, 1097–1106. 41
- [59] HOLTZ, R. (2003). Phenomenology of the effective stress intensity related to fatigue crack growth threshold. *International Journal of Fatigue*, **25**, 891–897. 117
- [60] HONG, H.P. (1997). Reliability analysis with non destructive inspection. *Structural Safety*, **19**, 383–395. 63

## REFERENCES

- [61] HUDSON, C. (1981). A root mean square approach for predicting fatigue crack growth under random loading. In J.C.C. Hudson, ed., *Methods and models for predicting fatigue crack growth under random loading*, ASTM STP 748, 41–52, American Society for Testing and Materials. 24
- [62] HUTAR, P., SEITL, S. & KRUML, T. (2009). Effects of specimen geometry on fatigue crack propagation in threshold region. In *ICF12 - 12<sup>th</sup> International conference on fracture*. 113
- [63] ISHIKAWA, H. & TSURUI, A. (1984). A stochastic model of fatigue crack growth in consideration of random propagation resistance. *Transaction of JSME*, **50**, 1309–1315. 27
- [64] ISHIKAWA, H., TANAKA, H. & WAKASA, S. (1995). A stochastic crack growth model with propagation resistance as a random field. In R. Rackwits, G. Augusti & A. Borri, eds., *Reliability and optimization of structural systems*, Chapman and Hall, London, UK. 27
- [65] KAUL, H. (1938). Statistische erhebungen über Betriebsbeanspruchungen von Flugzeugflügeln. *der Deutschen Luftfahrtforschung, Ergänzungsband*, 307–313. 15
- [66] KIM, H., CHOI, M., CHUNG, C. & SHIN, D. (2003). Fatigue properties of ultrafine grained low carbon steel produced by equal channel angular pressing. *Materials Science and Engineering: A*, **340**, 243–250. 113
- [67] KITAGAWA, H. & TAKAHASHI, S. (1975). Applicability of fracture mechanics to very small cracks or the cracks in the early stage. In *Proc. Second International Conference on Mechanical Behavior of Materials*. 10
- [68] KORDA, A.A. (2007). Fatigue crack growth behaviour in ferritic-pearlitic steels with networked and distributed pearlite structures. *International Journal of Fatigue*, **29**, 1140–1148. 14, 113, 116, 117
- [69] LAHAM, S.A. (1998). Stress intensity factor and limit load handbook. Tech. rep., British energy generation Ltd, SINTAP, task 2.6. 63, 65, 67
- [70] LAL, D. (1992). The combined effects of stress ratio and yield strength on the LEFM fatigue threshold condition. *Fatigue and Fracture of Engineering Materials and Structures*, **15**, 1199–1212. 115
- [71] LARDNER, R. (1966). Crack propagation under random loading. *Journal of the Mechanics and Physics of Solids*, **14**, 141–150. 16
- [72] LARDNER, R. (1966). Crack propagation under random loading - II. *Journal of the Mechanics and Physics of Solids*, **14**, 281–288. 16
- [73] LARDNER, R. (1967). A theory of random fatigue. *Journal of the Mechanics and Physics of Solids*, **15**, 205–221. 16
- [74] LAUSCHMAN, H. (1987). A stochastic model of fatigue crack growth in heterogeneous material. *Engineering Fracture Mechanics*, **26**, 707–728. 27
- [75] LAWSON, L., CHEN, E. & MESHII, M. (1999). Near threshold fatigue: a review. *International Journal of Fatigue*, **21**, S15–S34. 56, 111, 115, 116
- [76] LIDIARD, A.B. (1979). Probabilistic fracture mechanics. In *Fracture mechanics, current status, future prospects*, Pergamon Press. 26
- [77] LILLIEFORS, H.W. (1967). On the Kolmogorov-Smirnov test for normality with mean and variance unknown. *Journal of the American Statistical Association*, **62**, 399–402. 55
- [78] LIN, X. & SMITH, R. (1999). Finite element modelling of fatigue crack growth of surface cracked plates, Part I: The numerical technique. *Engineering Fracture Mechanics*, **63**, 503–522. 22
- [79] LIU, H. (1998). A dislocation barrier model for fatigue crack growth threshold. *International Journal of Fracture*, **93**, 261–280. 13, 111, 114, 117
- [80] LIU, P.L. & KIUREGHIAN, A.D. (1986). Multivariate distribution models with prescribed marginal and covariances. *Probabilistic Engineering Mechanics*, **1**. 90
- [81] LIU, Y. & MAHADEVAN, S. (2007). Stochastic fatigue damage modelling under variable amplitude loading. *International Journal of Fatigue*, **29**, 1149–1161. 6
- [82] LIU, Y. & MAHADEVAN, S. (2009). Probabilistic fatigue life prediction using an equivalent initial flaw size distribution. *International Journal of Fatigue*, **31**, 476–487. 6, 86
- [83] LUTES, L. & SARKANI, S. (2004). *Random vibrations: Analysis of structural and mechanical systems*. Butterworth - Heinemann, Oxford. 17
- [84] MADSEN, H.O., KRENK, S. & LIND, N.C. (1986). *Methods of structural safety*. Prentice Hall, New Jersey. 17, 21, 27, 30
- [85] MALJAARS, J., STEENBERGEN, H. & VROUWENVELDER, A. (2012). Probabilistic model for fatigue crack growth and fracture of welded joints in civil engineering structures. *International Journal of Fatigue*, **38**, 108–117. 23
- [86] MATTRAND, C. & BOURINET, J. (2011). Random load sequences and stochastic crack growth based on measured load data. *Engineering Fracture Mechanics*, **78**, 3030–3048. 17
- [87] MCCLUNG, R. (1991). The influence of applied stress, crack length and stress intensity factor on crack closure. *Metallurgical Transactions A*, **22A**, 1559–1571. 46, 66, 120
- [88] MCCLUNG, R. (1994). Finite element analysis of specimen geometry effects on fatigue crack closure. *Fatigue and Fracture of Engineering Material and Structures*, **17**, 861–872. 7, 46, 120
- [89] MCCLUNG, R. & SEHITOGU, H. (1989). On the finite element analysis of fatigue crack closure-1. basic modelling issues. *Engineering Fracture Mechanics*, **33**, 237–252. 46, 120
- [90] MCKAY, M., BECKMAN, R.J. & CONOVER, W. (1979). A comparison of three methods for selecting values of input variables in the analysis of output from a computer code. *Technometric*, **21**. 33



## REFERENCES

---

- [91] MELCHERS, R. (2002). *Structural reliability analysis and prediction*. John Wiley & Sons. 29, 93
- [92] MILLER, K.J. & DE LOS RIOS, E.R. (1982). *Short Fatigue Cracks*. Mechanical Engineering Publications. 10
- [93] MINER, M. (1945). Cumulative damage in fatigue. *Journal on Applied Mechanics*, **12**, A159–A164. 9
- [94] MIRANDA, A., MEGGIOLARO, M., CASTRO, Z., MARTHA, L. & BITTENCOURT, T. (2003). Fatigue life and crack path predictions in generic 2D structural components. *Engineering Fracture Mechanics*, **70**, 1259–1279. 22
- [95] MONTGOMERY, D. (2008). *Design and analysis of the experiments*. John Wiley & Sons. 40, 51
- [96] MONTGOMERY, H., RUNGER (2009). *Engineering Statistics, Student Study Edition*. John Wiley & Sons. 40, 55, 78
- [97] MOORE, H. & KOMMERS, J. (1927). *The fatigue of metals*. McGraw Hill, New York. 26
- [98] MOSLEMI, H. & KHOEI, A. (2009). 3D adaptive finite element modeling of non-planar curved crack growth using the weighted superconvergent patch recovery method. *Engineering Fracture Mechanics*, **76**, 1703–1728. 19
- [99] MURAKAMI, Y. (1987 - 1992 - 2002). *Stress intensity factor handbook*, vol. 1-2 and 3 and 5-6. Pergamon Press, Japan. 18
- [100] MURAKAMI, Y. (2002). *Metal fatigue: Effects of small defects and nonmetallic inclusions*. Elsevier Science, Oxford. 11
- [101] NELSON, W. (1982). *Applied life data analysis*. John Wiley & Sons, New York. 77
- [102] NELSON, W. (1990). *Accelerated testing*. John Wiley, Sons, New York. 77
- [103] NEWMAN, J.C. (1984). A crack opening stress equation for fatigue crack growth. *International Journal of Fracture*, **24**, 65, 119
- [104] NEWMAN, J.C. (1997). Crack growth under variable amplitude and spectrum loading. In *TMS symposium proceedings to honor P. Paris*. 20
- [105] NEWMAN, J.C. & RAJU, I. (1986). *Stress intensity factor equations for cracks in three-dimensional bodies subjected to tension and bending loads*, vol. 2, chap. 9. Elsevier Science, computational methods in the mechanics of fracture edn. 18, 19
- [106] NEWMAN, J.C. & RAJU, I.S. (1986). Stress intensity factor equations for cracks in three-dimensional bodies subjected to tension and bending loads. In *Computational methods in the mechanics of fracture*, Elsevier Science. 63, 64
- [107] NEWMAN, J.C. & SCHNEIDER, J. (2005). Compression pre-cracking to generate near threshold fatigue-crack-growth rates in two aluminium alloys. *International Journal of Fatigue*, **27**, 1432–1440. 41
- [108] NEWMAN, J.C. & YAMADA, Y. (2010). Compression pre-cracking methods to generate near-threshold fatigue-crack-growth rate data. *International Journal of Fatigue*, **32**, 879–885. 41
- [109] NEWMAN, J.C., BROT, A. & MATIAS, C. (2004). Crack-growth calculations in 7075-T7351 aluminum alloy under various load spectra using an improved crack-closure model. *Engineering Fracture Mechanics*, **71**, 2347–2363. 22
- [110] ORTIZ, K. & KIREMIDJIAN, A. (1988). Stochastic modeling of fatigue crack growth. *Engineering Fracture Mechanics*, **29**, 317–334. 26, 27, 28
- [111] PALMGREN, A. (1924). Die Lebensdauer von Kugellagern. *Verfahrenstechnik, Berlin*, **68**, 339–341. 9
- [112] PÄR, J. (2002). On rainflow cycles and the distribution of number of interval crossings by a Markov chain. *Probabilistic Engineering Mechanics*, **17**, 123–130. 17
- [113] PÄR, J. (2006). Extrapolation of load histories and spectra. *Fatigue and Fracture of Engineering Materials and Structures*, **29**, 201–207. 82
- [114] PARIS, P., TADA, H. & DONALD, J. (1999). Service load fatigue damage - a historical perspective. *International Journal of Fatigue*, **21**, S35–S46. 20
- [115] PARK, Y.H. & TANG, J. (2006). An efficient methodology for fatigue reliability analysis for mechanical components. *Journal of pressure vessels technology*, **128**, 293–297. 9
- [116] PHILIPPS, E. & NEWMAN, J. (1989). Impact of small cracks effect on designlife calculations. *Experimental mechanics*, **29**, 10
- [117] PICKERING (1978). *Physical metallurgy and the design of steels*. Applied Science Publishers. 111, 118
- [118] PRAWOTO, Y. (2009). Designing steel microstructure based on fracture mechanics approach. *Materials Science and Engineering A*, **507**, 74–86. 111, 116
- [119] PROVAN, J. (1986). *Probabilistic fracture mechanics and reliability*. Martinus Nijhoff, Dordrecht. 27
- [120] RACKWITZ, R. (2011). Reliability analysis—a review and some perspectives. *Structural Safety*, **23**, 365–395. 33
- [121] RACKWITZ, R. & FLESSLER, B. (1978). Structural reliability under combined random load sequences. *Computers and Structures*, **9**, 489–494. 29, 33, 89, 93
- [122] RAIFFA, H. & SCHLAIFER, R. (1961). *Applied Statistical decision Theory*. Cambridge University Press. 11
- [123] RAO, S. (1992). *Reliability based design*. McGraw-Hill. 32
- [124] RAU, I. (1970). On fatigue-crack propagation under stationary random loading. *International Journal of Engineering Science*, **8**, 175–189. 16
- [125] RAVICHANDRAN, K. (1991). A rationalisation of fatigue thresholds in pearlitic steels using a theoretical model. *Acta Metallurgica et Materialia*, **39**, 1331–1341. 14, 116, 117

## REFERENCES

- [126] RAVICHANDRAN, K. & DWARAKADASA, E. (1991). Theoretical modelling of the effects of grain size on the threshold for fatigue crack growth. *Acta Metallurgica et Materialia*, **39**, 1343–1357. 13, 14, 111, 113, 114, 117
- [127] RIGHINIOTIS, T.D. & CHRYSANTHOPOULOS, M.K. (2004). Fatigue and fracture simulation of welded bridge details through a bi-linear crack growth law. *Structural Safety*, **26**, 141–158. 7, 18, 23, 35
- [128] RITCHIE, M. (2002). Crack closure and the fatigue crack propagation threshold as a function of load ratio. *Fatigue and fracture of Engineering materials and Structures*, **21**, 847–855. 114
- [129] RITCHIE, R.O. & LANKFORD, J. (1986). Overview of the small crack problem. In *Small Fatigue Cracks*, The Metallurgical Society. 10
- [130] RYCHLIK, I. (1996). Simulation of load sequences from rainflow matrices: Markov method. *International Journal of Fatigue*, **18**. 17
- [131] SADANANDA, K. & VASUDEVAN, A. (2003). Fatigue crack growth mechanisms in steels. *International Journal of Fatigue*, **25**, 899–914. 117
- [132] SANKARAN, S., SARMA, V., PADMANABHAN, K., JAEGER, G. & KOETHE, A. (2003). High cycle fatigue behaviour of a multiphase microalloyed medium carbon steel: a comparison between ferrite-pearlite and tempered martensite microstructures. *Materials Science and Engineering: A*, **362**, 249–256. 114
- [133] SCHIJVE, J. (1973). Effect of load sequences on crack propagation under random and program loading. *Engineering Fracture Mechanics*, **5**, 269–280. 16
- [134] SCHIJVE, J. (2001). *Fatigue of structures and materials*. Kluwer Academic Publishers. 115
- [135] SCHÖLLMANN, M., FULLAND, M. & RICHARD, H. (2003). Development of a new software for adaptive crack growth simulations in 3D structures. *Engineering Fracture Mechanics*, **70**, 249–268. 19
- [136] SCHÜTZ, W. (1996). A history of fatigue. *Engineering Fracture Mechanics*, **54**, 263–300. 16
- [137] SNEDECOR, G.W. & COCHRAN, G.W. (1989). *Statistical Methods*. Iowa State University Press. 51
- [138] SOBczyk, K. (1986). Modelling of random fatigue crack growth. *Engineering Fracture Mechanics*, **24**, 609–623. 28
- [139] SOBczyk, K. & SPENCER, B. (1992). *Random fatigue: from data to theory*. Academic Press, London, UK. 28
- [140] SONSINO, C. (2004). Principles of variable amplitude fatigue design and testing. *Journal of ASTM International*, **1**, 3–23. 16
- [141] SONSINO, C. (2007). Fatigue testing under variable amplitude loading. *International Journal of Fatigue*, **29**, 1080–1089. 16
- [142] STRAUB, D. (2004). *Generic approaches to risk based inspection planning for steel structures*. Ph.D. thesis, Swiss Federal Institute of Technology Zürich. 11, 21
- [143] SURESH, S. (1985). Crack initiation in cyclic compression and its applications. *Engineering Fracture Mechanics*, **21**, 453–463. 41
- [144] SURESH, S. (1998). *Fatigue of materials*. Cambridge University Press. 10, 112, 113, 115
- [145] SURESH, S. & RITCHIE, R.O. (1984). Propagation of short fatigue cracks. *International Metals Review*, **29**. 10
- [146] TADA, H., PARIS, P. & IRWIN, G. (2000). *The stress analysis of cracks handbook*. ASME Press, New York, 3rd edn. 18
- [147] TANAKA (1990). Metallurgical and mechanical factors affecting fatigue crack propagation and crack closure in various structural steels. In *Fatigue 90*, Honolulu, Hawaii. 115
- [148] TAYLOR, D. (1989). *Fatigue thresholds*. Butterworth Co Ltd. 13, 14, 15, 111, 113, 114, 116, 117
- [149] TORIBIO, J., GONZÁLEZ, B. & MATOS, J. (2008). Micro and macro analysis of the fatigue crack growth in pearlitic steels. *Ciencia e Tecnologia dos Materiais*, **20**, 68–74. 56, 113, 117
- [150] TSURUI, A. & ISHIKAWA, H. (1986). Application of the Fokker-Planck equation to a stochastic fatigue crack growth model. *Structural Safety*, **4**, 15–29. 27
- [151] TUCKER, L. & BUSSA, S. (1977). The SAE cumulative fatigue damage test program. In R. Wetzel, ed., *Fatigue under complex loading - analyses and experiments*, 1–54. 16
- [152] VANMARCKE, E. (1983). *Random fields. Analysis and synthesis*. MIT Press, Cambridge, MA. 90
- [153] VARANASI, S.R. & WHITTAKER, I.C. (1976). Structural reliability prediction method considering crack growth and residual strength. In *Fatigue crack growth under spectrum loads*, ASTM STP 595. 26
- [154] VASUDEVAN, A. & SADANANDA, K. (2007). Transient stress effects on fatigue crack growth thresholds due to testing methodology. *International Journal of Fatigue*, **29**, 1985–1989. 117
- [155] VIRKLER, D., HILLBERRY, B. & GOEL, P. (1979). The statistical nature of fatigue crack propagation. *Journal of Engineering Materials and Technology*, **101**, 148–153. 26, 27
- [156] WESÉN, J. & HEIER, E. (1998). Fatigue crack growth thresholds – the influence of Young’s modulus and fracture surface roughness. *International Journal of Fatigue*, **20**, 737–742. 113, 117
- [157] WHEELER, O.E. (1972). Spectrum loading and crack growth. *Journal of basic engineering - Transaction ASME*, **4**, 181–186. 20
- [158] WILLENBORG, J.D. (1971). A crack growth retardation model using an effective stress concept. Tech. rep., USAF Flight Dynamics Lab. 20
- [159] WIRSCHING, P. & CHEN, Y. (1988). Considerations of probability-based fatigue design for marine structures. *Marine Structures*, **1**, 23–45. 24

## REFERENCES

---

- [160] WIRSCHING, P. & NGUYEN, H.P. (2001). Fatigue reliability: a review of recent advances. *International Journal of Materials Product Technology*, **16**, 285–294. 9
- [161] WU, X. & CARLSSON, A. (1991). *Weight functions and stress intensity factor solutions*. Pergamon Press, Oxford, UK. 18
- [162] XING, J., ZHONG, O. & HONG, Y. (1997). A simple log normal random process approach of the fatigue crack growth considering the distribution of initial crack size and loading conditions. *International Journal of Pressure Vessels and Piping*, **74**, 7–12. 27
- [163] YANG, J., SALIVAR, G. & ANNIS, C. (1983). Statistical modeling of fatigue-crack growth in a nickel-base superalloy. *Engineering Fracture Mechanics*, **18**, 257–270. 28
- [164] YANG, J.N. & MANNING, S.D. (1996). A simple second order approximation for stochastic crack growth analysis. *Engineering Fracture Mechanics*, **53**, 677–686. 26, 27
- [165] ZERBST, U., SCHÖEDEL, M., WEBSTER, S. & AINSWORTH, R. (2007). *Fitness-for-service. Fracture assessment of structures containing cracks*. Elsevier Science. 19, 30, 38, 66, 67
- [166] ZHANG, R. & MAHADEVAN, S. (2001). Fatigue reliability analysis using nondestructive inspection. *Journal of Structural Engineering*, **27**, 957–965. 63
- [167] ZHENG, R. & ELLINGWOOD, B. (1998). Stochastic fatigue crack growth in steel structures subject to random loading. *Structural Safety*, **20**, 303–323. 6
- [168] ZHU, M. & XUAN, F. (2009). Effect of microstructure on appearance of near-threshold fatigue fracture in Cr-MoV steel. *International Journal of Fracture*, **159**, 111–120. 14, 116, 117